Some Case Histories with Lessons to Learn in Dam Engineering

Luiz Guilherme de Mello[1]

1 INTRODUCTION

Honouring Prof. Victor de Mello is a very hard task; doing it in his hometown raises the responsibility many steps higher.

I have decided to look into one of his loved fields of expertise, sharing with a broad community a less known but important contribution he has conceived, coordinated design and tests, and lead throughout the implementation in the field, following its success through monitoring results. This contribution is not as well-known as his discussion and proposal of understanding compacted fine grained / clayey fills as pre-consolidated materials, of using an inclined upstream stepped chimney filter in different earth fill dams, and the optimization of the wrap-around interface between concrete structures and the adjacent compacted earth fill in dams, as illustrated in Figures 1.1, 1.2 and 1.3, and discussed in detail in his Rankine Lecture - de Mello, V. (1977).

.

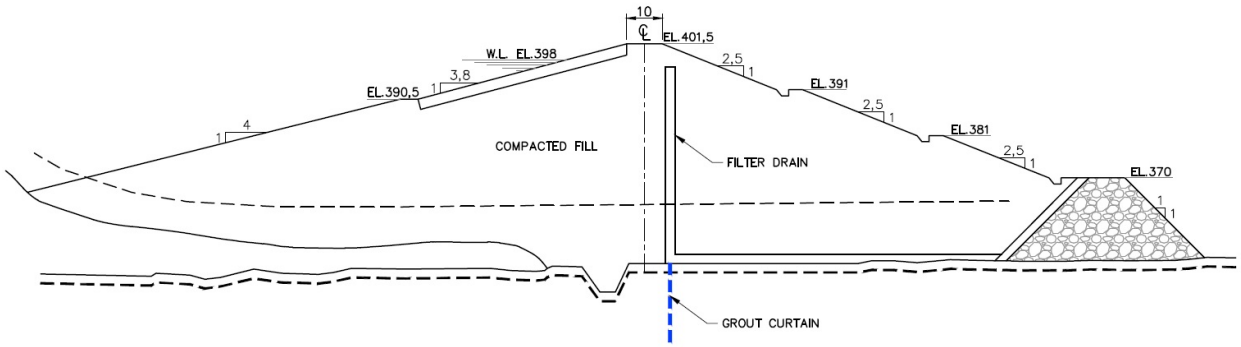

Figure 1.1 - Traditional earthfill cross section, in Brazil attributed to Terzaghi

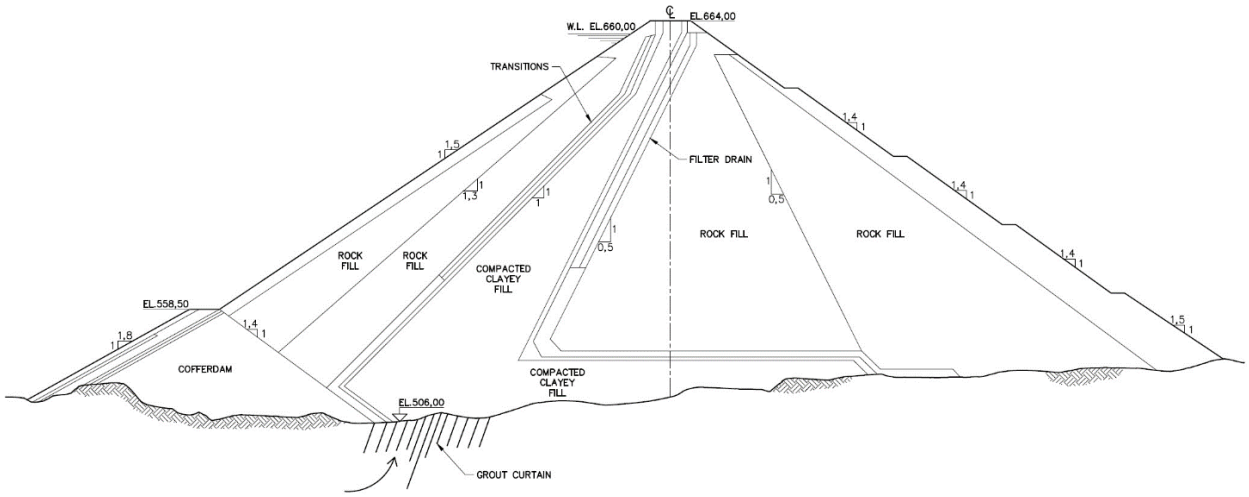

[1] Assistant Professor – Escola Politécnica Universidade de São Paulo, Geotechnical Consultant – Vecttor Projetos, São Paulo, Brasil

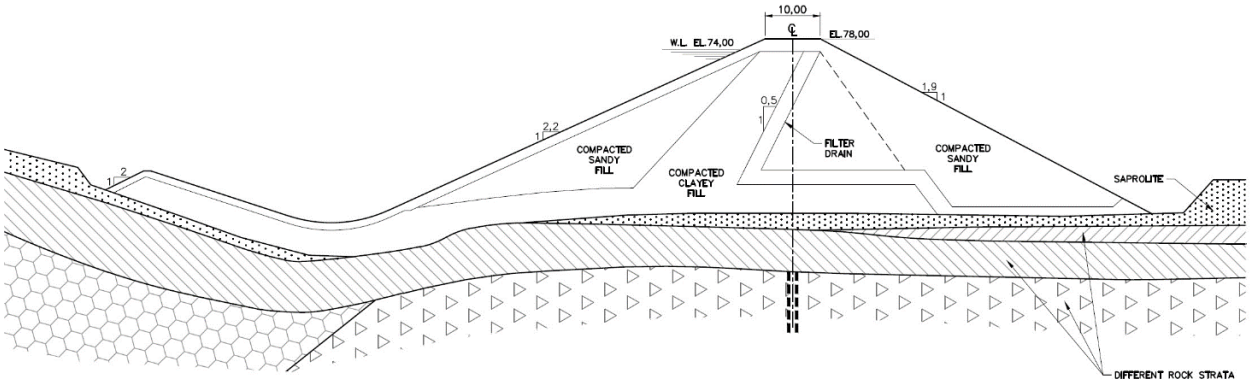

Figure 1.2 – Cross section optimized by Victor de Mello with upstream inclined impervious core and internal impervious blanket

It was a pioneer solution at the time it was conceived, impacted positively the dam where it was implemented, and was used in other situations of my knowledge

This technical paper presents other two case histories focusing on particular geological situations faced during dam construction or final stages of commissioning, both also in the tropical environment of Brazil's Amazon region. One led to the need of completely changing the geological / geomechanical model for the stability calculations of its intake structure, and the other led to the failure of a headrace tunnel following a mechanism not previously reported in the specialized literature. Geological particularities of the three sites are described in detail for two of the sites, with contribution of the geologists involved, endorsing many other authors (for example Fookes, P.G. et all 2000) on the need of having a sound geological model to work with.

The idea of discussing geotechnical challenges, either in time to take the best decisions possible or after a failure happens and repair is to be discussed, comes from the validity of sharing the experience gained when unforeseeable situations arise, so that equivalent future cases are prevented. Case histories add an important source of information for practitioners and even researchers when reporting situations properly documented. In all these cases a clear understanding of both the geological and physical model, leading to identifying the prevailing and conditioning behaviour(s) is fundamental. It is understood that case histories are an important tool to disseminate gained experience; in a previous lecture the author has shared some other situations of failures discussing his views on this important source of knowledge (de Mello, L.G., 2005).

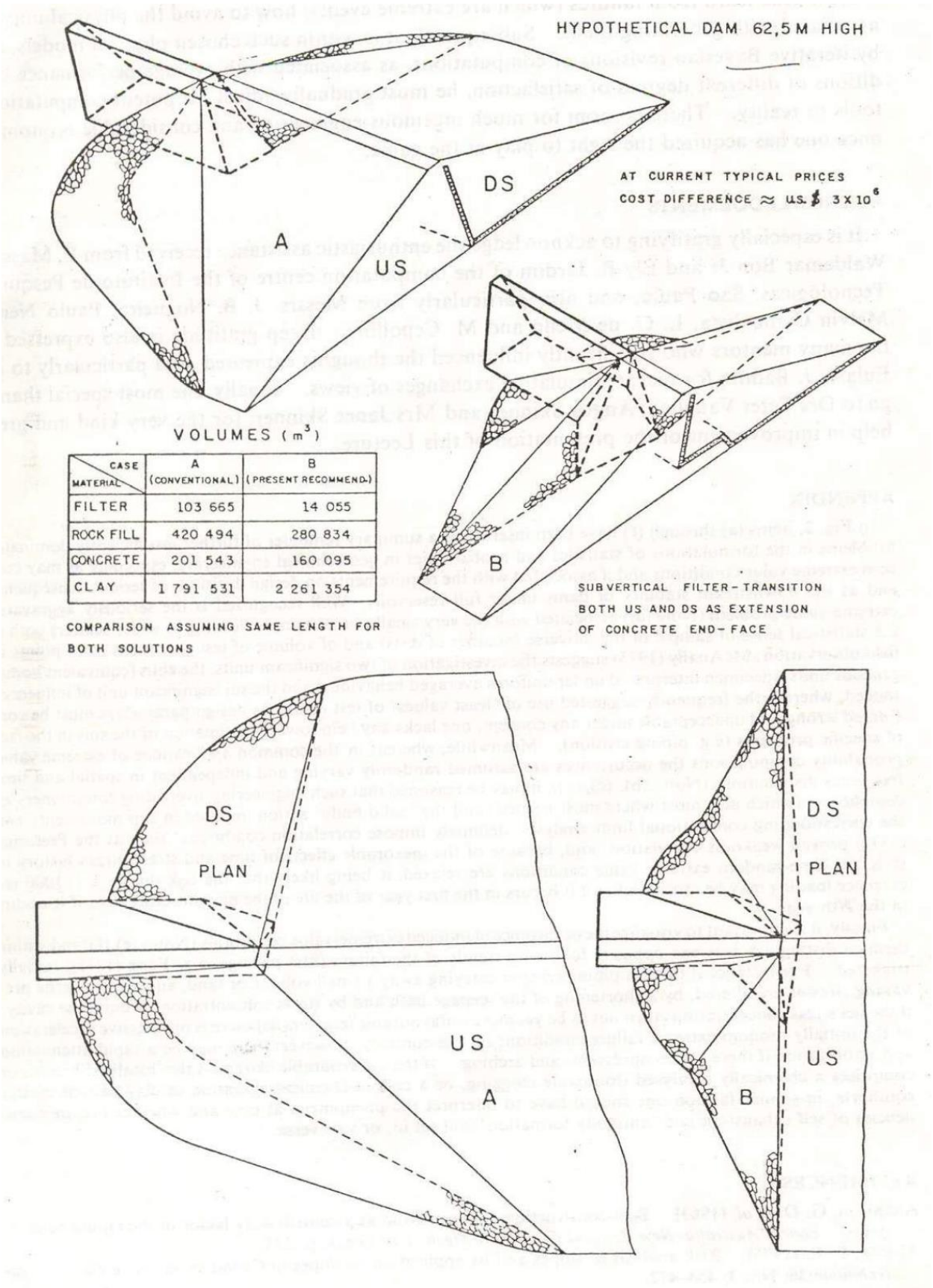

Figure 1.3 - From V. de Mello's Rankine Lecture - optimizations proposed and routinely used in South America for the wrap around interface of concrete structure and earthfill dam

2 BALBINA HYDROELECTRIC POWER PLANT

The Balbina Hydroelectric Scheme is located 170km north of Manaus, in the Uatumã River, left side contributor of the Amazon River. Its embankment dam is a homogeneous earth fill with average height of 30m, having as foundation silty-clayey residual and saprolitic soils generated by the weathering of volcanic rocks, called volcanites to keep the same simplified terminology used during the works. The main features associated to the plant are: installed capacity 250MW, generating since 1989; concrete volume 350,000m^3; volume of the compacted soil 5,000,000m^3; total length of dam 3,300m, 330m of which correspond to the concrete structure; maximum height of the structures 34m and 33m for the earth fill dam.

2.1 Local geology

The volcanic rocks present at the site show all features of a theoretical weathering profile. The main characteristic of the materials is the relatively low thickness of the weathered rock (usually fractured), being about 2m thick. The saprolite and residual soils capping the rock present typical thickness greater than 10m; the saprolite and saprolitic soil predominate in 80% of the strata, the mature residual soil being often eroded, remaining only the saprolitic soil. Another important aspect is the extremely irregular topography of the interface with the volcanic rock top, as well as the absence of boulders or core stones in the soil mass, which is very favorable to investigation and/or soil grouting.

Among the geotechnical-geological features conditioning the design of the embankment dam the existence of regions points with permeability higher than 10^{-3}cm/s needs to be emphasized. These high values of permeability were measured in constant level in situ permeability tests carried out in the clayey and silty saprolitic soil, as well as in in situ tests performed in trenches.

This layer of low density (dry density between 5 and 10 kN/m^3) saprolitic soil showed areas with high occurrence of tubular cavities denominated ‘’canaliculi’’, with typical diameters of a few millimetres to 2 cm, and, in exceptional cases, of 2 to 10 cm.

Figure 2.1 presents the distribution of the measured permeability values in the saprolitic soil; it can be seen that 38% of the values are higher than 10^{-4} cm/s, and 10% are higher than 10^{-3} cm/s, values which are not compatible with the existing experience in saprolitic soils. No sample from the SPT tests recovered every meter exhibited any feature that could justify the high permeability values encountered, such as sand or gravel.

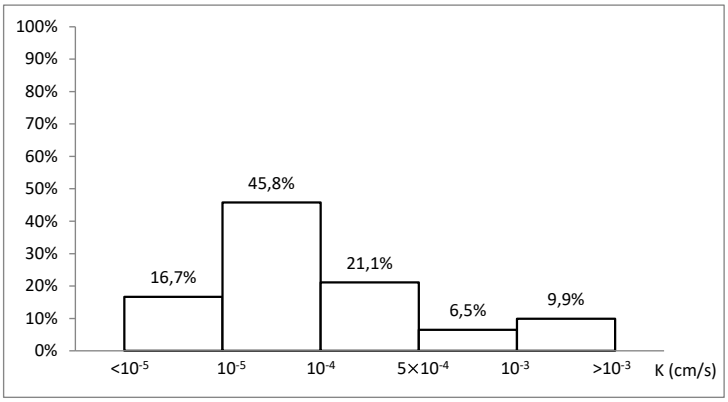

Figure 2.1 - Distribution of Measured permeability values

On this basis, the high permeability values were put under suspicion; in early stages of design, the saprolitic soil was treated as a low permeability soil, consistently with its grain size curve and plasticity characteristics. Basic design conceived foundation treatment with a shallow cut off down to the bottom of the alluvial layer, associated with an upstream impervious blanket and relief wells downstream.

Different phases and sophisticated subsoil investigation associated the high permeabilities to the presence of tubular cavities, canaliculi, in the saprolitic soil profile, with diameters varying from millimetric to centimetric (2 to 3cm), intercommunicating and with an erratic geometric pattern. They were detected in most trenches, with a frequency, which would vary grossly between one or two per square meter for the largest diameters, and one per square decimeter (100 per m^2) for the canaliculi of 2 mm diameter. This frequency varies along the foundation, and some trenches did not detect any canaliculi at all.

The previously described sequence of in situ investigations and observations lead to the following conclusions:

- The saprolitic soil underlying the alluvium and overlying the highly fractured weathered rock consists mainly of a silty matrix. This matrix has a typical permeability of 10^{-5} cm/s, in tune with Brazilian experience.
- Criss-crossing the soil matrix, tubular cavities / canaliculi ranging in diameter from 2 to 30mm are present, conditioning flow of water and giving the soil mass an equivalent permeability which can locally reach values as high as 10^{-2} to 10^{-1} cm/s.

Since it was found impossible to follow the canaliculi into the soil mass, no determination of their length, continuity, interconnections and preferential direction could be made. Visually they seemed to be distributed in all directions with their diameter varying along their course by a factor of approximately two. The interconnection between the canaliculi was demonstrated by the excavation and dewatering adjacent trenches; the addition of a tracer in a trench lead to its sure in the other in only 20 seconds. These investigations lead to the conclusion that the canaliculi needed to be considered continuous at least over a distance of the order of 5m.

Another very important question was associated with the stability of the canaliculi's walls when submitted to a continuous flow of water.

These canaliculi were interpreted as being generated by intense termite activity linked with the last glacial period and the associated lowering of water table linked to the ocean regression (de Mello, L.G. et al, 1987). The action of termites was proposed by the Portuguese biologist Machado A.B (1983), confirming the activity of these insects in all the samples, through traces, essentially composed of faecal and oral pellets, found inside the canaliculi. According to Machado the canaliculi developed probably in the last glacial quaternary era (12.000 to 18.000 years ago), when the region had relatively dry climatic conditions, decisive for the existence of vegetation formations designated as ''credo'' and ''caatinga'', propitious for the proliferation of termites. These insects became rare after the formation of the amazon forest and were not found inside the canaliculi studied. Machado also suggested that the canaliculi of higher diameters should correspond to ramifications of roots, which the termites had eaten, and that those with diameter smaller than 0.8 millimetres would have their origin associated with the disintegration of thin roots, still partially preserved in the regional soils. Photo 2.1, Photo 2.2 and Photo 2.3 illustrate said canaliculi in inspection trenches just excavated.

Photo 2.1 – Canaliculi at Balbina Hydroelectric Power Plant Dam foundations (1)

Photo 2.2 – Canaliculi at Balbina Hydroelectric Power Plant Dam foundations (2)

Photo 2.3 – Canaliculi at Balbina Hydroelectric Power Plant Dam foundations (3)

2.1 Foundation Treatment

Many different alternatives were evaluated prior to the definition of the foundation treatment to be used in the dam (Sathler and Camargo, 1985; Remy, J.P.P. et al, 1985), including conventional cut-offs, use of diaphragm walls to implement a cut-off, use of impervious blankets, etc. Grouting of the saprolitic soils at high pressures, generating hydraulic fracturing using the tube a manchette technique and thus intercepting the net of canaliculi was proved to be the best cost-effective alternative, when proper consideration of logistic and climatic peculiarities of the Amazon Region were included in the analysis.

The essence of the concept behind treating the foundation by grouting, aimed at creating a zone under the embankment's core in which all localized permeability singularities were eliminated, allowing all foundation studies to treat it as homogeneous, in terms of statistics of averages, in tune with the de Mello, V. (1977) Rankine Lecture. The same grout holes were used to extend and grout through the weathered and fractured rock beneath the saprolitic soils. The self-testing characteristics of the treatment methodology by grouting was also valued, leading to the concentration of treatment where specifically required.

Figure 2.2 illustrates a typical cross section for the proposed hydraulic fracturing grouting foundation treatment. The goal of grouting was defined as creating, by grout pressure fracturing, a net of grout planes which would intercept each other and the canaliculi, filling them with grout over part of their length, in order to create a zone 5m to 6m wide with reduced and homogenised permeability. A maximum value of permeability of 10^{-4} cm/s was expected after treatment.

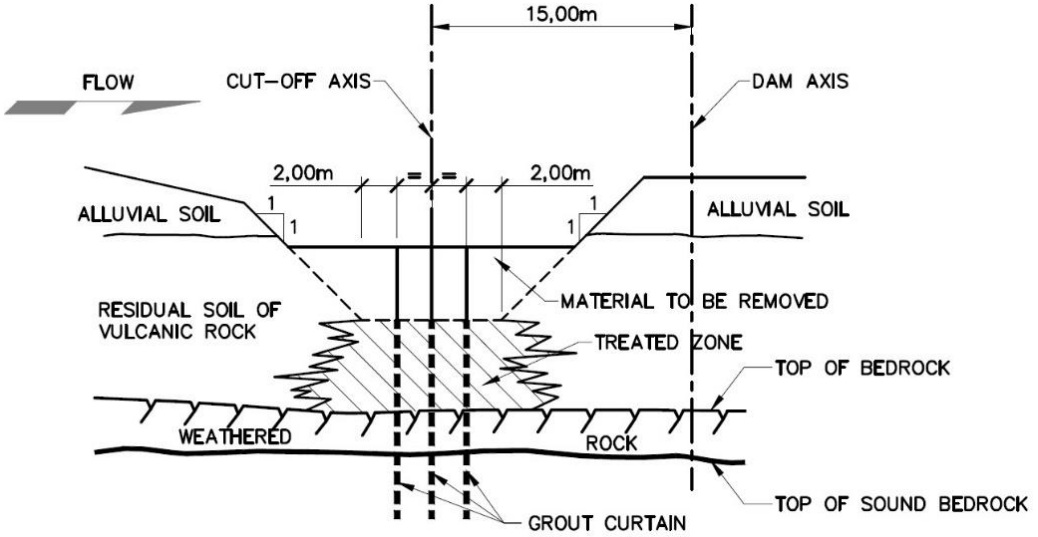

Figure 2.2 – Balbina Dam foundation treatment typical cross section

Using the tube a manchette technique, grouting in phases and localized was performed, applying pressures high enough to generate hydraulic fracturing of the soil, to allow penetration, interception and filling of the canaliculi and voids intercepted by the lenses of grout. The tube a manchette grouting apparatus used in Balbina is shown schematically in Figure 2.3.

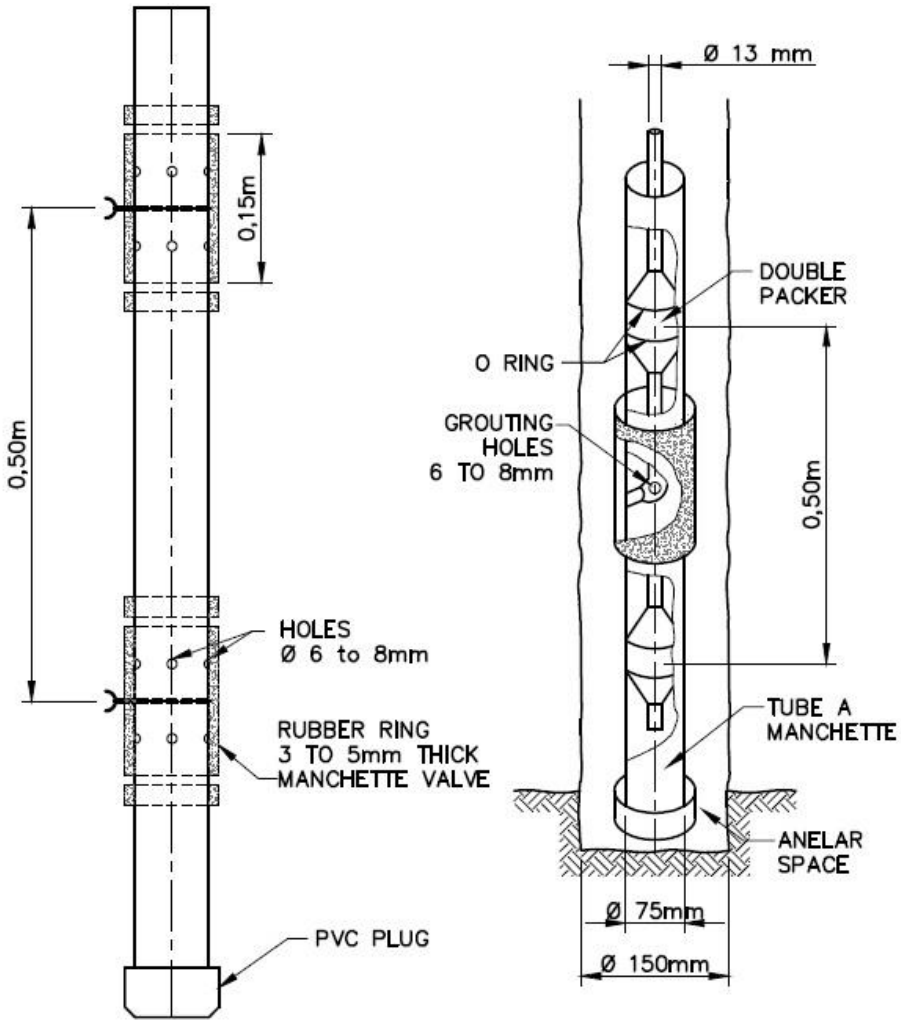

Figure 2.3 – Tube with manchette valve and grouting packers

The advantages of this concept of treatment are:

a) grouting can be intensified in regions were intake was higher;
b) treatment can be done all year round, despite of climatic changes which are drastically conditioning in the Amazon Region;
c) use of conventional equipment;
d) the same boreholes can be used to treat the weathered and sound rock underneath the saprolitic soil.

An in situ inspection trench of a grouted borehole is shown in Photo 2.4.

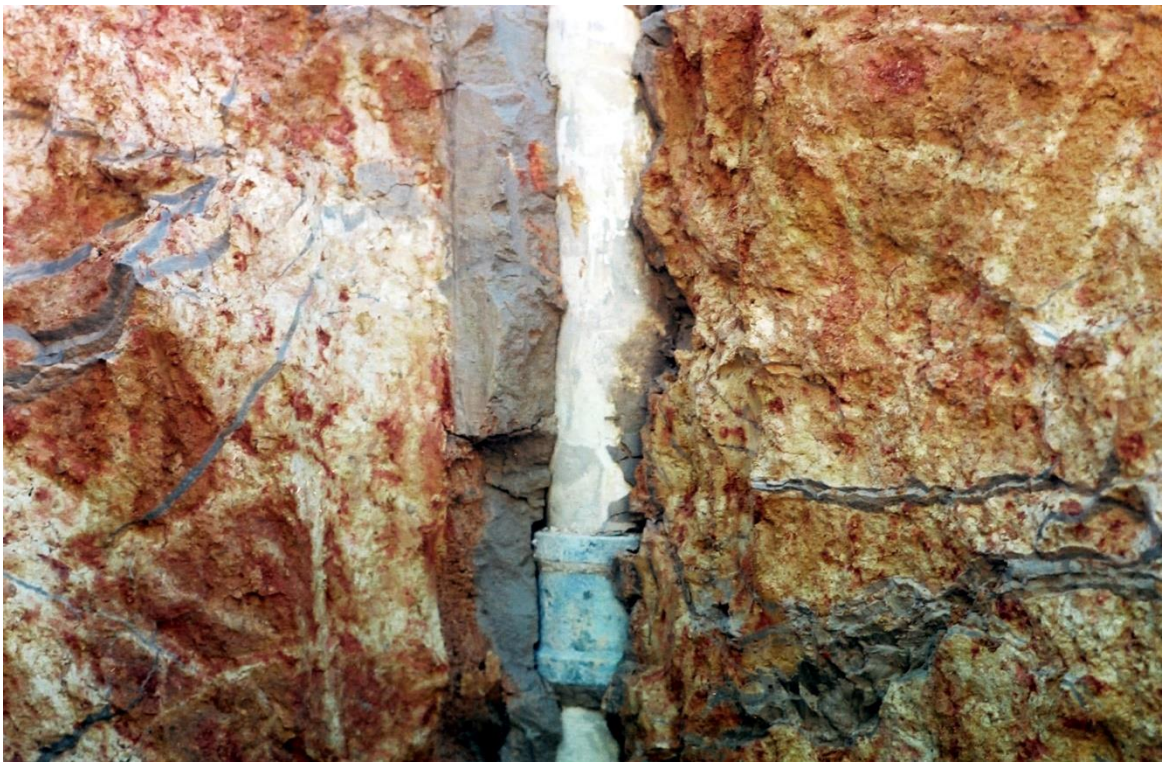

Photo 2.4 – Inspection trench - Tube a manchette in grouted borehole, with grout planes generated by hydraulic fracturing

2.2 Grouting Experimental Stretch

The pioneer characteristics of the proposed foundation treatment in saprolitic soils led to scheduling and performing an experimental grouting stretch about 180m long to allow selection of the criteria and methodology for the abovementioned treatment. This grouting test was carried out in the dam foundation area so as to be a part of the whole treatment of the dam's foundations.

The main aspects considered on the experimental stretch are summarized in Table 2.1, as well as the variables, which were analyzed on each of the four sub-segments grouted as presented by Santos et al (1985).

Table 2.1 – Balbina Dam foundation grouting experimental stretch main aspects and analyzed variables

Characteristics	Parts of the experimental grouting line			
	I	II	III	IV
Length (m)	40	24	50	68
Borehole disposition (m)	2 x 4	2 x 2	2 x 4	2 x 2
Phases of grouting (un.)	3	2	1	1
Volume grout per phase (l)	333	125	1000	300
Total grout vol. per valve (l)	1000	250	1000	300
Order of execution	Soil/rock	Rock/soil	Soil/rock	Soil/rock

2.3 Treatment Methodology

At the beginning of the treatment, special tests and a experimental stretch of work were performed to supply the engineers involved with data, which, in turn, helped optimize the treatment specifications. The special tests included:

- Carefully performed water loss tests in drained and in undrained conditions. Figure 2.4 presents two of the referred tests, from which the pressure causing hydraulic fracturing and the minor principal total stress σ_3, were interpreted. Following Bjerrum and Andersen (1972) discussions, the coefficient of earth pressure at rest K_o was estimated, provided that σ_3 is assumed to be horizontal. This value was estimated to very between $0.21 \leq K_o \leq 0.36$.
- After grouting with different colored cement pigments added to each grouting phase, inspection trenches showed valid the assumption of the orientation of σ_3.

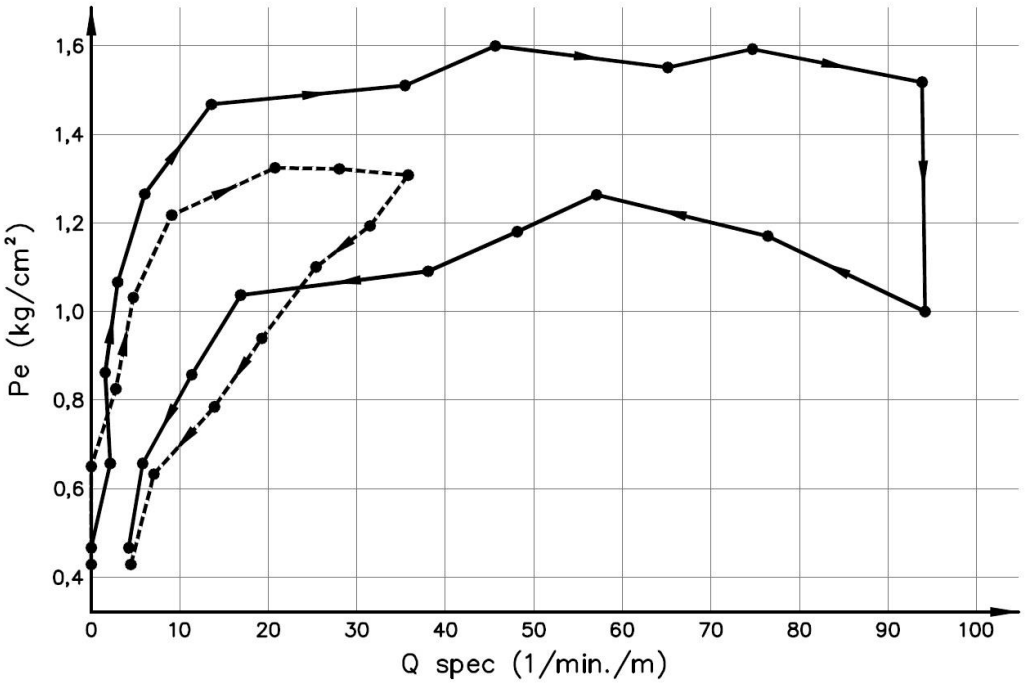

Figure 2.4 – Groutability Test example – Hydraulic fracturing of the saprolitic soil

Once the value of K_o is known with some degree of confidence, many theories exist which enable the pressure of hydraulic fracturing of a massif to be estimated (Bjerrum et al, 1972; Kennard, 1970; Haimsom and Fairhurst, 1967; Morgenstern and Vaughan, 1963). The data collected allowed the following relation to be established between the formulation proposed by Bjerrum and the observed values:

$$\Delta\mu_{obs} = 78.3 + 1.02\ \Delta\mu_{Bjerrum}\ \text{(kPa)}$$

The grouting methodology used in the treatment resulted from the experience of the professional team involved and was optimized many times as a function of the results and data collected. The methodology used during the major part of work can be summarized as:

a) Double packers developed at the site were used for testing and for grouting, which sealed through O-rings against a PVC tube left in each grouting borehole, weakly grouted in its external side to develop close contact with the saprolitic soil (as shown in Photo 2.4).

b) Initially, water loss tests were done in the saprolitic soils with pressure stages of 20; 40; 60 ... kPa until hydraulic fracturing occurred. Through this testing the determination of the coefficient of permeability prior to treatment and relevant indications of the pressures in which treatment was to be performed were gathered. Figure 2.5 presents some of the results obtained.

   Special techniques to assure perfect contact of the expansible packers with the walls of the boreholes were developed in order to avoid preferential vertical seepage due to deformation of the saprolitic soil when submitted to the packer pressure, which would invalidate all the testing.

   Spacing between valves was defined as 0.5m.

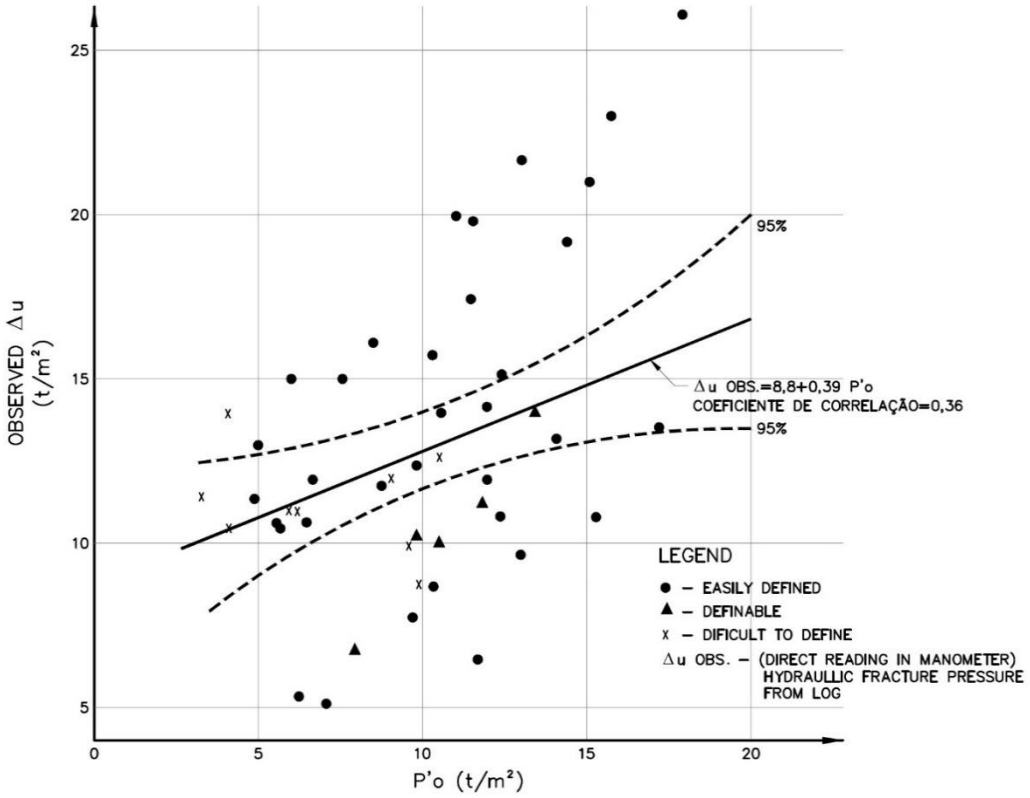

Figure 2.5 – Relationship between the increase of pressure to generate hydraulic fracturing and effective stresses in water loss tests

c) Three lines of grouting holes were planned – central/upstream/downstream - with grouting starting from the external lines in order to confine and improve treatment through the central holes.

d) The soil-cement grouts postulated to treat the soil were different to those used to fix and seal the PVC grouting tube. Both used as much as possible the local clayey saprolitic soils in order to reduce costs of treatment, due to the difficulties in hauling bentonite to the site.

The physical characteristics of the grout necessary to fix and seal the PVC tube needed to be carefully evaluated so that it would not condition the pressure values required for its rupture when grouting of the foundation soil. Several grouts were prepared in PVC pipe molds, with variable thickness and grout resistance. Tests simulated rupture processes of the annular seal grout, as a function of its thickness, grout strength and confining pressure. The results of these tests showed that the increments of the seal grout rupture pressure as a function of the three variables tested were higher with the confinement pressure and with the seal thickness, for rupture pressure values within the same order of magnitude, as shown in Figure 2.6.

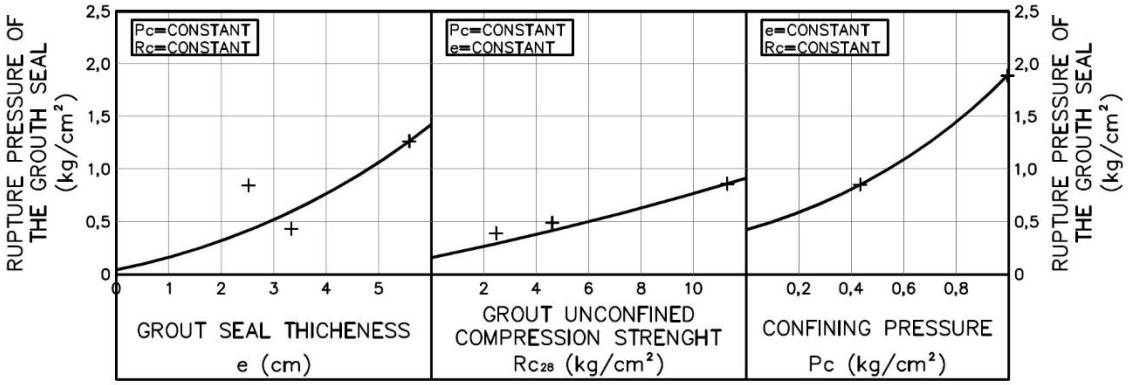

Figure 2.6 – Results of tests with grout seal models

Based on these results, a grout mixture for the annular seal was defined as: cement: 285kg / soil: 290kg / water: 805l

The specification of the soil-cement foundation grout asked for:

- Uniaxial compressive strength at 28 days of 1.5kg/cm^2;
- Viscosity ≤ 50cP;
- Sedimentation factor ≤ 5%;
- Fluidity in Marsh cone of 40s to 45s;
- Yield limits ≤ 0.1g/cm^2, which was achieved with the following mixture: cement: 73kg / soil: 310kg / water: 860kg.

It is worth noting that the initial amount of cement considered was of 375kg in the proportion above and was reduced substantially during the tests.

e) Grouting of the saprolitic soils was undertaken bottom-up, from the lowest manchette valve towards the top under a 3m high compacted earth fill, at pressures compatible with the hydraulic fracturing pressures as a function of depth previously determined. Tests were also performed to investigate if the ideal grouting sequence was to initially grout the saprolitic soils, and then to grout the underlying weathered rock horizon, or to inverse this sequence. Water loss tests were made in the contact zone between saprolitic soil and weathered rock horizons showing that foundation treatment was more efficient when the weathered rock was grouted first.

The possible explanation for the lower effectiveness of grouting close to the horizons' interface in a top-down sequence was interpreted as probably associated to soil-cement grout migration to the untreated weathered rock fractures. As grouting of the

higher depths of saprolitic soils was implemented with constant grout volumes, such migration would reduce grout quantity at the bottom of the saprolitic soil, consequently reducing the effectiveness of treatment in this interface.

f) Grout flow was usually 60l/min, and this value was sporadically reduced to control and reduce occasional grout surge at the surface.

g) Grouting, in stages, until the postulated volume per manchette is completed, was conceived to create hydraulic fracturing planes in several directions, associated to each grouting stage.

   Initially, a 1,000l grout volume per manchette was postulated in analogy with permeation grouting in sands, estimated as a function of the soil porosity. Tests showed this volume to be excessive, due to the long reach of the hydraulic fracturing planes as inspected in trenches, often at points over 10m away from the grout hole.

   Treatment was defined to stop when 300l of grout was absorbed by the soil or after 10min of no intake of grout.

   Inspection trenches were opened and visual inspection showed that grouting planes of different stages generally formed parallel planes, often overlapping. These observations lead to defining grouting in a single stage per manchette.

h) Water loss tests were performed in specially located additional boreholes to document the benefit of the treatment, limiting the maximum pressure of the test at 1.0kg/cm^2 not to hydraulically fracture the soil.

Grout pressures suffer loss of applied head pressure during grouting, at the manchette borehole seal and at the hydraulic fracturing planes. This head loss depends on the physical characteristics of the rupture planes in the borehole seal as well as in the hydraulic fracture planes, not allowing an effective control of the grouting process.

During the works the control of the grout flow, by recording the manometric pressure resulting from the process, was pursued. It was postulated that the resulting manometric pressure, as read at gauges immediately at the surface, did not exceed in more than 50% the pressure recorded immediately after hole seal rupture.

Such control parameter derived from the relation between initial and final manometric pressure recorded during the execution of the experimental stretch. It was also observed that the occurrence of cracks at the surface followed by surge of grout, generally happened when this relation was greater than 1.5

2.4 Evaluation of the Subsoil Treatment

The evaluation of the improvement of the saprolitic soil of the foundation of Balbina Dam with respect to its permeability was done through water loss tests carefully performed after the treatment, having as target the value of permeability of 10^{-4}cm/s.

In Figure 2.7 some test results are presented in relation to the information collected before grouting. The benefit of the treatment is obvious. In the mentioned figure, the

interpretation of the water loss tests following Babouchkine's (1965) formulation is presented. The control tests indicated that after grouting there was considerable reduction in permeability coefficients, especially with the elimination of coefficients above 5.10^{-3}cm/s.

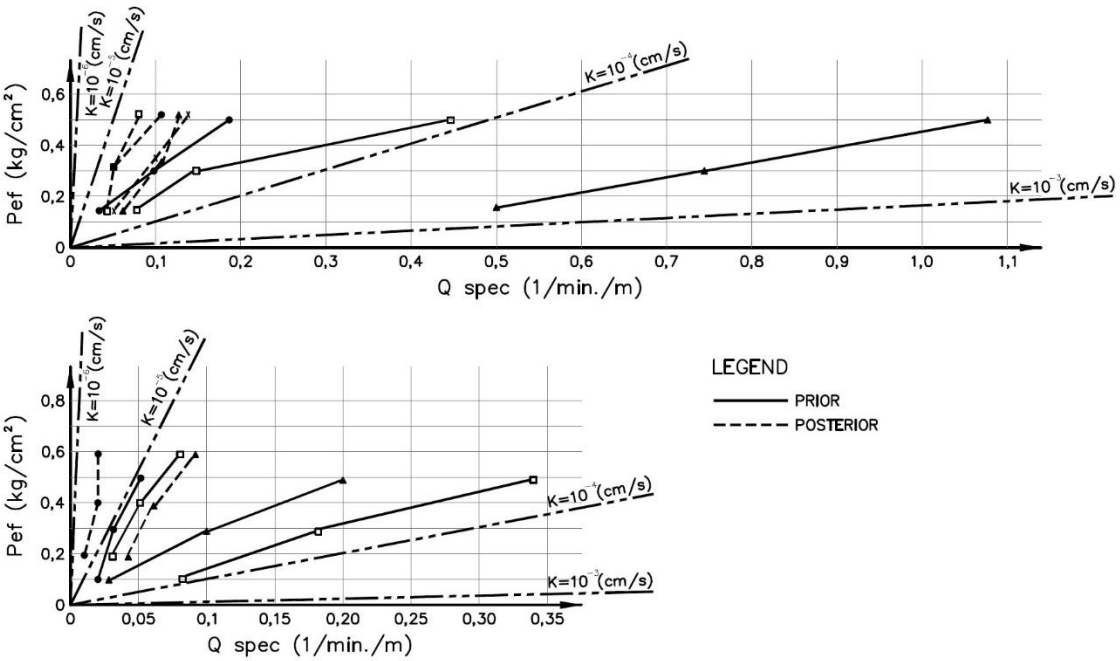

Figure 2.7 – Comparison of water loss tests prior and posterior to treatment

An analysis of this data demonstrated the success of the treatment applied considering the elimination of high permeability zones and the consequent foundation homogenization with respect to its permeability.

Photos 2.5 to 2.8 were taken at the inspection trenches, depicting the successful treatment of the canaliculi.

Photo 2.5 – Inspection trench – clacage planes intersecting and treating canaliculi (1)

Photo 2.6 - Inspection trench – clacage planes intersecting and treating canaliculi (2)

Photo 2.7 - Inspection trench – clacage planes intersecting and treating canaliculi (3)

Photo 2.8 - Inspection trench – treated canaliculi (4)

2.5 Filling of the Reservoir

Two different embankment cross sections were used during construction in order to separate the activities of foundation treatment from the earthmoving and compacting of embankment raising, which had to be done in a very defined time of the year due to the heavy rains that affect the Amazon Region. For this reason, in a region the grout buffer was positioned in the upstream of the dam and linked to the impervious core of the dam by a compacted berm, while in other region the grout buffer was positioned just underneath the core of the dam, where the applied stresses are higher.

Monitored filling of the reservoir started in mid-1987; the first rainy season was not able to fill the reservoir, and data during partial filling is available. It documents the benefit of the treatment.

Figures 2.8 to 2.11 present cross sections of the dam in the described situations with plots of the water level in the reservoir and measured pore pressures in hydraulic piezometers.

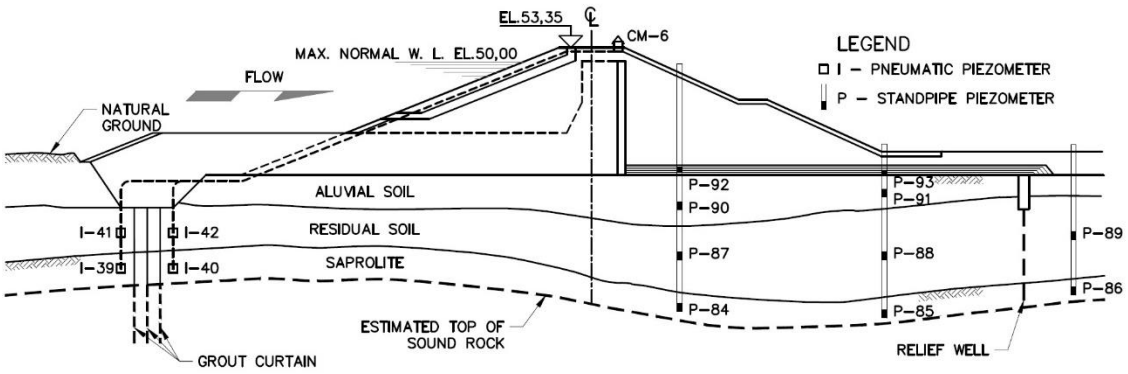

Figure 2.8 – Typical instrumentation on the right abutment

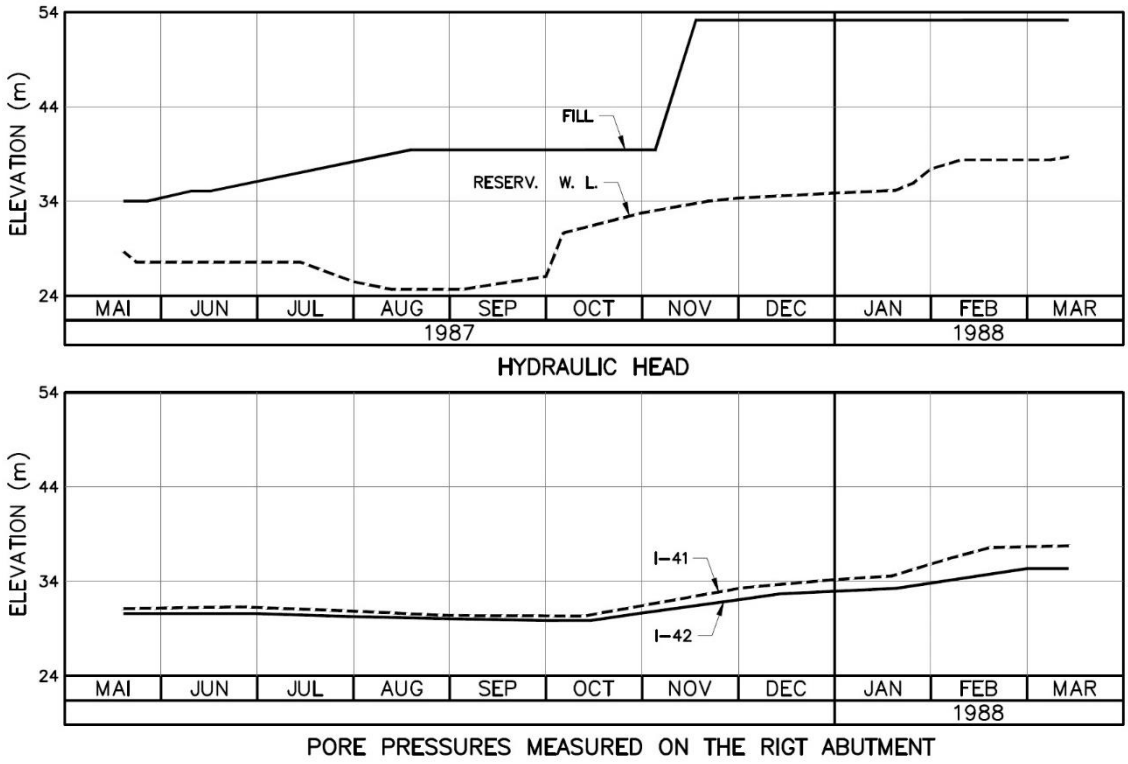

Figure 2.9 – Hydraulic head and pore pressure monitoring data for the right abutment

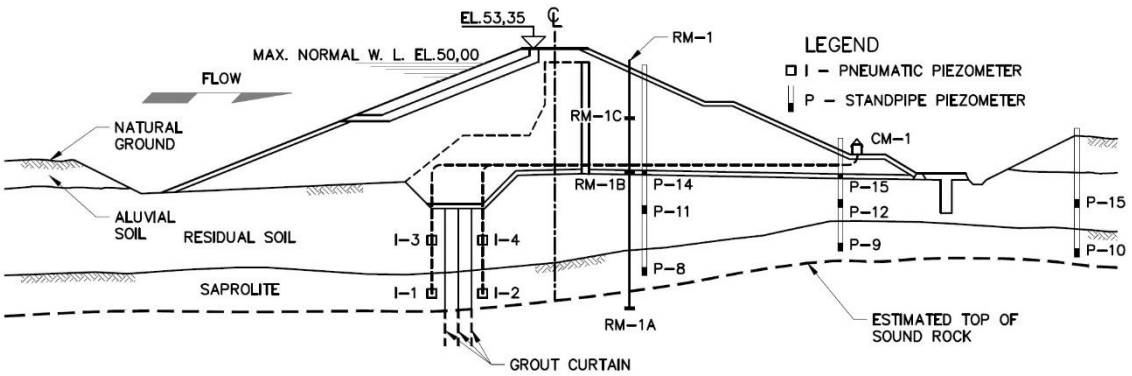

Figure 2.10 – Typical instrumentation on the left abutment

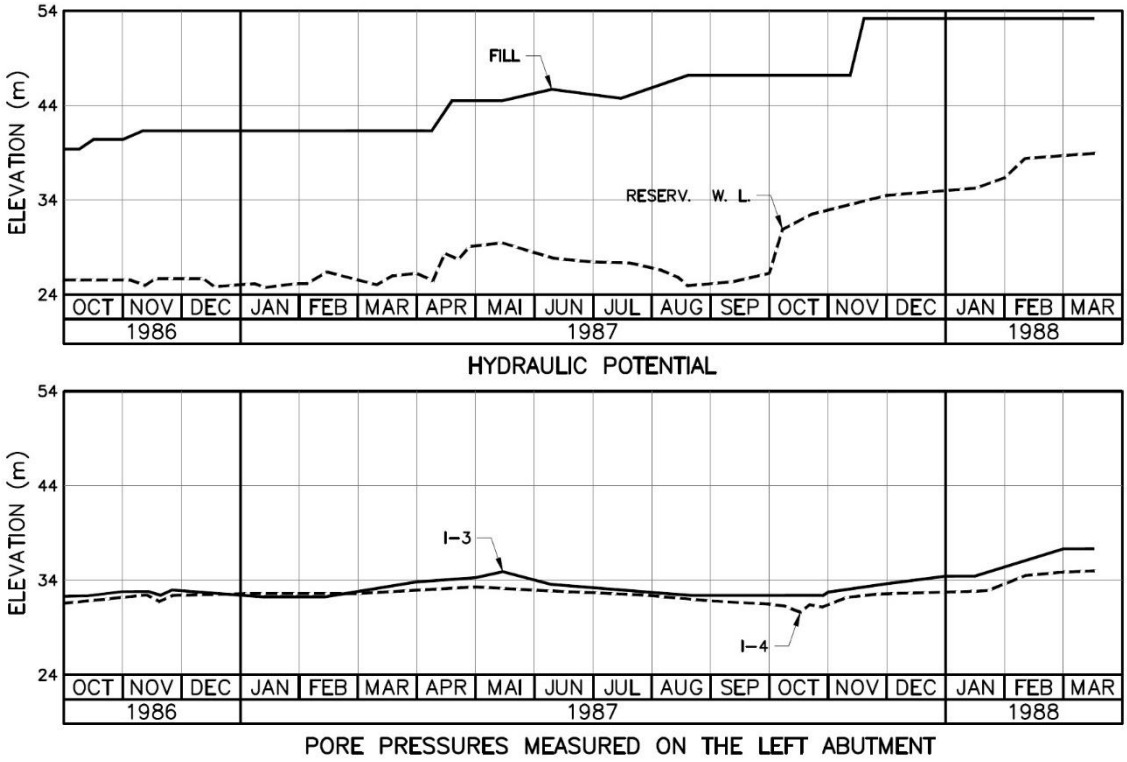

Figure 2.11 – Hydraulic head and pore pressure monitoring data for the right abutment

The data collected as well as situ inspections demonstrated the validity of the use of the discussed treatment to homogenize and diminish the permeability of a saprolitic soil with a net of open canaliculi. Prof. Victor F. B. de Mello and Eng. Joaquim Franco were of crucial importance in conceiving and implementing this solution for Balbina HPP.

3 TELES PIRES HYDROELETRIC POWER PLANT

The Teles Pires HPP is located in the Teles Pires River, contributor of the Tapajos River in the Amazon Basin at the border of Mato Grosso and Pará States. The main features associated to this power plant are: installed capacity 1,820MW, generating since 2015; its structure includes a section in roller compacted concrete (RCC) and an embankment dam of rock fill with impervious earth fill core with maximum height of 80m, and total crest length of 1,650m, 330m of which corresponds to the concrete structure; volume of the compacted soil 5,000,000m^3, maximum height of the structures 34m and 33m for the earth fill dam.

3.1 Local Geology

The site is located in the north portion of the Teles Pires granitic batholite, not far away from its contact with the Colider volcanites. The most recent rocks found in this igneous body are basic dikes sheared by posterior events.

Two large sinistral wrench faults striking N40W generated an important tectonic binary responsible for a system of subvertical joints that affected the Teles Pires granite (Figure 3.1). Other important vertical EW faults present a component of sinistral slip and cut the region together with extensive NE linears of an assumed gravitational distensive character.

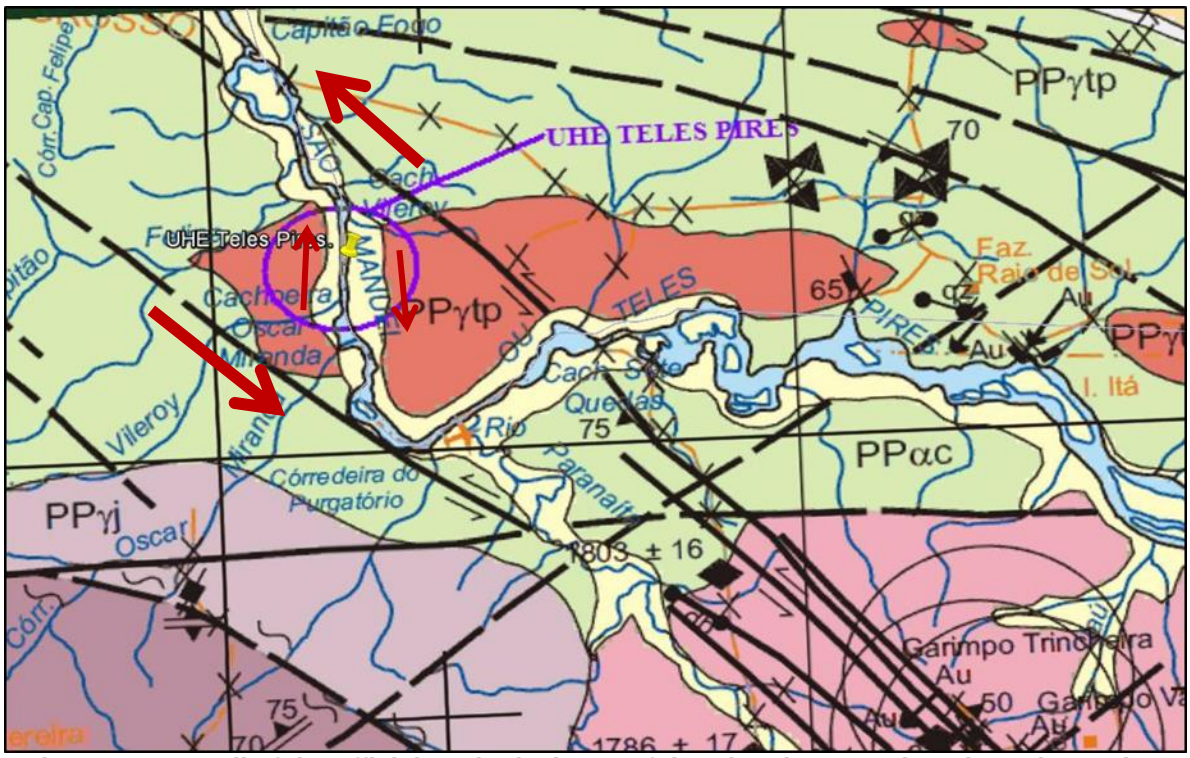

Figure 3.1 - Detail of the official geological map of the Alta Floresta mineral province. The Teles Pires granite (PPγtp) intruded the Colider Group (in green). Both are cut by large strike slip component subvertical faults (thick black lines). Relative binary dynamics is expressed through the red arrows as also the slip component of the NS fault along the Teles Pires River.

As the mentioned faults are superimposed to the Teles Pires intrusion, the initial geologic model of the project was based on the presence on brittle tectonic features. These features are represented by subvertical and inclined shear fractures with slickensides,

which could be identified in drill cores and excavation cuts. Such features are common in the transcurrent regime (Figure 3.2).

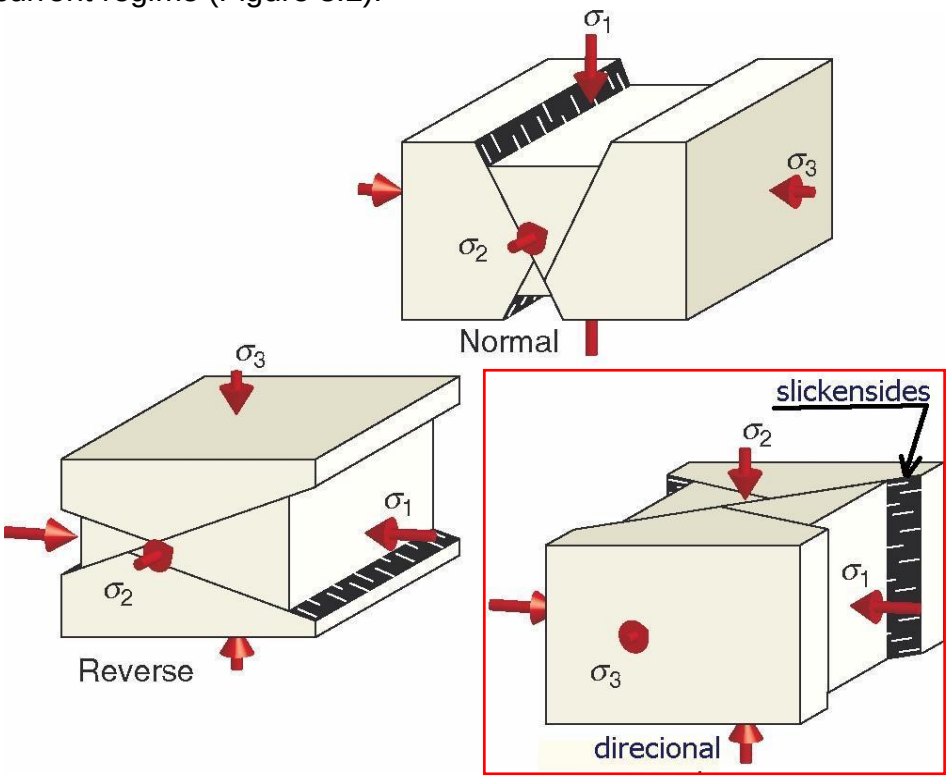

Figure 3.2 - Illustration of the dominant transcurrent and reverse type of faulting (adapted from Fossen, 2010)

In Riedel's model for conjugated fault systems (Figure 3.3) the NW and sub EW subvertical and inclined striking fractures are of a typically dominant left lateral strike slip dynamics, while the NE fractures should be essentially of distensive character. In conclusion, the tectonic environment should be essentially transcurrent compressive represented by subvertical and inclined discontinuities.

Additionally, the whole region was subjected to an intense hydrothermal activity along the different faults and shear zones. Therefore, the presence of caolinized zones, fillings of white and green clay minerals and even, locally, sulphides, are expected to mingle together with evidences of brittle tectonism such as gouges and slickensides.

During the initial design studies for this power plant, the geologic model assumed also incorporated presence of relatively shallow sub-horizontal stress relief joints that would gradually vanish with depth. This pattern of relief joints attenuating with depth is a trivial established in geological literature and also clearly exposed along several Brazilian dam foundations (Santa Clara, Santo Antônio and Jirau dams, for example) as also internationally in some important engineering geological texts, such as the classical paper of Terzaghi and several other authors (Dale, 1923; Carlsson and Olsson, 1977; Holzhusen, 1989; Fookes et al., 2000; Hencher et al., 2011).

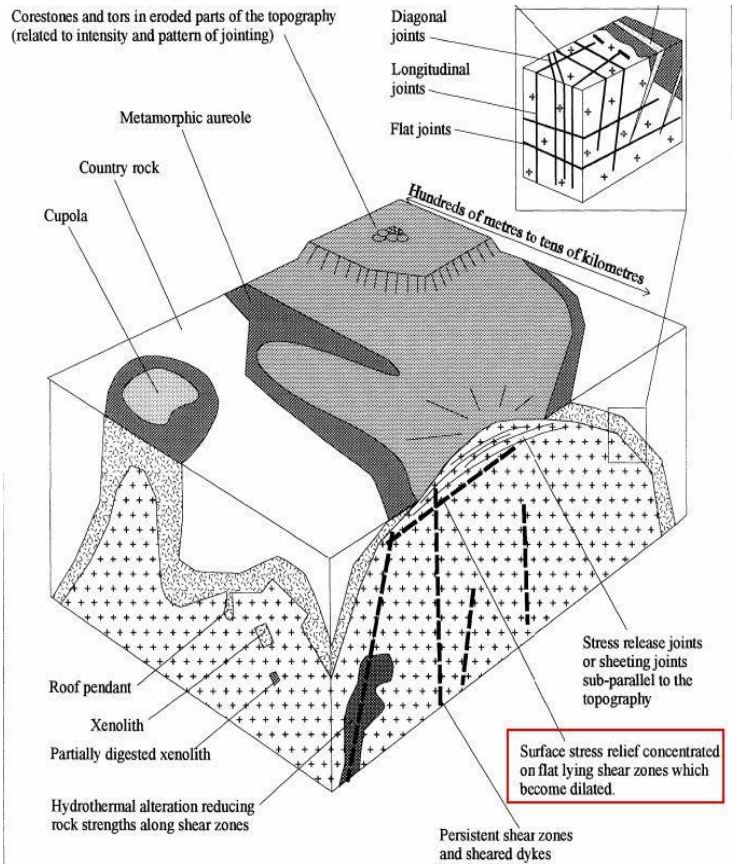

Figure 3.3 - Stress relief sub-horizontal discontinuities and sub-horizontal shear zones dilated due to the vertical stress relief in granites

3.2 Update of the Geologic Model and of Design

For detailed design, local difficulties prevented that detailed investigations were performed before beginning of the excavations in some regions, principally at the dam's right abutment, where the intake and the powerhouse structures are located. As soon as access was permitted, 38 additional rotatory borings were initially done, 4 with optical imaging, which allowed the visualization of the spatial position of the weathered zones. This allowed the separation of the horizontal from the inclined or vertical discontinuities, which is difficult and very debatable when the correct control of the discontinuities' strike is not known due to the mechanical fragmentation of the rock cores during drilling and core recovery. A high frequency of weathered sub-horizontal discontinuities was observed but the difficulty of correlating its continuity inhibited its extrapolation in the design cross sections used for design decisions and calculations, as shown in Figure 3.4.

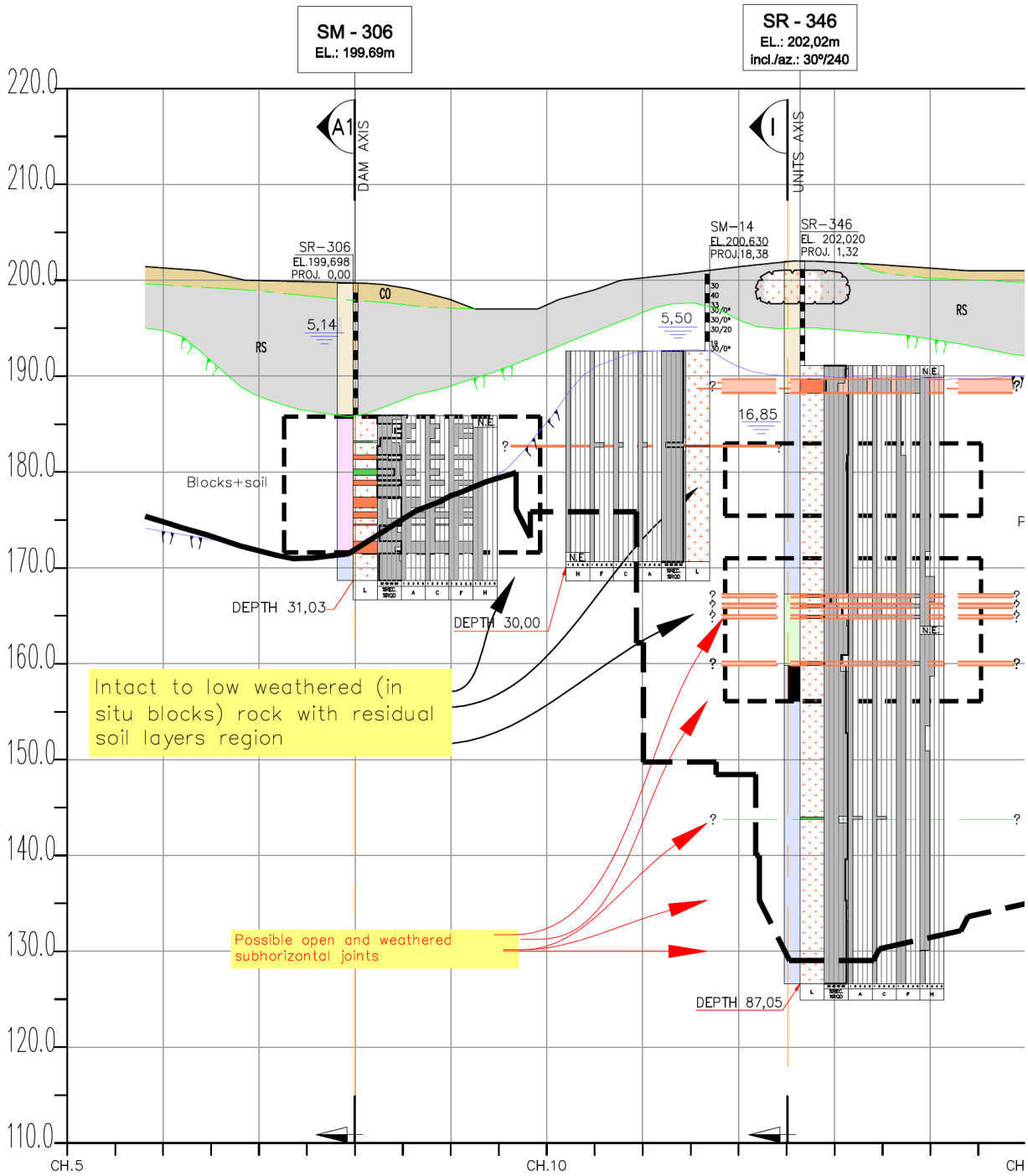

Figure 3.4 – Teles Pires Intake structure foundation geological cross section after initial additional investigations for detailed design

The gradual increase in data acquisition clearly showed that the necessary revision of the geological model previously conceived had a major impact in the project's structures' stability. The incidence of weathered sub-horizontal discontinuities (Figure 3.5) combined with the joints pattern had direct practical implications in the excavations' design, leading to the need to lower the foundation of the water intake structure.

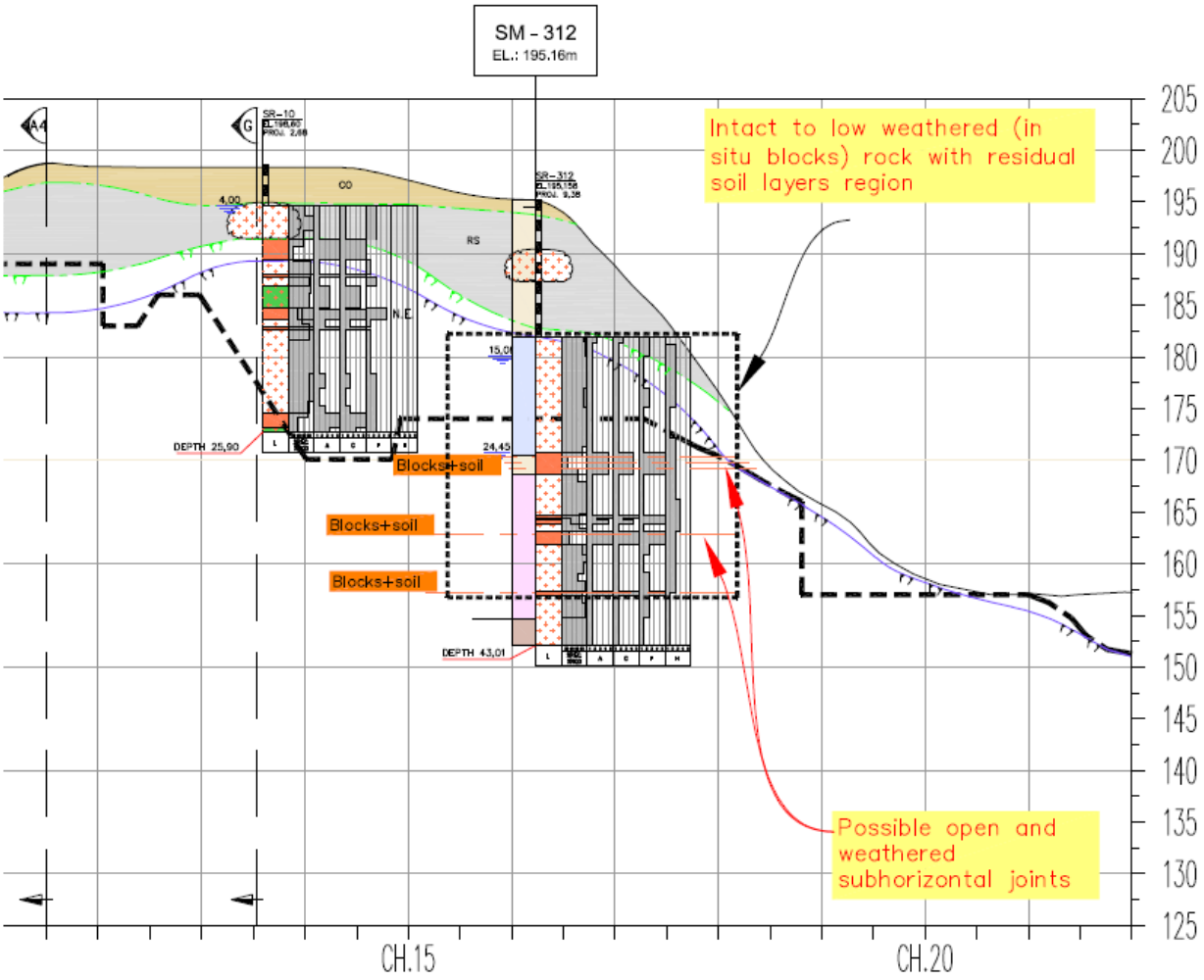

Figure 3.5 - Teles Pires Intake structure foundation geological cross section after further investigations, showing denser pattern of weathered subhorizontal joints

A comprehensive investigation program based on a dense array of rotopercussive borings, described by qualified geologists, was performed to better and quickly map the substrata underneath this structure, leading to the proposition of a much more complex discontinuities pattern than initially predicted (Figures 3.6 and 3.7). It clearly indicated the presence of thick discontinuities with soil filling concentrated between elevations 155m and 170m.

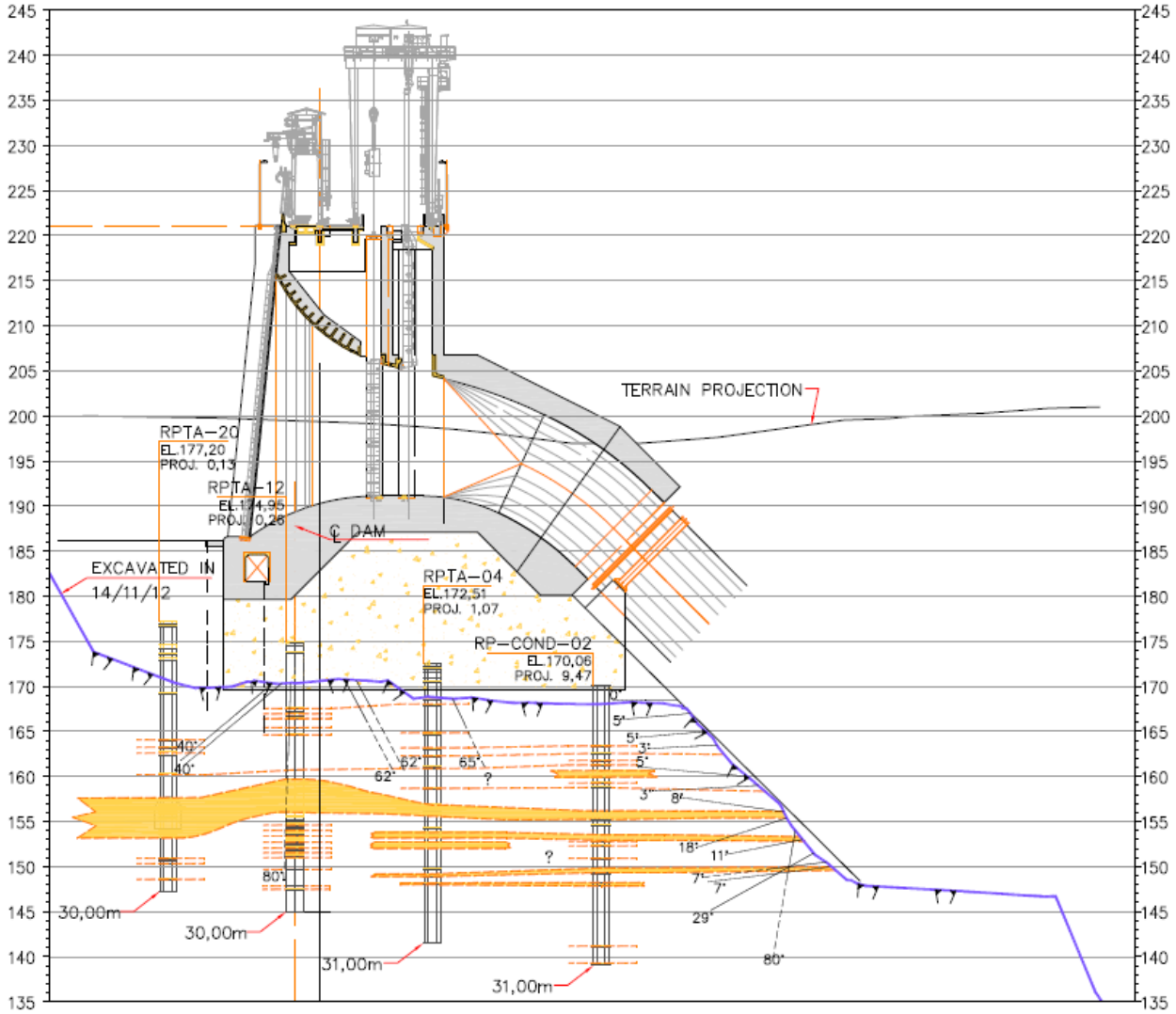

Figure 3.6 – Updated discontinuity pattern at water intake structure foundation – Cross section after rotopercussive dense array investigations

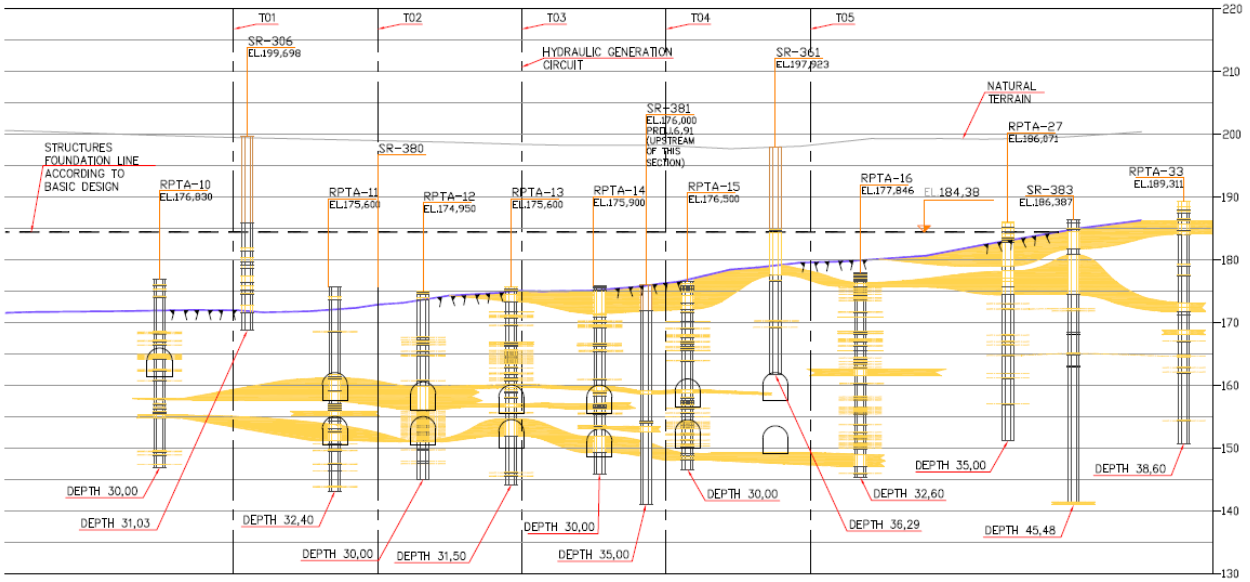

Figure 3.7 – Updated discontinuity pattern at water intake structure foundation – Longitudinal section

Later, during excavations, geological mapping confirmed that numerous of the sub-horizontal discontinuities presented decametric extension with weathered soils filling frequently laminated and pre-sheared, with presence of estriae and slickensides. This characterized a sub-horizontal shear zone with indication of displacements accompanied by its subparallel secondary joints.

This shear zone, identified as master joint, has its trace clearly visible on all walls of the excavation (Photo 3.1), dipping downstream with local components towards the river as shown in Figure 3.8.

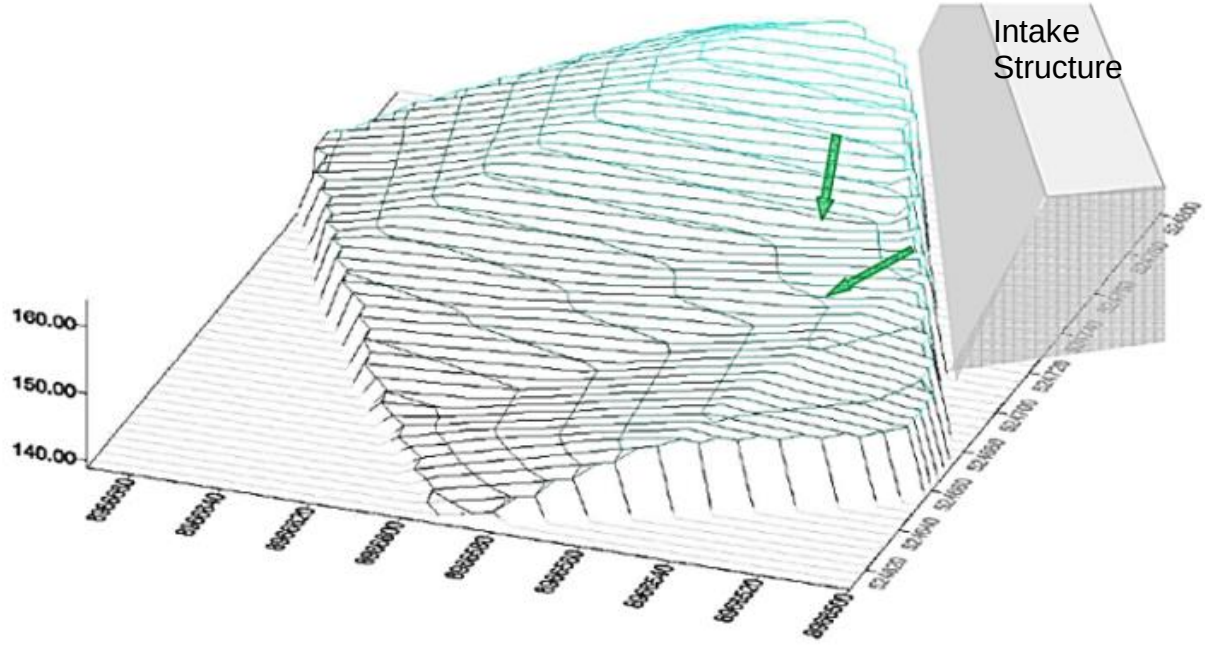

Figure 3.8 – Master joint 3 D surface model

Photo 3.1 – Master joint trace emphasized in yellow, as visible at the excavation walls

Features of the tectonic of displacements between the rock strata were gradually determined allowing to characterize a particular situation, distinct from the usual stress relief joints common in granites. A package of various sub-horizontal shear zones with

different indications of thrust in the NS direction was identified, in a non-previously described pattern for the region.

Photos 3.2 (a) to (e) and 3.3 (a) to (e) illustrate the typical characteristics and the variability of these characteristics in the master joint and its secondary structures.

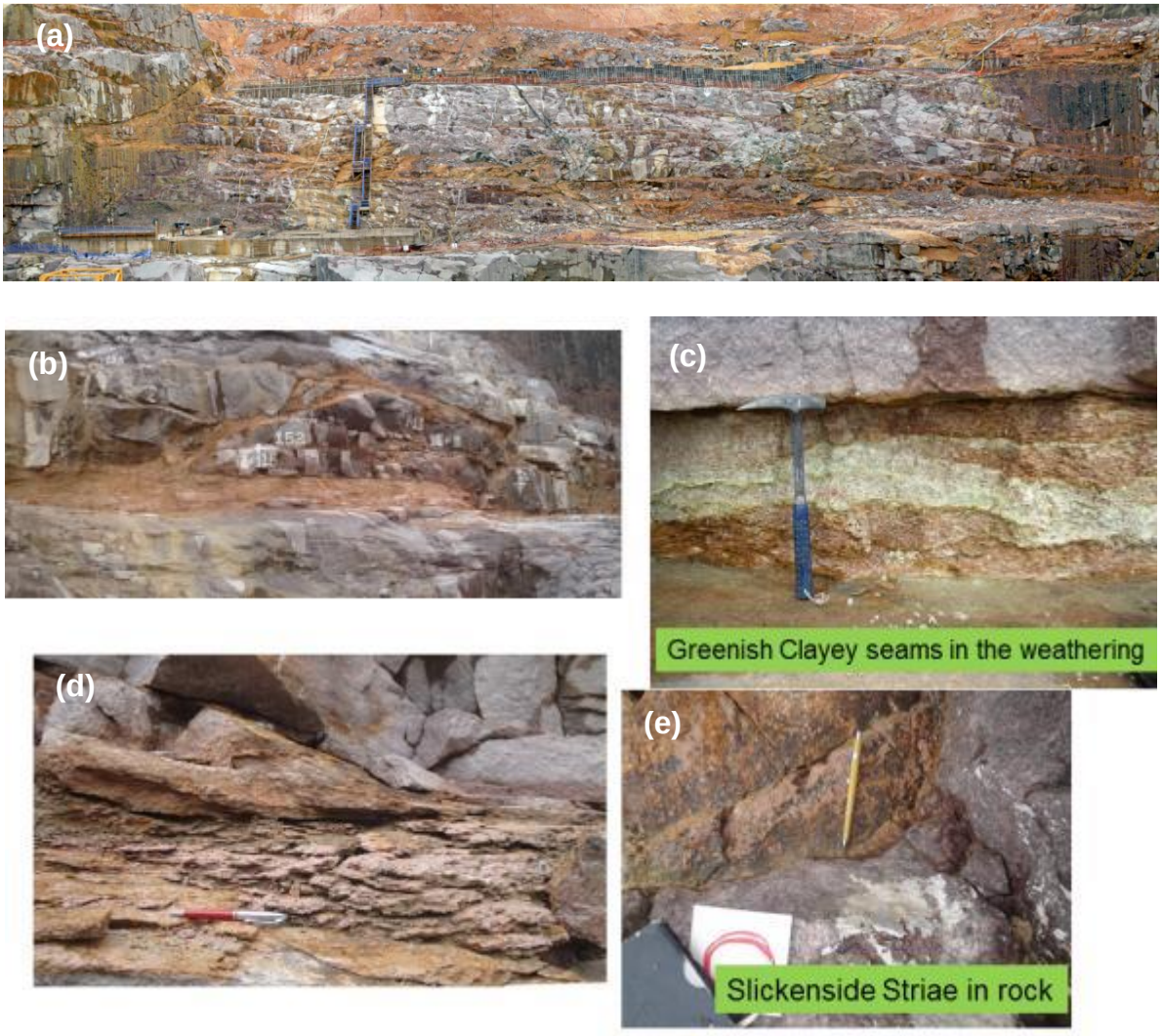

Photo 3.2 – Typical shear features in the master joint (1): (a) General view of excavation wall; (b) Isolated shear lens; (c) Clayey zone in a lens; (d) Lenticular lamination; (e) rock-rock displacement estriae.

The indications of thrust tectonism along extensive sub-horizontal discontinuities confirm the presence of pre-shearing, including in the rock / rock surfaces as observed in different locations of the excavated face, as well as, later, in the stabilizing structures excavated in the area (Photo 3.3 (a) to (e)).

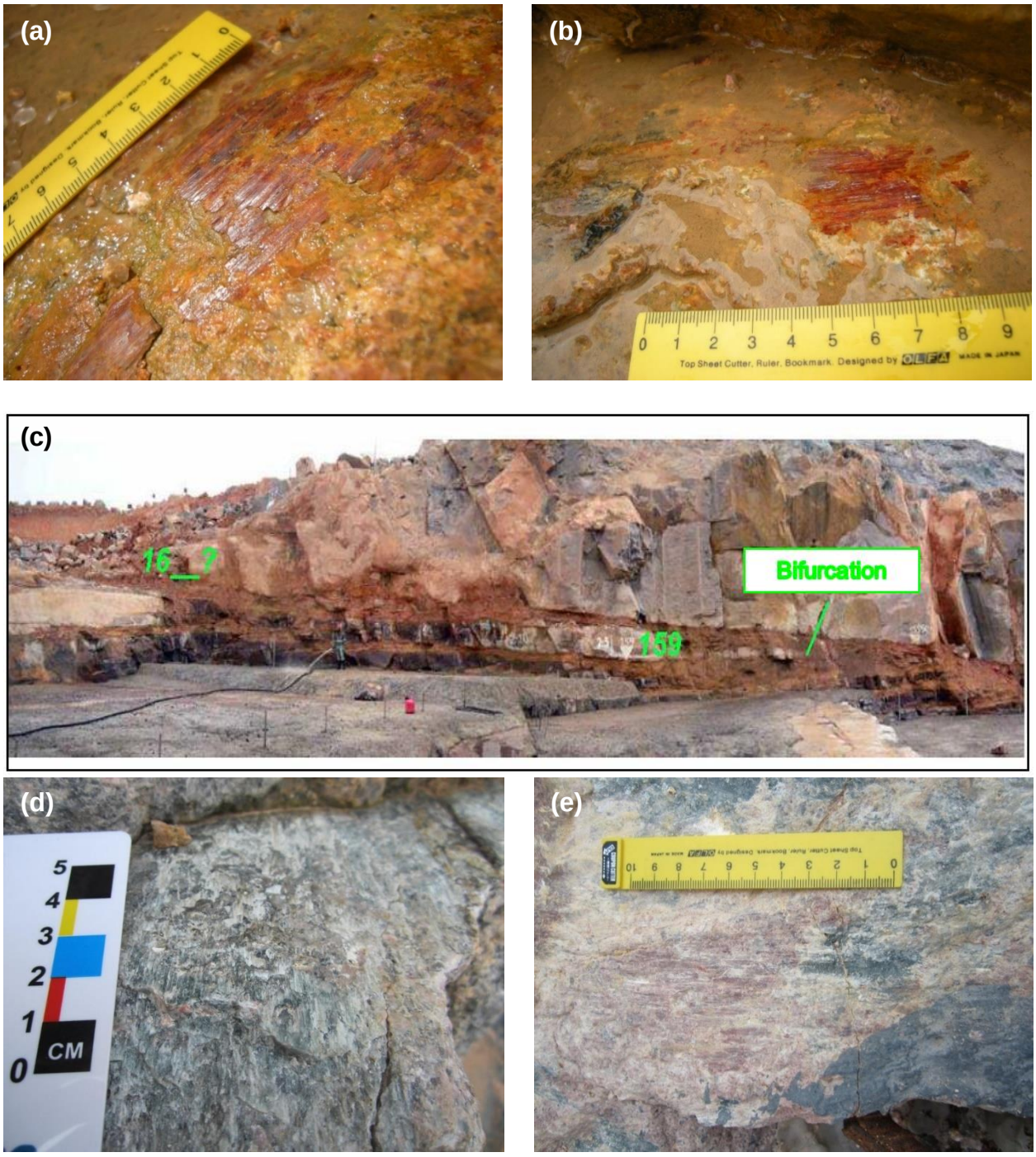

Photo 3.3 – Typical shear features in the master joint (2): (a) (b) Slickensides; (c) Bifurcation at master joint; (d) and (e) Estriae in non-weathered rock / rock interface

Based on this revised geological model the stability of the intake structure with relation to its sliding became intrinsically conditioned by the master joint, requiring special attention. Photo 3.4 presents the discontinuity pattern mapped at the water intake structure foundation's as seen in the penstocks excavation face, and Figure 3.9 displays a cross section for the water intake structure, presenting the identified discontinuity pattern as used in the geomechanical model proposed.

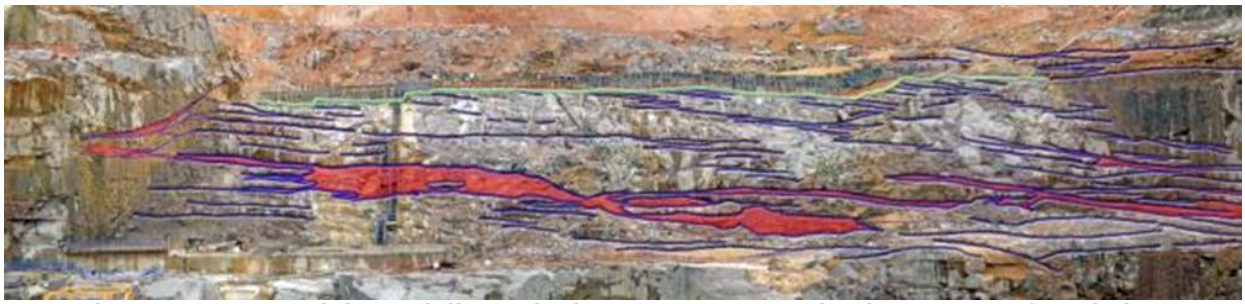

Photo 3.4 – Master joint and discontinuity pattern at water intake structure foundations

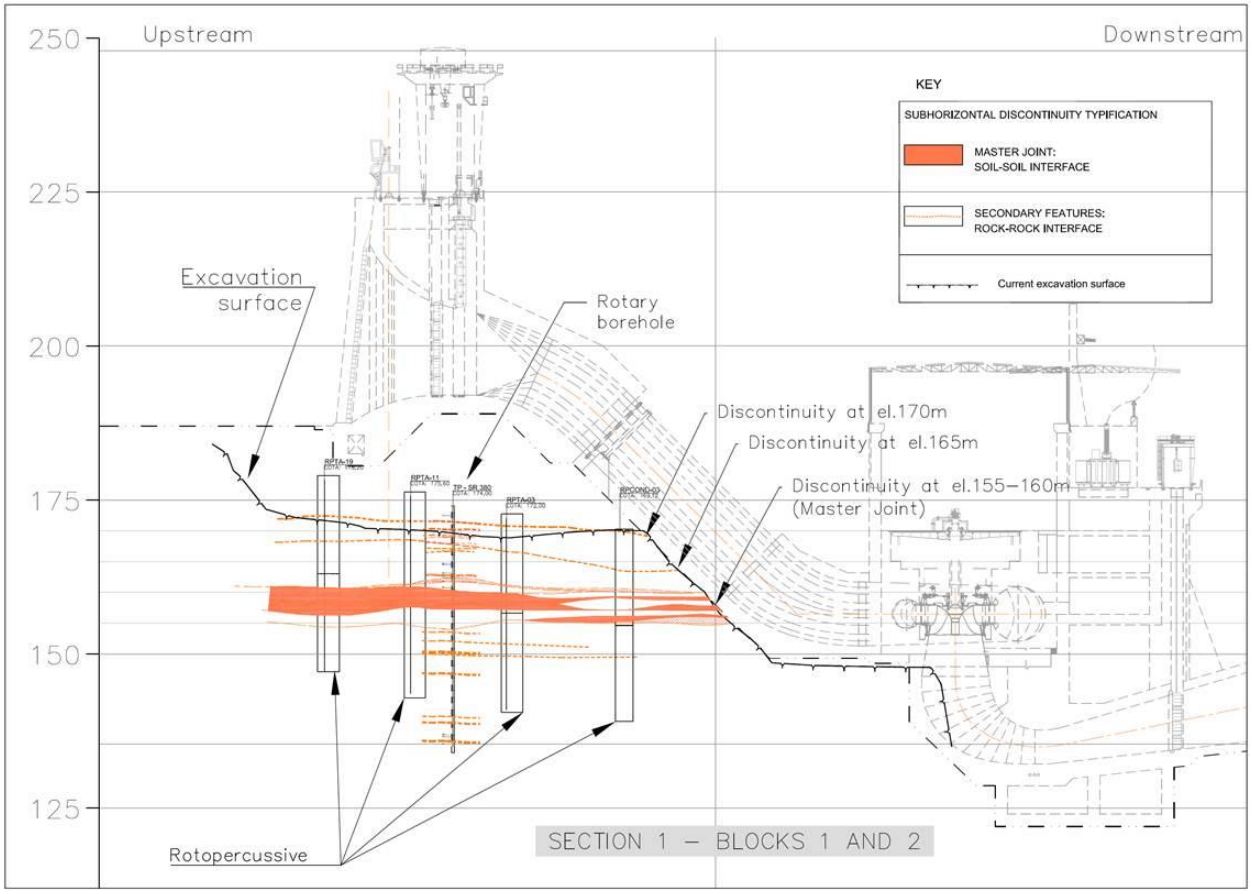

Figure 3.9 - Water intake structure cross section with discontinuity pattern in tune with proposed updated geological model

3.3 Laboratory tests

In order to characterize the geomechanical properties of the more intensively weathered material present in the master joint a series of laboratory tests were performed in samples prepared from undisturbed blocks. Full characterization of the material and shear strength determination were pursued, through direct shear and triaxial tests. In order to try to bypass the problem of sample heterogeneity, step incremental stress tests on the same samples were performed, with partial success.

The interpretation of the test results was done trying to postulate the shear strength available at strains of 0.5% in the triaxial tests and displacements of 0.5mm in the shear box, of 1.0%/1.0mm, and 2.0%/2.0mm, as well as at peak values.

Figures 3.10 to 3.13 plot the laboratory shear strength test results and proposed envelope. The results are presented plotting the normal and shear stresses acting at the oriented plane; a Mohr-Coulomb failure envelope with null cohesion tangent to the Mohr's Circle is proposed for each hypothesis of strain at failure.

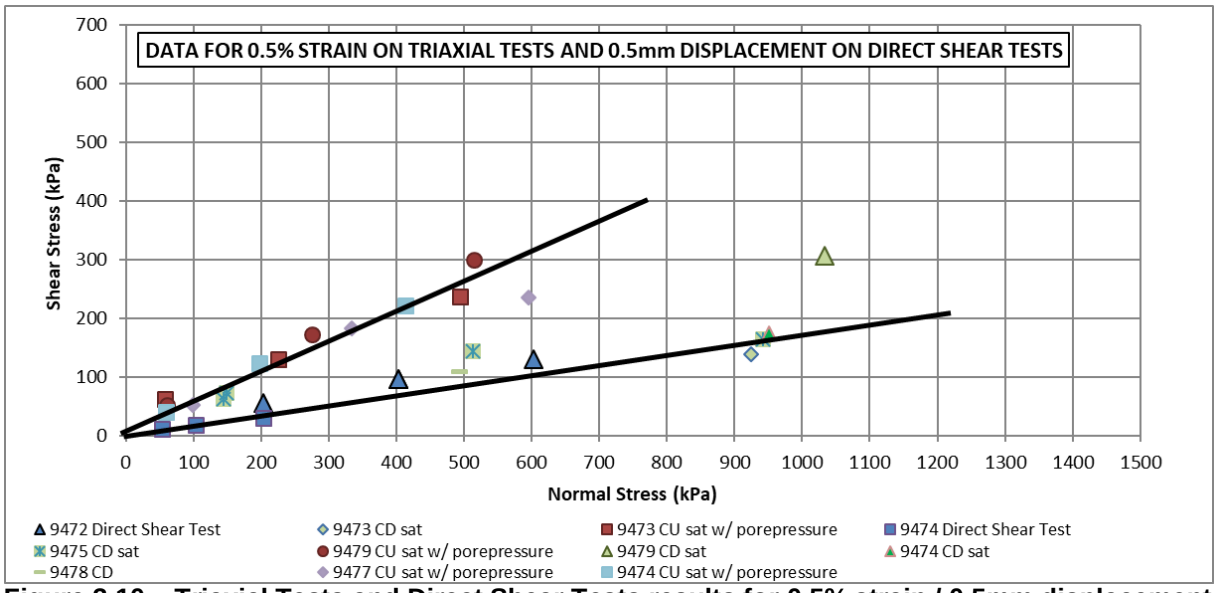

Figure 3.10 – Triaxial Tests and Direct Shear Tests results for 0.5% strain / 0.5mm displacement

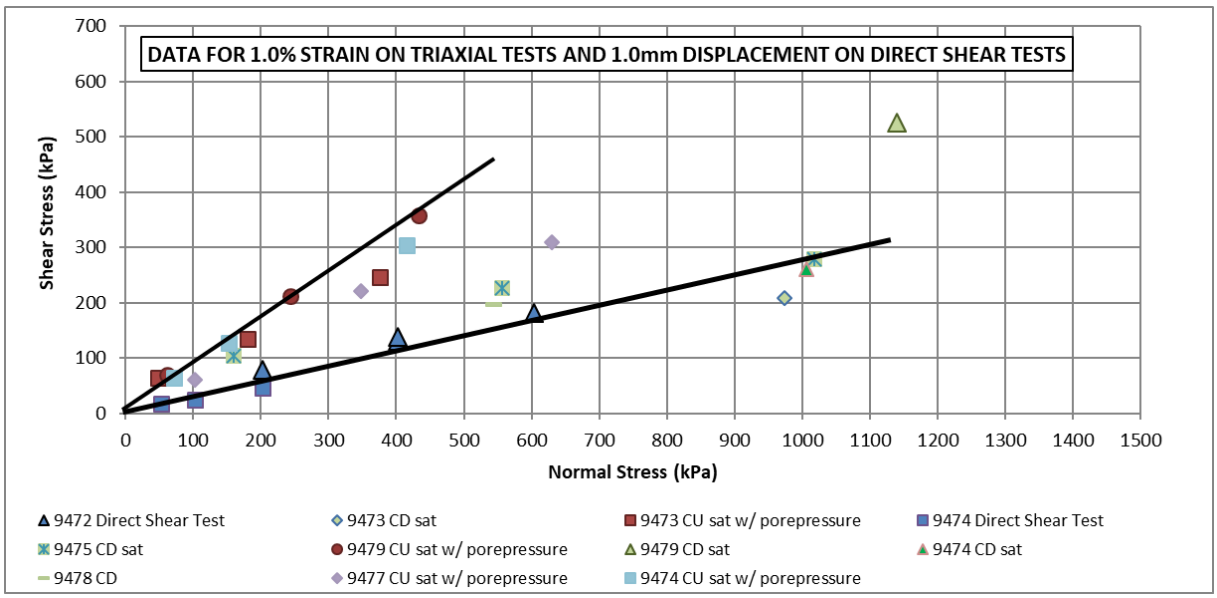

Figure 3.11 – Triaxial Tests and Direct Shear Tests results for 1.0% strain / 1.0mm displacement

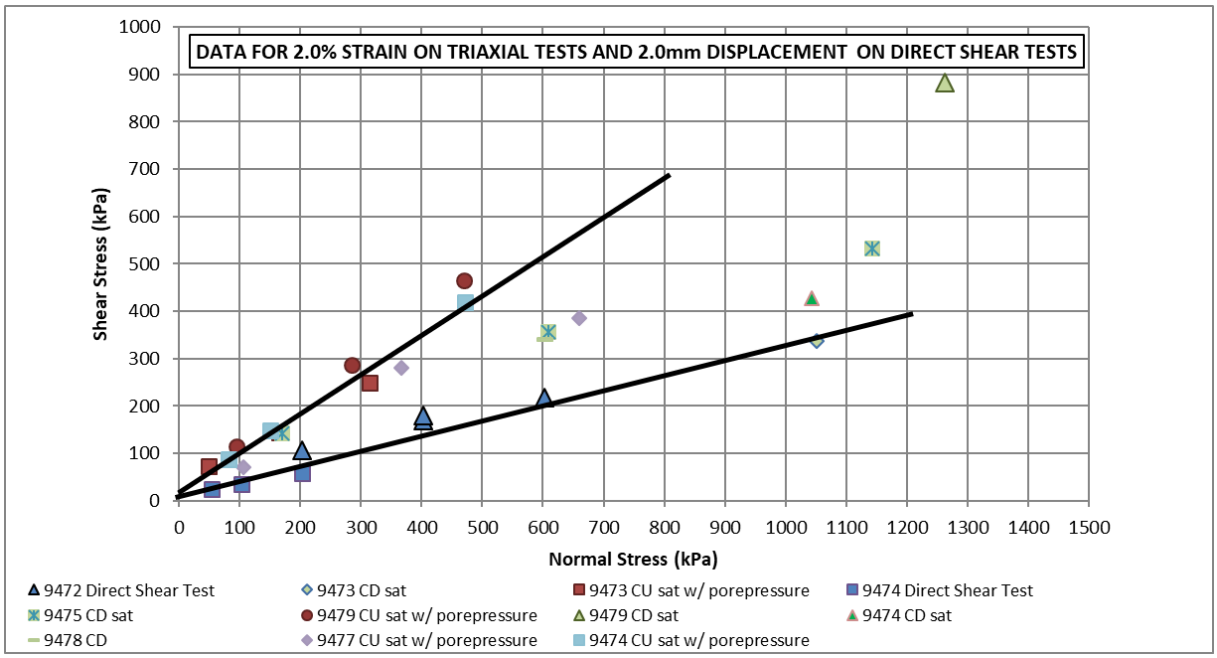

Figure 3.12 – Triaxial Tests and Direct Shear Tests results for 2.0% strain / 2.0mm displacement

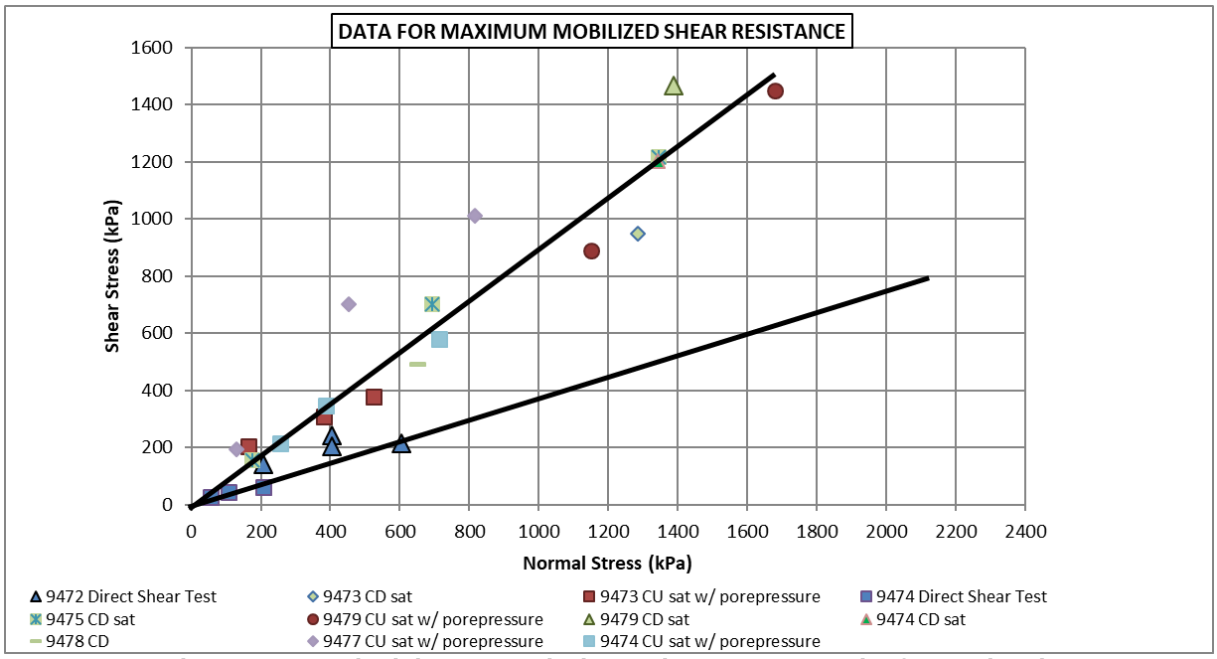

Figure 3.13 - Triaxial Tests and Direct Shear Tests results for peak values

Fixing a null cohesion intercept, the range of values of friction angle, ϕ', obtained vary between: 10º and 27º for strains / displacements of 0.5% / 0.5mm; 16º and 40º for strains / displacements of 1.0% / 1.0mm; 18º and 40º for strains / displacements of 2.0% / 2.0mm; and 20º and 42º for peak stress-strain values.

Additionally to the shear strength parameters of the more intensively weathered material present in the master joint, parameters for the secondary features associated to the master joint were also necessary. Considering that these secondary features present less weathered to rocky characteristics in some regions, associated to difficulties of obtaining undisturbed samples of these materials to fit in a shear box, estimates of the shear strength available in these locations was pursued from Barton's classification parameters *Jr* (joint roughness number) and *Ja* (joint alteration number). For regions where these

structures present themselves associating soil like material with saprolites / slightly weathered rock with lateral continuity this procedure lead to postulating values of angle of friction, ϕ', varying between 7º and 11º; and finally, in locations where less weathered rock dominates a friction angle, ϕ', of 20º was postulated.

Difficulty remained in interpreting and postulating average shear strength value representative of the master joint as a whole.

3.4 Design of the Stabilizing Structure

Safety of the water intake structure was verified against sliding, overturning, flotation and maximum stresses at its base, for different loading hypothesis, as routinely done in design procedures. Specifically, the sliding verifications were performed following the basic equation:

$$FSD = \frac{\frac{\Sigma N_i tg(\phi_i)}{CSD\phi} + \frac{\Sigma C_i A_i}{CSDc}}{\Sigma T_i} \geq 1{,}0$$

where:
FSD = Factor of safety against sliding
CSDϕ = Reduction factor on the friction angle ϕ'
CSDc = reduction factor on the cohesion c'
Ni = Resultant of normal forces to the sliding surface being analysed
ϕi = Characteristic friction angle of the sliding surface being analysed
Ci = Characteristic cohesion along the surface being analysed
Ai = Structure contact effective area in the plane being analysed
Ti = Resultant of the forces parallel to the sliding surface

The Brazilian codes require values of partial factors of safety *CSD*ϕ and *CSDc* of 1.3 and 1.5 respectively for the angle of friction and the cohesion, for normal loading conditions.

Initially, reverse calculations were performed to check what values of shear strength parameters were necessary to comply with the safety requirements. With zero cohesion intercept, as associated to surfaces with pre-existing slickensides, a value of 34.9° was shown to be required to comply with stability safety factors. As this value of shear strength could not be anticipated to prevail in the master joint or any other discontinuity with slickensides, a drainage gallery was conceived and designed at elevation 140m linked to the water intake structure gallery by a series of vertical drains. The reduction of water pressure in the base of the intake structure lead to a reduction of the required shear strength of the conditioning discontinuities, which under this hypothesis resulted in 29.5°.

Again, this value of shear strength could not be anticipated to prevail in the master joint or any other persistent discontinuity with slickensides, leading to the decision to design underground galleries filled with concrete to contribute as shear keys, increasing the safety factors to sliding to the required value. Having in consideration the distinct stress-strain behaviour of the concrete in the shear keys with relation to the soil filling of the discontinuities, it was decided that the shear keys should sustain all the horizontal stresses applied at the elevations where discontinuities prevailed, with no load being

transmitted through the rock massif. Two longitudinal shear keys linked by five transversal shear keys were designed. The geometry of these galleries was not rigidly fixed in design, the specifications being that the galleries should follow the master joint (Figure 3.14), excavating an additional 2.5m of the rock massif above its crown and 1m below its invert.

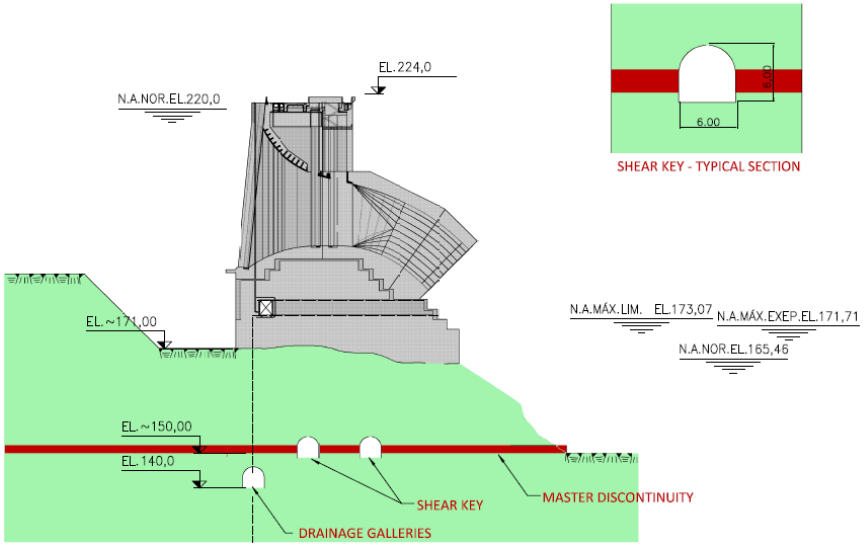

Figure 3.14 – Modeled Shear key geometry

An international Board of Consultants was invited to contribute in the difficult decision of postulating a representative value of average operating shear strength in the master joint; the results of the shear strength tests performed were used to help in the postulation of the average representative values to be used in stability analysis. The estimative of an angle of friction for the master joint postulated by the BoC was between 25º and 28º, with worst-case scenarios to be verified with 22º.

Stabilizing shear keys were designed to guarantee safety of the structure from sliding as conditioned by the master joint (Figures 3.15, 3.16, Photos 3.5 (a), (b) and 3.6), associated to a drainage gallery previously conceived, also at the foundation of the intake structure, at elevation 140m, and relieving the water pressure as drained by a battery of vertical drains (Figures 3.14, 3.15, 3.18 and 3.17).

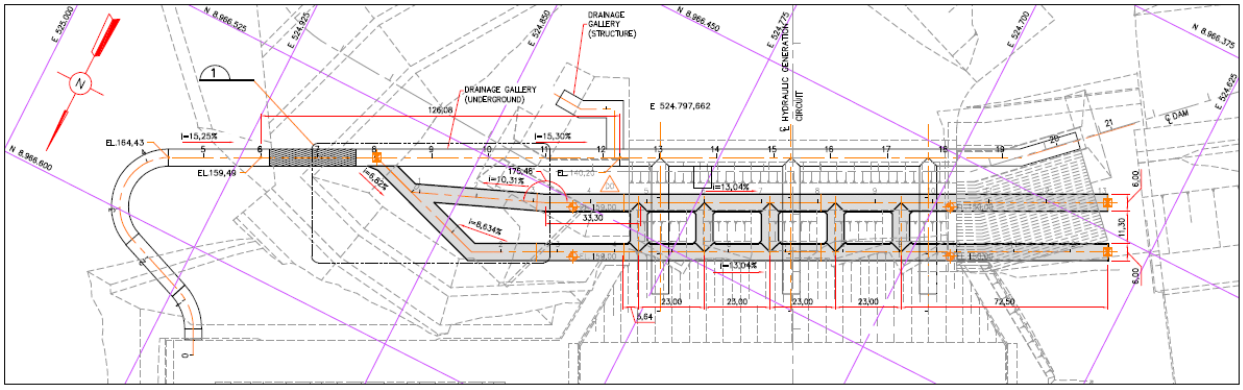

Figure 3.15 – Shear keys and drainage galleries – Plan View

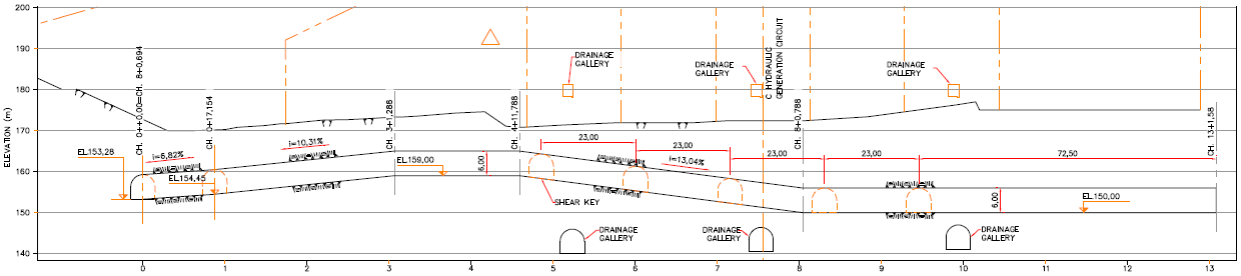

Figure 3.16 - Shear keys and drainage galleries – Longitudinal Profile – Access to shear keys

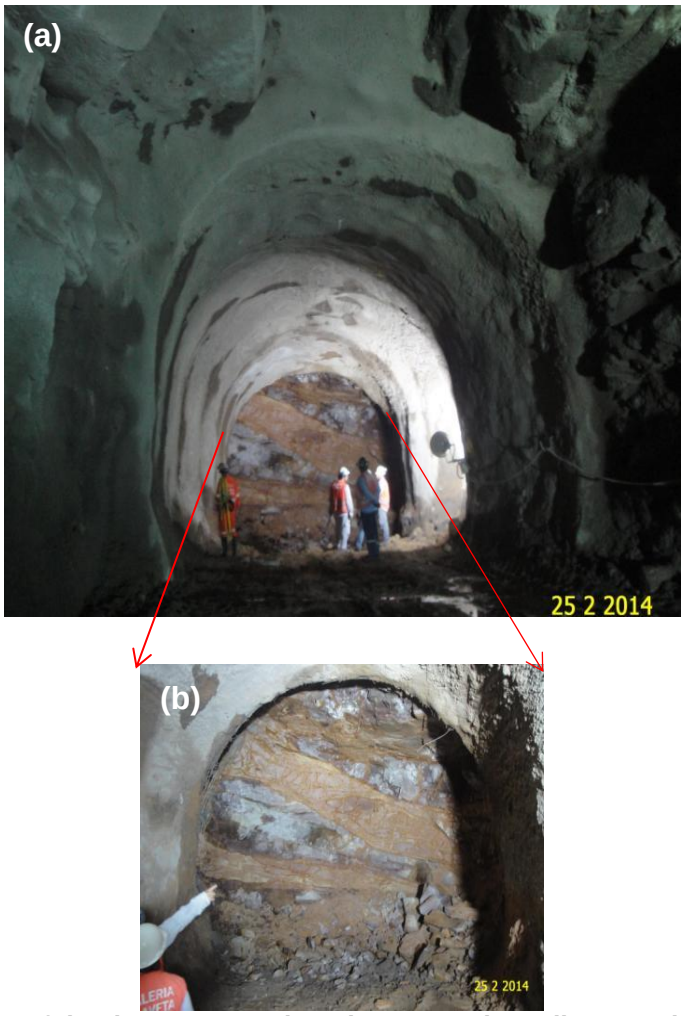

Photo 3.5 - Front view of the downstream shear key. Note the gallery overbreak above the steel ribs (a), and the detail of the downstream dipping of the weathered master joint (b).

Photo 3.6 – Detail of the weathering pattern in the Master Joint

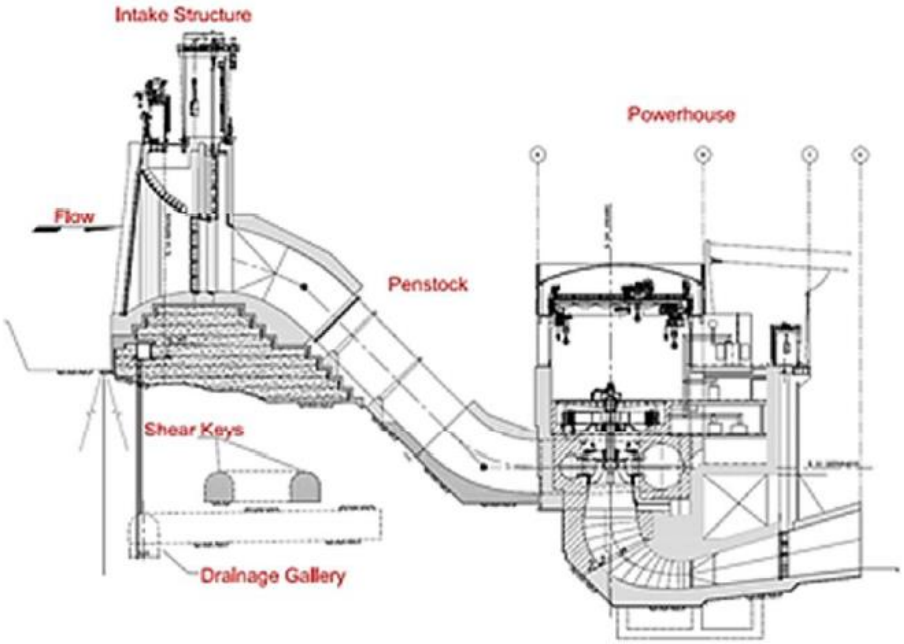

Figure 3.17 – Cross section of intake structure foundation shear keys, drainage galleries and drainage curtain

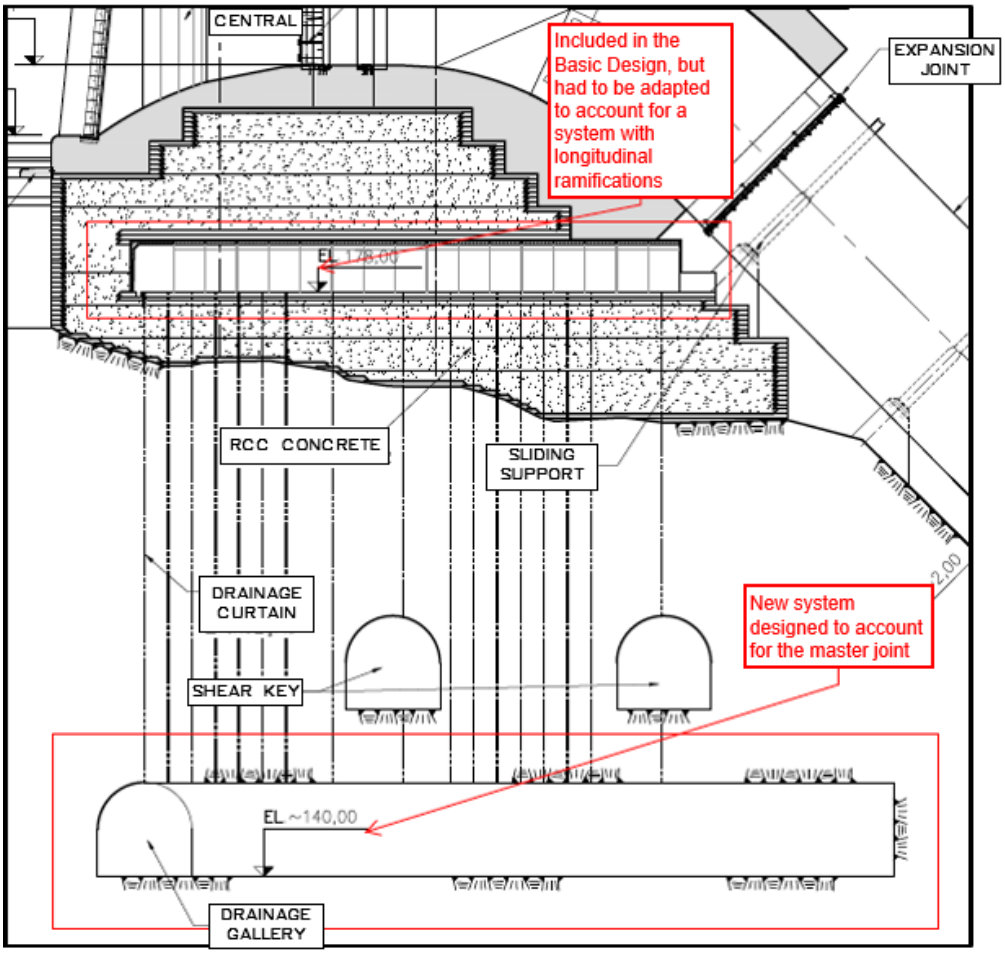

Figure 3.18 – Detail of the cross section of Water intake structure foundation showing the shear keys, drainage galleries and drainage curtain

Secondary parallel joints above the master joint were also identified and mapped during excavation (Figure 3.19); their influence in the stability of the intake structure had to be discussed and evaluated together with that of the master joint itself, taking in consideration their spatial random variation.

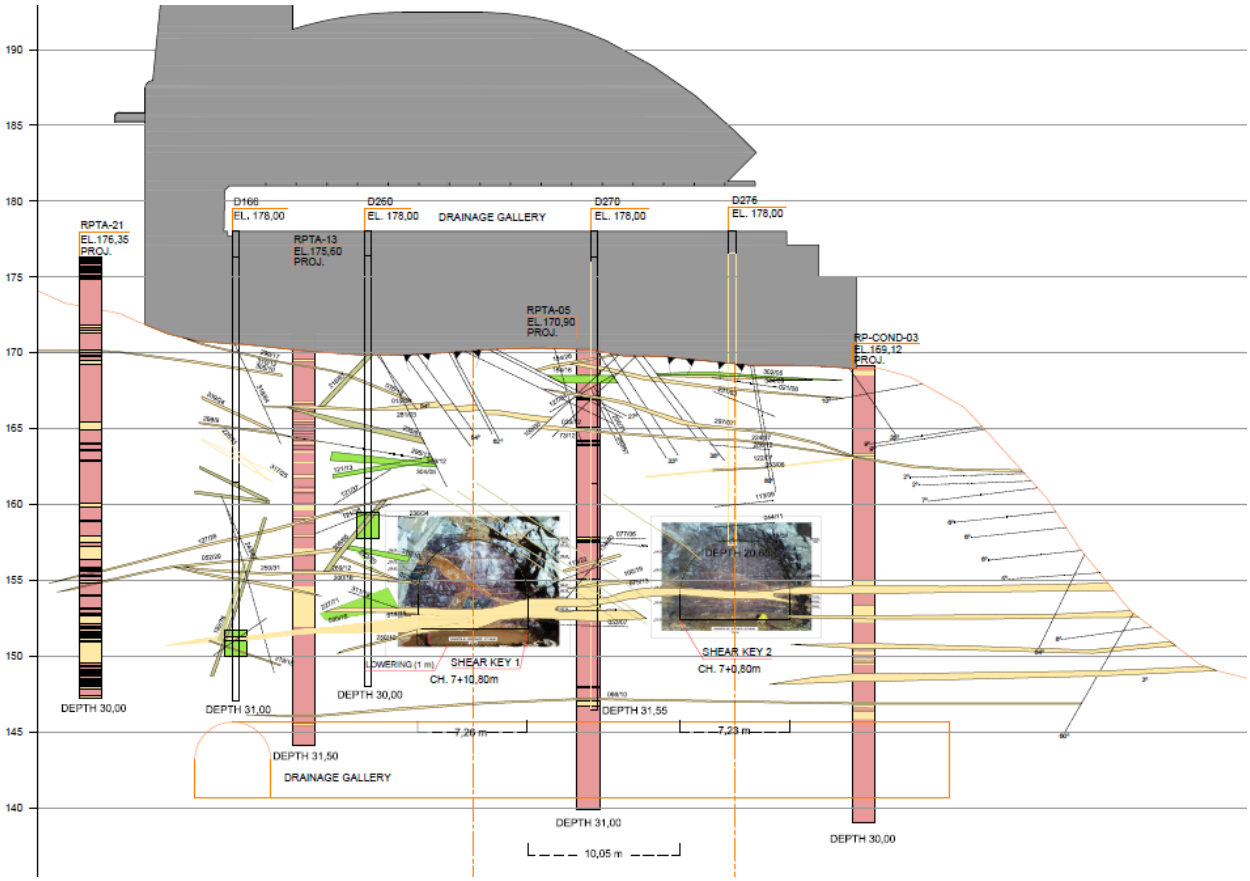

Figure 3.19 – Water intake structure foundation cross section with master joint and secondary parallel joints

Further sliding stability verifications were performed, leading to the decision to install an upstream impervious blanket with two PEAD layers (Figure 3.20) to reduce the water pressures in the intake structures' foundation, as well as of 55 passive subvertical anchors of 57mm diameter, working in shear. These additional stabilizing details increased the factor of safety by 12% to 18%, depending on the loading case and depth of the discontinuity, also guaranteeing the stability of all secondary sub-horizontal planes / features existing between the foundation of the water intake structure and the master joint.

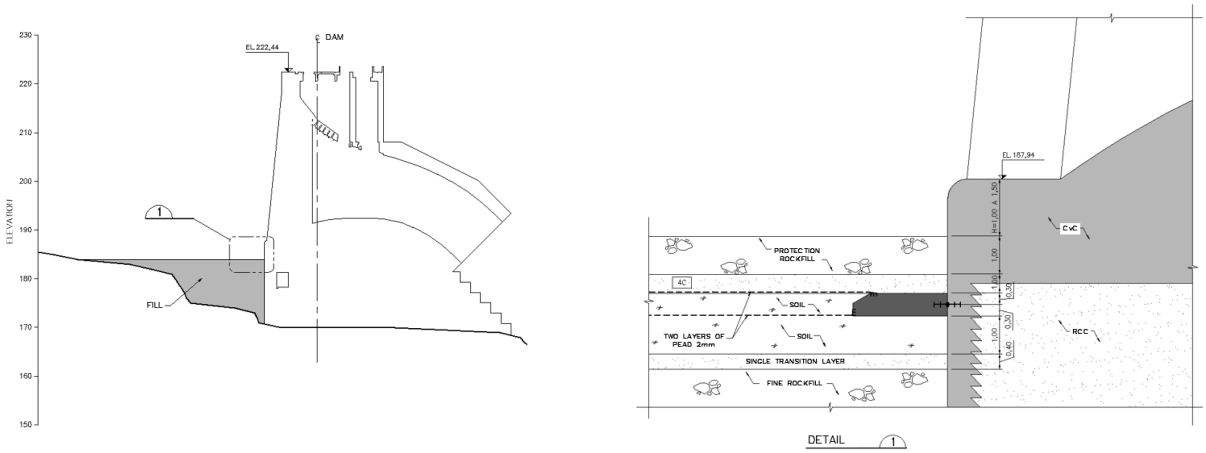

Figure 3.20 – Upstream impervious blanket – Detail showing fill and PEAD layers

3.5 Monitored behaviour of the dam during initial filling and subsequent period

Reservoir filling began in December 2014 and was very fast, with 85% filling happening in only 8 days; after all environmental issues were properly dealt with, the last 1.8m of reservoir was filled after 1 month. Readings of the extensive monitoring program after 8 months of maximum reservoir level are summarized below.

Among many instruments installed in the water intake structure, the behaviour of this structure can be represented by the behaviour of extensometers and piezometers installed in the structure's foundation underneath one of its concrete blocks.

The extensometer measurement results presented in Figure 3.21 is representative of the behaviour shown in all such instruments.

Readings show that deformations of approximately 10mm happened when the galleries were being excavated in the region of influence of the instrument, especially as tunnel excavation suffered important overbreak in following the master joint within the design criteria, leading this excavation to being only 4m to 5m from the foundation of the intake structure. Additionally, the load imposed by the concrete around the penstocks before filling the shear keys with concrete is considered to have influenced the behaviour monitored. Soon after concrete filling of each gallery/shear key deformations stopped completely, and were not affected or mobilized by reservoir filling at all.

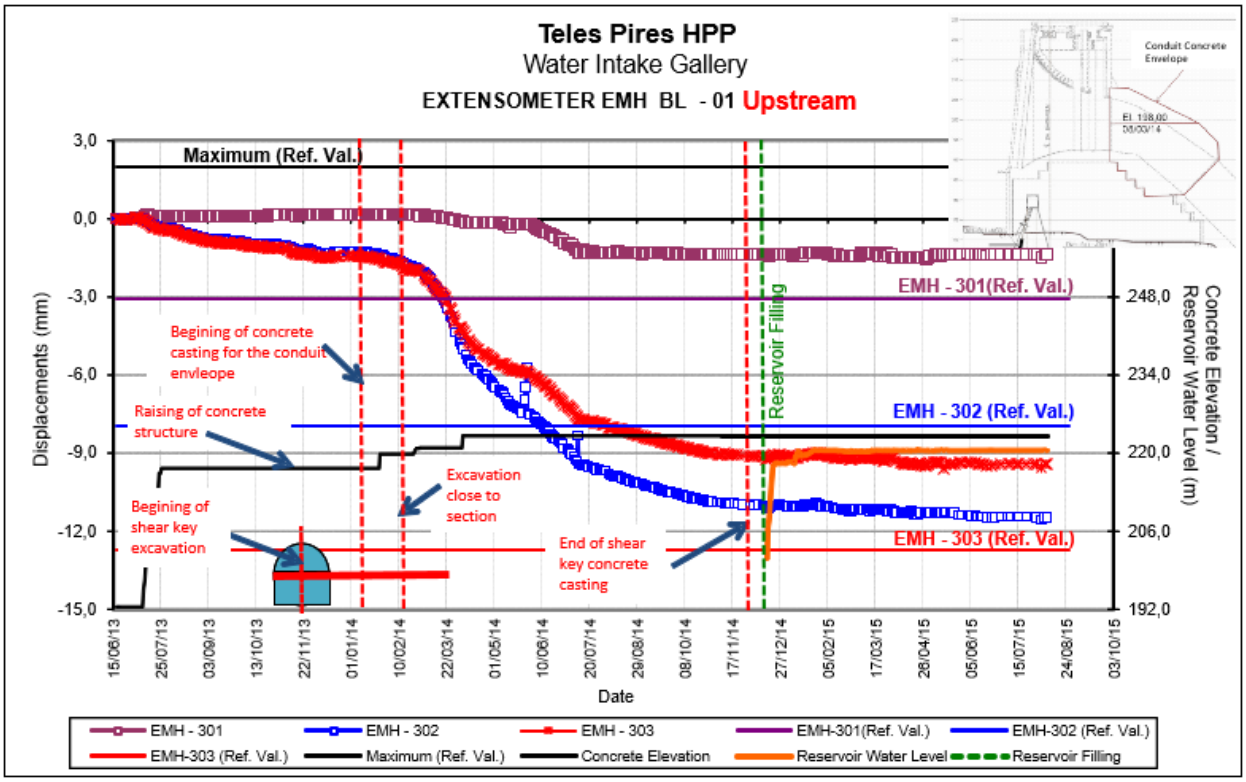

Figure 3.21 – Typical data for extensometer installed in the water intake structure's foundation underneath one of its concrete blocks

Standpipe and electric piezometers were installed from the intake structure drainage and monitoring gallery, inclined 10º upstream and 15º downstream in order to check the real hydrostatic thrust acting on the structure's foundation and compared to the design hypothesis. The comparison of the hydraulic head measured with relation to that used in

design verifications is an important parameter to judge the efficiency of drainage on the thrust diagram acting in the structure's foundation. Two distinct water thrust diagrams were used in these verifications: one suggested by the international BoC (Figure 3.22 (a)), and another that does not include the contributing efficiency of the PEAD impervious upstream blanket (Figure 3.22 (b)).

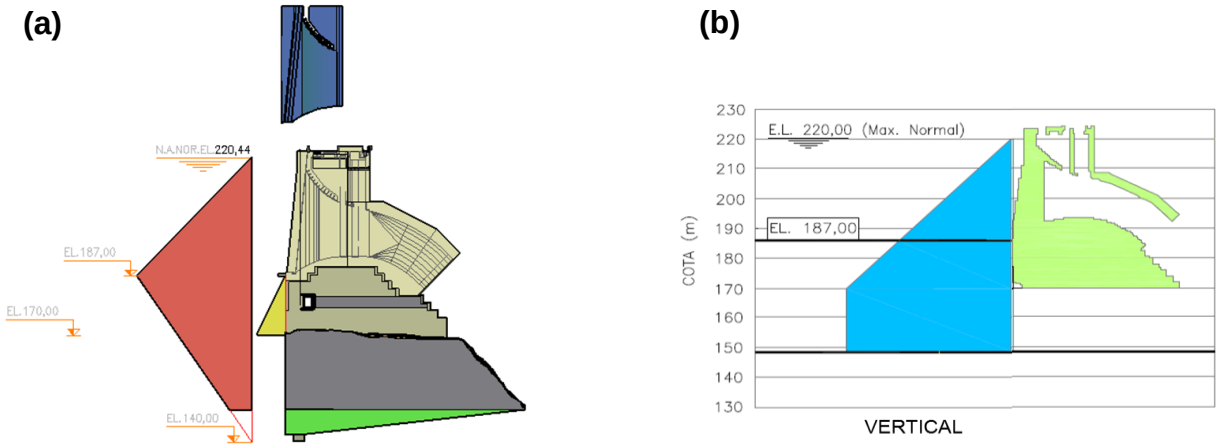

Figure 3.22 - Water thrust diagrams: (a) Diagram 1 - Proposed by the BoC; (b) Diagram 2 – Without PEAD

The measured piezometric values (Figure 3.23) lead to conclude that the diagram of water thrust suggested by the BoC for the structure's foundation was surpassed in some of the intake blocks, while all readings were lower than the piezometric levels associated to the hypothesis of a non-efficient PEAD upstream impervious blanket in the foundation.

Having in consideration that no incremental deformations were measured by the extensometers when the water thrust diagram started to be imposed by reservoir filling, the fact that some readings were higher than those postulated by the BoC did not raise any further concerns.

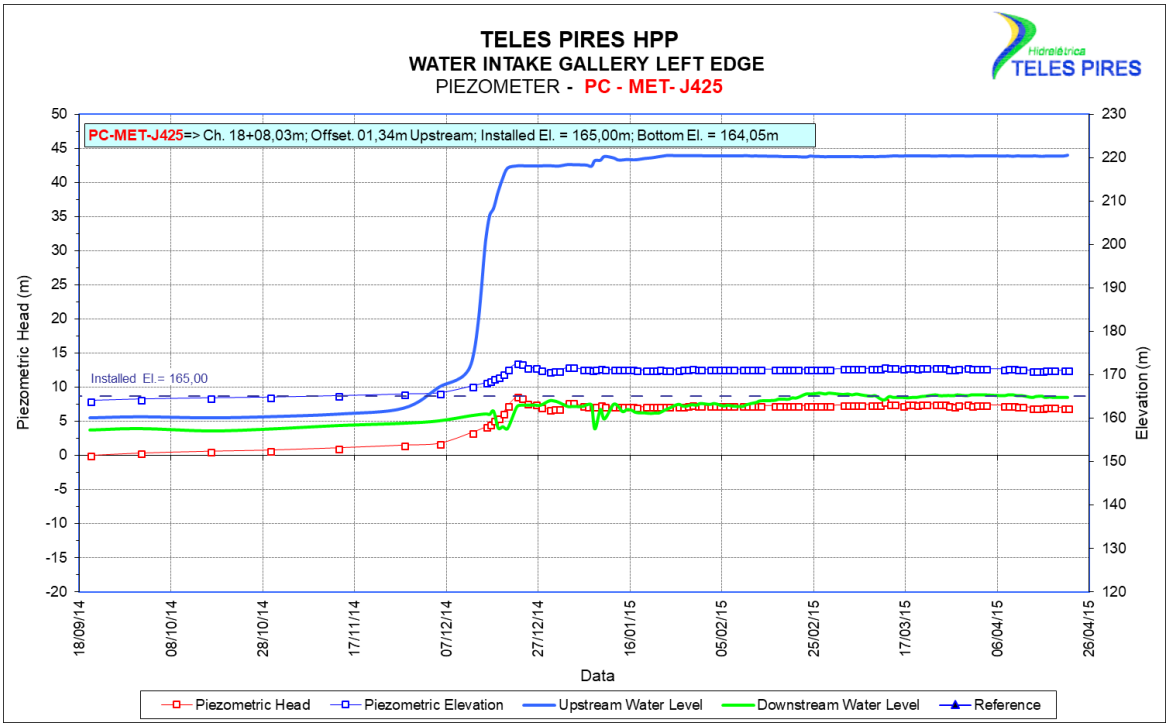

Figure 3.23 – Piezometer and reservoir level data

The piezometers also allow the verification of the efficiency of the grouting curtain. The measured values allow to interpret that this efficiency is on average associated to a reduction of 60% of the measured upstream water pressure.

All readings stabilized soon after reservoir filling and are considered to be in compliance with design predictions and criteria.

4 CHAGLLA HYDROELETRIC POWER PLANT

The Chaglla Hydroelectric Power Plant is located on the Huallaga River in the Chaglla and Chinchao districts, department of Huánuco, Peru. The dam axis is located downstream from the confluence of the Panao River and the Huallaga River and the total catchment area is around 7,150km². It comprises a 202m high concrete face rockfill dam (CFRD) with a crest length of 274m, three tunnel spillways for a design flow of 3620m³/s, a headrace tunnel 14,4km long, excavated by drill and blast in an 8m span horse-shoe shape cross section, feeding two vertical axis Francis turbines each of 225MW capacity. The discussion below refers to the headrace tunnel.

4.1 Local Geology

The rocks in the region of the project are of sedimentary origin, ranging in age from Permian to Mesozoic periods, 350 to 65 Mya ago. The project area is located within the calcareous rocks of the Pucará Group.

This geological group is of marine origin and forms a fringe in an NNW-SSE direction, and is usually subdivided into three formations, which, in a simplified description can be described:

- its base consists of dolomitic, bituminous and limestones with medium to thick stratification;
- in the middle lutite and limestone intercalations occur; the lutites are stratified, forming medium-sized layers, and dark gray to black in color; the limestones are dark gray to black, well stratified in thin to medium-sized layers, somewhat bituminous and occasionally clayey silty, with chert nodules;
- the top of the sequence consists of light-gray limestones in thin to very thick layers.

The carbonate rocks present some karstic action, as discussed below.

The headrace tunnel is located on the left bank of the Huallaga River, on the east flank of a large anticlinal structure trending NW-SE with layers that always dip between 40º and 80º towards NE. The carbonate rocks are characterized by ductile structures with broad folds oriented mainly in a NE-SW direction, these being the features that impact the project structures, particularly in the headrace tunnel, as it runs at right angles to these geological structures and, therefore, intersects them in some stretches, such as the Lluto and Chimao creeks.

The main discontinuities in these rock masses are the bedding planes, which are very persistent with thin to medium layers, 20cm to 60cm thick. Other discontinuities correspond to two families of tension fractures caused by folding, as well as systems resulting from the shear stresses to which these rocks were subjected.

Thrust faults in a NW-SE direction were mapped on the left bank of the Huallaga River. Various strike-slip faults in a NE-SW direction with regional dimensions that leave deep slopes on the creeks coming down from the mountains were also observed.

In summary, the headrace tunnel is intercepted by beddings and faults, of which only two are effectively major pressure-relief zones (Lluto and Chimao creeks). Most of these

beddings have a general NE-SW orientation, corroborating the regional structural characteristics.

4.1.1 Geological-Geotechnical Investigations

To assess the geological characteristics of the project structures area dipole-dipole array, vertical electrical sounding, seismic refraction and MASW (Multichannel Analysis of Surface Waves) geophysical methods were used. The local topography of high and steep slopes impacted the performance of the geophysical surveys, especially in matching the most appropriate lines.

Due to the difficult access in virtue of the steep slopes in the project region as well as the dense vegetation, in some cases field geological surveys were made in locations near to or parallel to the project axis and structures. Along the headrace tunnel axis, 22 surface geomechanical stations conveniently located were defined and used to determine the structural characteristics of the rock mass.

Boreholes were drilled at the tunnel portals, at the adits' entrance and at locations of lower massif cover, like the creeks mentioned.

4.1.2 Hydrogeological Model

The hydrogeological model developed during the design studies concluded that the supply to the aquifer was the result of:

- infiltration of rainwater and water from tributary creeks or water from remote areas seeping through the longitudinal and transverse fault planes that affect the zone;
- the flow of underground water through the limestone rock mass as a result of its secondary permeability, the final direction of the water flow being the banks of the Huallaga River, which acts as an important natural drain;
- eventual perched aquifers in the limestone rock mass.

Considering that the bedding planes are subvertical, incursions into the caves in the region detected that the main karst access points (sinkholes and dolines) could be investigated to depths of 80m to 100m or even more, down to location where the presence of fallen blocks hindered further access.

4.2 Description of the Headrace Tunnel

The headrace tunnel´s horizontal and vertical alignments were selected in order to ensure adequate rock cover in the left-bank side valleys while minimizing the maximum rock cover and the length of the intermediate construction adits. It has a total length of 14.38km and a 7.85m high, 8.5m wide horse-shoe shape excavated cross section. It was excavated by drill and blast method with full face blasting for each round, using five intermediate adits. Figure 4.1 illustrates the headrace tunnel's alignment and the location of the adits.

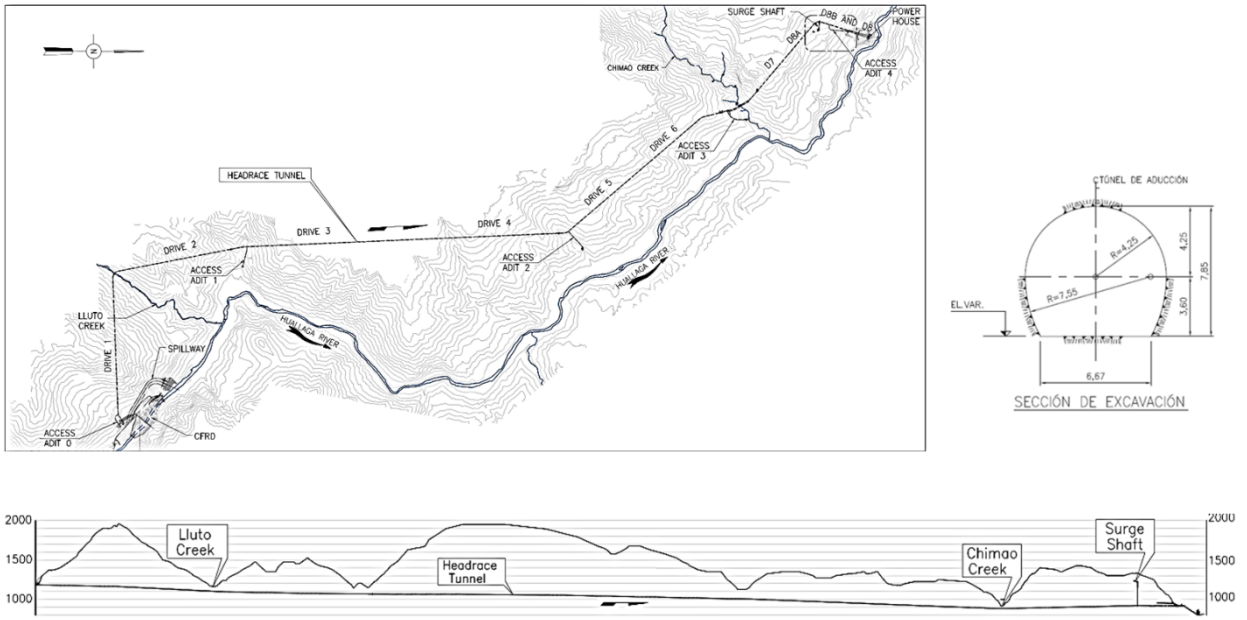

Figure 4.1 - Plan view, cross section and longitudinal section of the headrace tunnel

The maximum cover above the tunnel is around 880m. The average unconfined compressive strength (UCS) of the rock is about 100MPa for the massive grey limestone and about 85MPa for the bituminous limestone. Thus, considering an average specific weight of the rock of around 2.6tf/m³, the maximum in situ geostatic stresses are in the range of 23MPa, or about 25% of the intact rock UCS.

The tunnel alignment crosses two main side valleys at distances of about 2.3km (Lluto creek) and 12.2km (Chimao creek) from the intake.

Considering that a maximum hydraulic head of 313m is imposed at the Chimao creek crossing, hydro-jacking tests were performed from the surface, as well as from inside the tunnel itself, to check the minimum in situ stresses and adjust the lining design. A reinforced concrete lining was used in the low-cover section of the tunnel, about 200m and 180m long immediately upstream and downstream, respectively, of the steel lined siphon used to pass underneath the side valley, with length of 323m to guarantee safe hydraulic gradients during operation in this specific location.

4.3 Geological and geomechanical characteristics of the rock mass along the tunnel

During construction of the headrace tunnel, a very detailed geological mapping was obtained as the excavations progressed. The data collected from this survey included: geological formation, rock mass description, hydrogeology aspects, estimation of Barton's Q index, including the rock mass class and quality. Photographs showing the rock type, discontinuities, presence of water and other items of interest on the tunnel face at each excavation round were also produced. Figure 4.2 presents an example of such document.

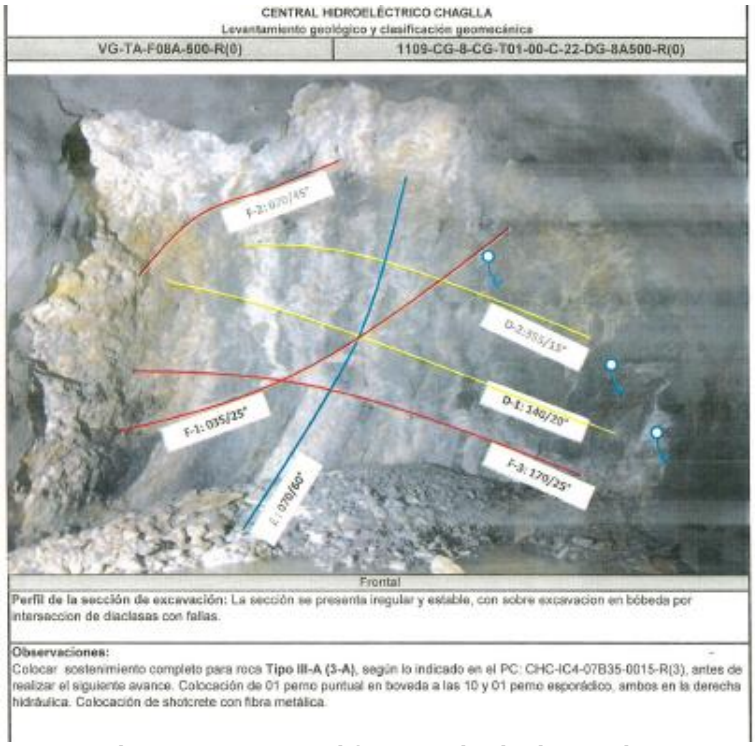

Figure 4.2 – Tunnel face geological mapping

Geological/geotechnical maps of 50m sections along the tunnel were prepared, presenting the different lithological types, the orientation of the bedding planes and other important geological structures. Stereograms showing the orientation of the bedding planes were included as it is the most persistent structure.

Barton's rock mass classification was done methodically at each excavation advance, showing the value attributed to each of the parameters from which it is derived, the GSI punctuation, alteration/consistency/jointing degrees and the features of the main discontinuities. Definition and adjustment of the tunnel support at each excavation round was postulated based on this data.

During excavation of the tunnel, various lithological types were crossed: gray and/or banded limestones, bituminous limestones, breccia and andesitic dykes. At some chainages shearing developed along the bedding planes was observed, which at these locations presented a clayey, silty or crushed rock filling. These particular features were named "stratigraphic fault"; Photos 4.1 and 4.2 illustrate these features in the excavation front.

No karstic cavities were found along the alignment of the headrace tunnel during excavation. The only cavity of karstic origin was intersected at chainage 0+234 of adit 3. At this spot, a cavern filled with clay approximately 6m wide by 8m high was found at the adit tunnel crown. It was interpreted to be related to a karstic duct which started at a doline placed about 100m higher than the level of the adit and ended in a cavity on the right bank of the Chimao creek. The cavity was backfilled with concrete and the infiltration water flowing through the karstic duct was conveyed through pipes to the portal of the adit 3 to allow the excavation to proceed.

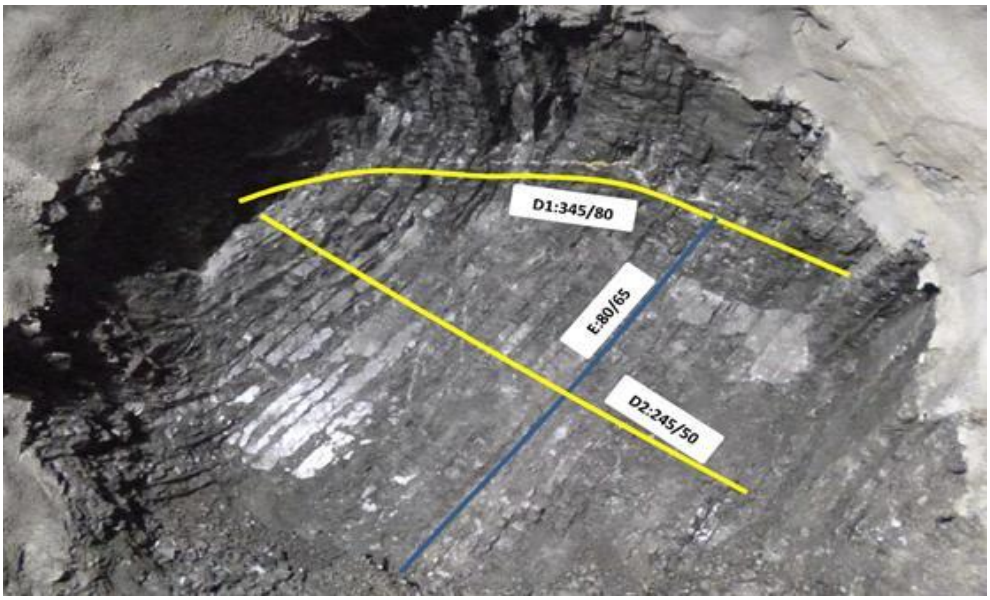

Photo 4.1 - View of the thinly stratified gray limestone at the excavation front

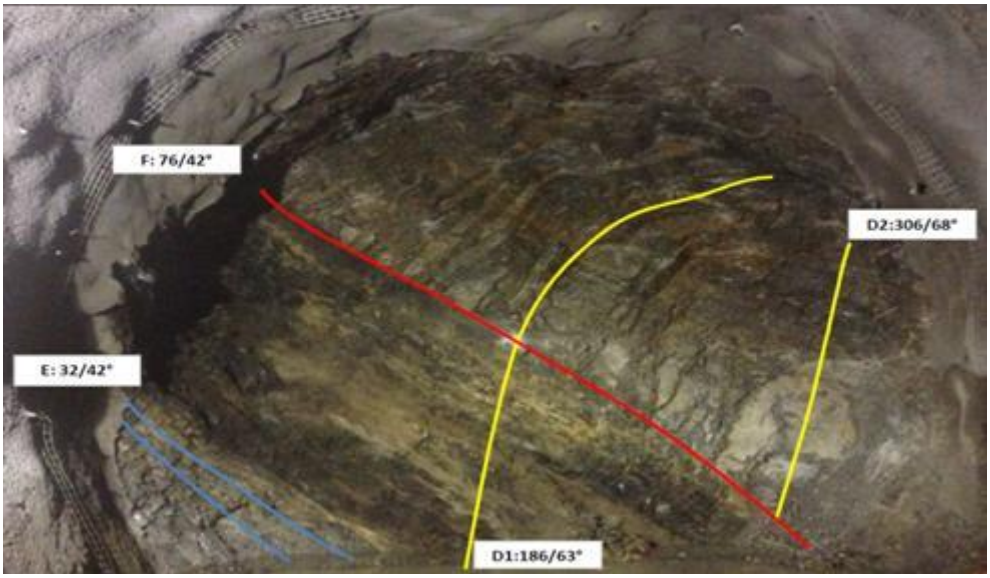

Photo 4.2 - View of the "stratigraphic faults" in the gray limestones at the excavation front

The banded limestones described were continuously and irregularly interbedded with the gray limestones and could, therefore, be grouped with them as they have similar geotechnical behaviour. The rock is dark gray with light bands with moderate degree of jointing and alteration, medium to low strength, thin to moderate bedding layers and three joint systems (Photo 4.3).

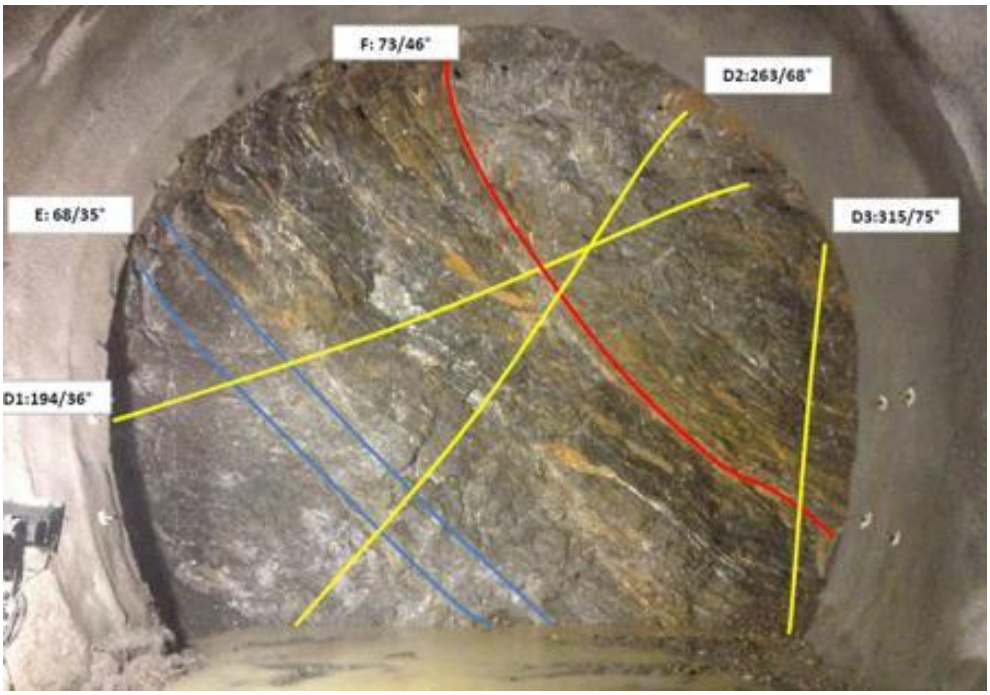

Photo 4.3 - View of the thinly stratified banded limestone at the excavation front

The bituminous limestones are part of the middle member of the Pucará Group and were found overlying the banded gray limestones. This lithological type is black and dark gray with moderate to intense degree of jointing and alteration, low to medium strength, thin to moderate bedding layers and three joint systems, with clayey silt or crushed rock fillings in some bedding planes, as well as thin layers of carbonaceous lutites (Photo 4.4).

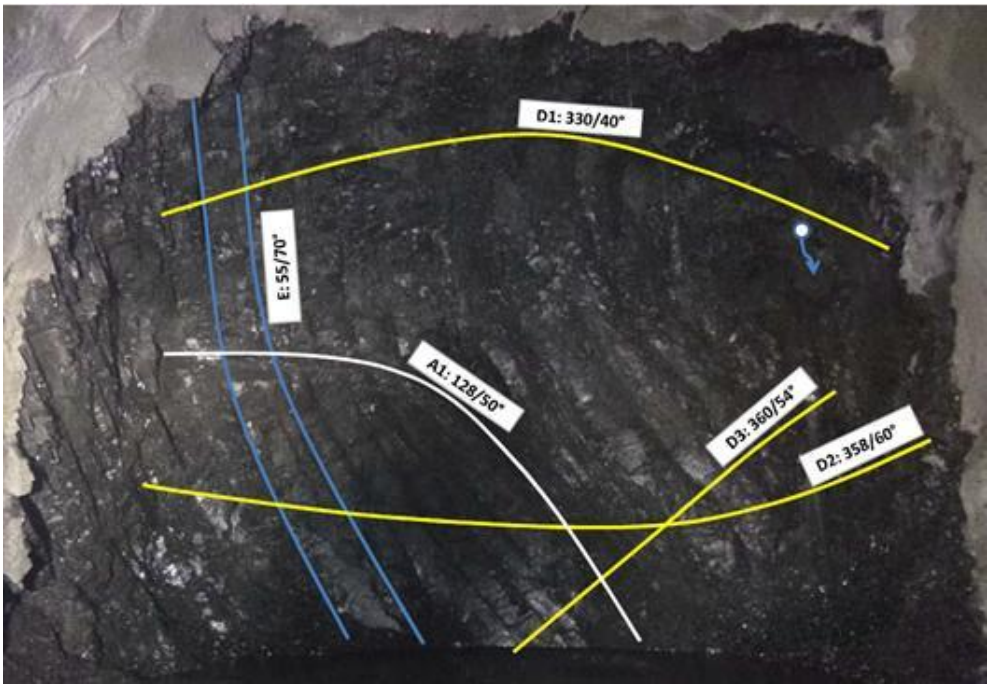

Photo 4.4 - View of the bituminous limestone at the excavation front

4.4 TUNNEL LINING DESIGN

4.4.1 Design Assumptions and Excavation Support

The tunnel support was defined according to the Q-System (Barton, Lien and Lunde, 1974; NGI, 2013). In the crossings under the Lluto and Chimao creeks, where the conventional empirical cover criteria were not met, steel and reinforced concrete linings were used and auxiliary measures taken to ensure safe operation of the tunnel in terms of water losses and the stability of the adjacent slopes.

The final lining for the operation phase in most of the headrace tunnel consists of shotcrete applied systematically as a permanent excavation support on the crown and sidewalls with a thickness varying between 7cm and 20cm according to the rock mass class, and a plain 25cm thick concrete slab on the tunnel floor poured over a layer of compacted muck. The systematic installation of a secondary lining of cast-in-situ concrete was discarded because the calcareous rocks encountered along the tunnel were considered durable under the foreseen operating conditions, and the 2.8m/s flow velocity in the tunnel was compatible with a shotcrete lining.

Table 4.1 summarizes the tunnel support as a function of Barton's Q value:

Table 4.1 – Summary of tunnel lining design as a function of Barton's Q value

Q	Rock Mass Class	Description of the tunnel support treatment
Q > 60	I (very good rock)	7cm thick fiber reinforced shotcrete (crown and sidewalls)
7 < Q ≤ 60	II (good rock)	7cm thick fiber reinforced shotcrete (crown and sidewalls); spot bolting where required
0.64 < Q ≤ 7	III (moderately good rock)	10cm thick fiber reinforced shotcrete (crown and sidewalls); 3m long passive bolt (ϕ=25mm) at 2m spacing in the crown; spot bolting where required
0.08 < Q ≤ 0.64	IV (poor rock)	15cm thick fiber or steel mesh reinforced shotcrete (crown and sidewalls); 4m long passive bolt (ϕ =25mm) at 2m centers in the crown and sidewalls
Q ≤ 0.08	V-A (very poor weathered rock)	20cm thick steel mesh reinforced shotcrete (crown and sidewalls); steel rib or lattice girder spaced at 1m centers; forepoles if necessary (crown)
	V-B (very poor altered rock)	20cm thick steel mesh reinforced shotcrete (crown and sidewalls); steel rib or lattice girder spaced at 1m centers; forepoles (crown); reinforced invert if necessary

4.4.2 Reinforced Concrete and Steel Lining Under the Chimao Creek

At the location where the tunnel passes under Chimao creek, at a tunnel chainage of around 12+340, the rock cover is approximately 20m with an applied hydraulic head reaching 313m at elevation 883m.a.s.l. Steel lining was designed for this section of the tunnel, 322.8m long and extending to both sides of the Chimao valley. Confinement of

the rock mass in the tunnel sections adjacent to the steel lining was checked by means of several hydro-jacking tests; the results showed a minimum safety factor against jacking of the rock of around 1.10. To ensure a safety factor of 1.30 and to avoid potential leakages from the tunnel, a hybrid impervious lining extending to the points where the rock cover is sufficient according to conventional empirical cover criteria was implemented on both sides of the valley. The hybrid lining is composed of the following elements:

- an outer ring of reinforced shotcrete applied over the existing tunnel support with a minimum thickness of 20cm and a circular inner profile;
- a sprayed 3mm thick waterproof membrane applied on the inner surface of the shotcrete ring (this membrane was considered an additional measure whose effect was disregarded in the dimensioning of the reinforced concrete);
- a 40cm thick inner ring of reinforced concrete poured over the waterproof membrane.

Additional grouting of the rock around the tunnel at pressures of up to 30bar (equivalent to the operating pressure of the tunnel in this section) was performed to further reduce the permeability of the rock mass and also to pre-compress the concrete lining.

The hybrid lining was applied along a 181.0m length of the tunnel downstream of the steel lining and a 201.0m length upstream of the lining. Thus, the lined section of the headrace tunnel in the region of the Chimao creek had a total length of about 704.8m.

4.5 Procedures for Filling the Headrace Tunnel

Special procedures for filling the headrace tunnel were defined in design, considering flow from the gates at the water intake and from the natural water table of the rock mass into the tunnel, this infiltration being estimated to be around 2m³/s. The water intake structure is divided into two bays, each equipped with a fixed-wheel gate. Each gate is divided into three panels; the lower two are rigidly coupled, while the middle and upper panels are linked with a special tie, forming a 50mm space between them. Opening the middle and upper panels without raising the whole gate is called a “cracking” operation.

Filling of the tunnel started on November 17th, 2015, using only the inflow in the tunnel provided by the natural water table. Figure 4.3 shows that from the beginning the water level inside the headrace tunnel rose at a rate of approximately 0.4m/h with the infiltration flow alone, well below the maximum recommended rate of 2m/h (Benson, 1988).

On November 26th the level in the reservoir reached the Intake structure, allowing crack opening of the gates to start, with the water level inside the tunnel at elevation 975m.a.s.l.

Filling continued at approximately 0.4m/h for the next seven days, when the water level inside the tunnel was observed to be stabilizing at approximately at elev. 1,050m.a.s.l. As the water level inside the tunnel rose, at this moment the exfiltration flow from the tunnel exceeded the infiltration rate.

Throughout this period, the site was inspected to check if water was daylighting and appearing anywhere or if there were any related surface changes, particularly inside the construction adits and respective concrete plugs. No significant changes were detected.

The maximum normal water level in the reservoir (elevation 1,196m.a.s.l.) was reached on December 4th, and one of the spillway gates was opened to control the level.

As the filling rate fell to 0.1m/h, it was decided to lower the reservoir level so that one of the gates at the water intake could be opened with a low head. In this way the inflow and water velocities could be controlled, avoiding damage to the concrete floor of the tunnel. Lowering of the water level in the reservoir to the elevation 1,182.2m.a.s.l. (just 0.7m above the gate sill) began on December 9th, and the reservoir level was kept at this elevation, corresponding to an inflow of 4.0m³/s.

With this procedure, the filling rate of the tunnel was increased to 1m/h for the next three days and dropped again to 0.3m/h, reaching elevation 1,160m.a.s.l. around noon on December 18th. As the last stretch of the tunnel would be less affected by the filling flow (the floor is less inclined), it was decided to raise the reservoir level again to finish filling the tunnel. This was done on December 19th in the morning. The filling rate during this last day was 1m/h.

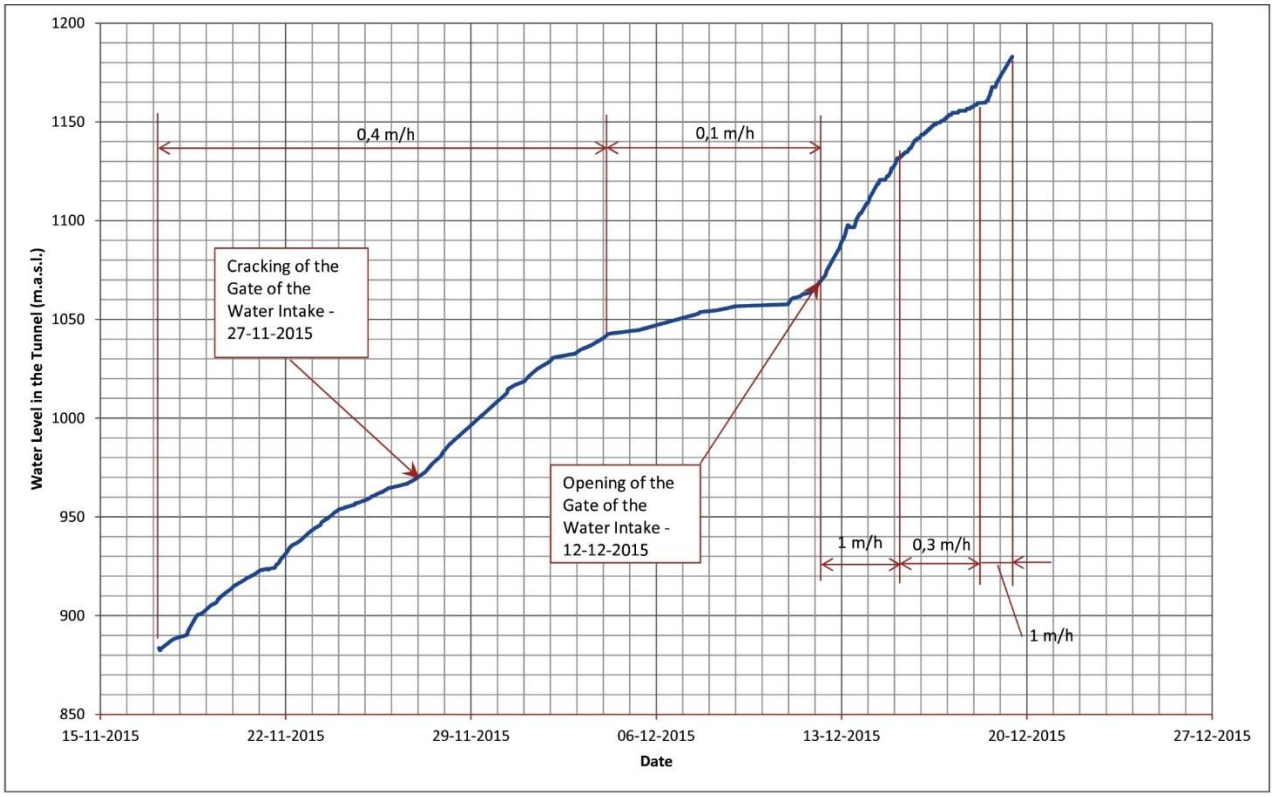

Figure 4.3 – Tunnel filling

The following changes were observed during the first half of December:

- Low seepage at the concrete plug in adit 4; complementary grout injections were performed.
- No change at adit 3.
- Increased seepage into a drainage gallery excavated under Chimao creek to control uplift water pressure in the syphon.
- Significant seepage in the lower half of adit 2.

4.6 Headrace Tunnel Incident on February 17th, 2016

4.6.1 Description of the Incident

Filling of the headrace tunnel happened between November 17th and December 19th, 2015. The tunnel remained pressurized with its normal operating pressure from that date till February 17th, 2016, a period of 61 days, without any record of abnormalities. During this period three crude measurements of overall tunnel leakage were performed, by closing the gates at the tunnel intake structure and measuring the drop in the water level in the adjacent adit 0 after a given time interval. The measurements indicated an exfiltration / leakage of around 2.5m³/s.

On February 17th, 2016, at 1:03 PM, a load rejection test was performed on one of the generating units with 80% of the maximum generating flow. At 6:57 PM, an earthquake of magnitude 4.2 on Richter scale was recorded. The epicenter was very close to the dam site, and the earthquake was perceived by the site personnel as an intense, very short shake.

On February 18th, 2016, a significant leakage of dirty water on the left bank of Chimao creek was observed and adit 3 flooded. In the same day, a load rejection in the second generating unit with the same 80% of the maximum generating flow was performed. The leakage increased further the next day, turning into a very intense surge of water (see Photos 4.8 (a) and (b)). On February 20th, 2016, another general leakage measurement was carried out in the headrace tunnel in the same way as previously. The results indicated a leakage of approximately 11.4m³/s, an increase of about 4.5 times over the previous measurements in the tunnel.

This led to the decision to dewater the tunnel in order to investigate the causes of the problem.

4.6.2 Seismic Data Recorded on the Day

On February 17th, 2016, at 6:57 PM an earthquake of magnitude 4.2 on Richter scale struck at a distance of approximately 3km from the Chaglla Hydroelectric Power Plant Dam and 13km from the powerhouse.

The location of the earthquake was initially determined by the Geophysical Institute of Peru (IGP). Figure 4.4 (a) shows the location of the earthquake on Google map of Peru (taken from an IGP web page) and Figure 4.4 (b) presents a larger scale image showing the locations of the earthquake (SISMO) and the Chaglla Dam (PRESA).

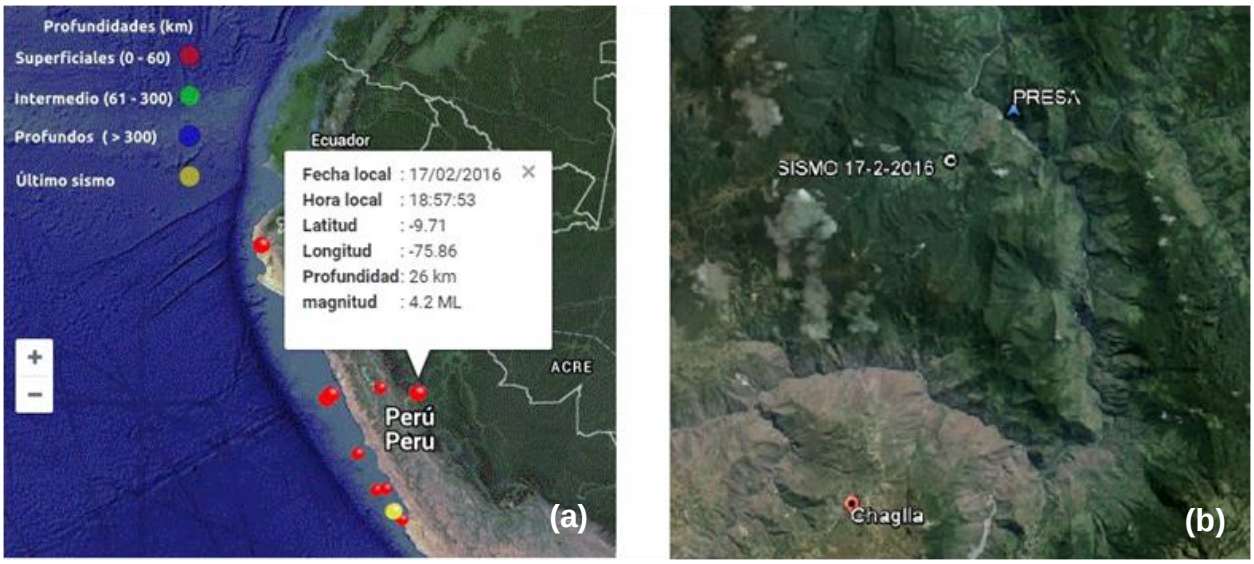

Figure 4.4 - Earthquake location: (a) Location (determined by the IGP) of the 4.2 ML earthquake that occurred on February 17th, 2016; (b) Close-up showing the location of the Chaglla Dam (PRESA), of the village of the same name and of the earthquake (SISMO).

Three accelerographs had been installed on the site to record movements generated by seismic activity. Two were installed at the dam: at the dam's the crest, and at its base. The third was installed in the powerhouse structure. At the time of the earthquake, the accelerograph at the base of the dam was out of service because of vandalism, and readings were only available for the crest of the dam and the powerhouse.

Earthquake records

Figure 4.5 shows the recordings of the three earthquake acceleration components over time at the dam. The estimated distances from the epicenter of the earthquake to the dam and power house (other recordings) are 3km and 13km, respectively.

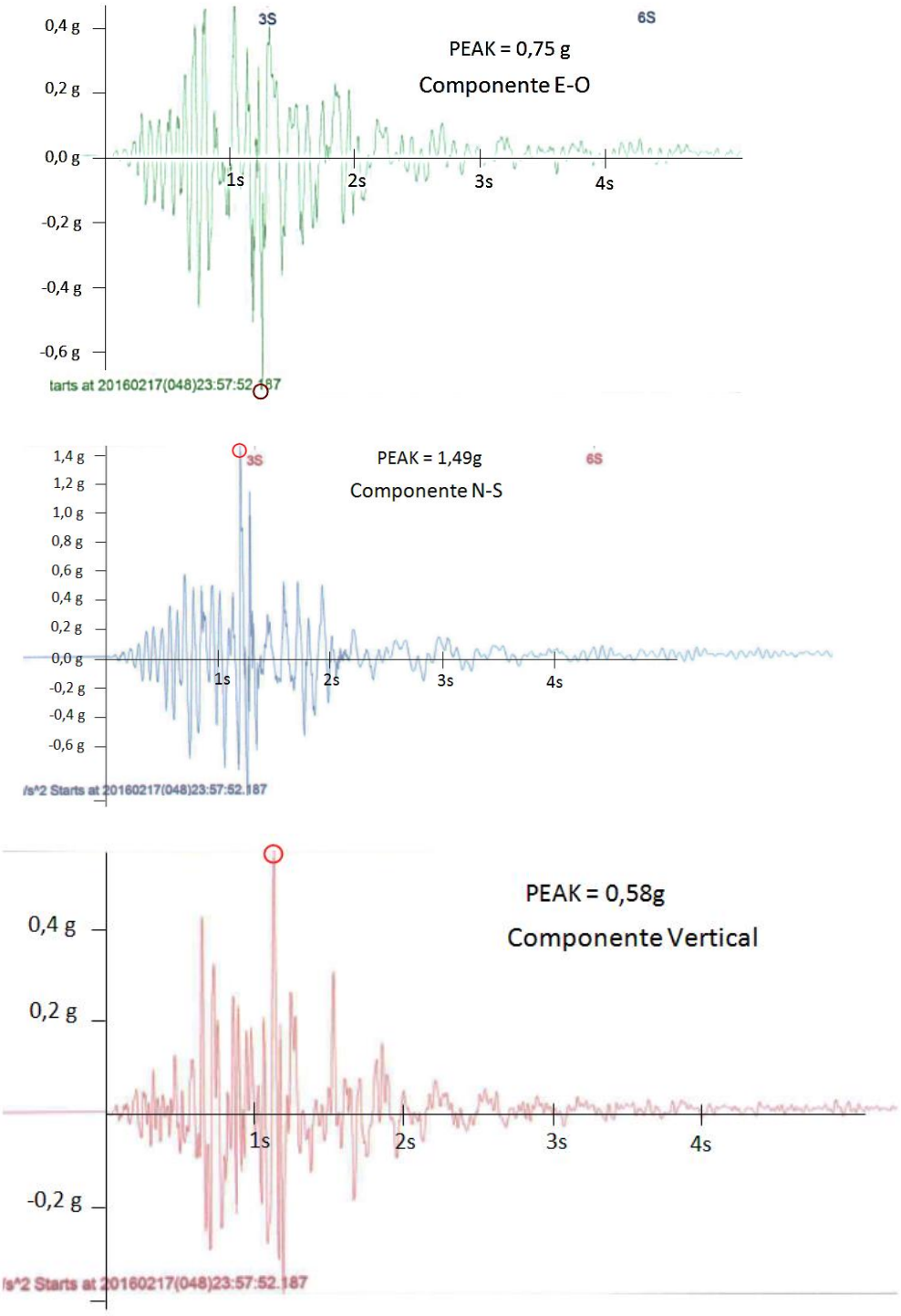

Figure 4.5 - Crest of the dam: Recording of the three acceleration components

Seismic interpretation of the records

Table 4.2 shows a list of the main parameters for recordings on the crest of the dam.

The most remarkable result is the high value of peak acceleration (1.5g) for the 01-02 (NS) component at the crest of the dam, approximately 150 times greater than the largest component (NS) for the powerhouse. The short distance between the epicenter and the dam would suggest that the peaks are the product of some near-fault effects, such as directivity or the hanging-wall effect.

All the values of the parameters recorded at the powerhouse are very small and of no significance from an engineering point of view, this fact being interpreted as being associated to the installation of the accelerograph in this structure.

Table 4.2 - Parameters measured by the accelerographs

Component	Recording crest of the dam		
	01-01 (vertical)	**01-02 (NS)**	**01-03 (EW)**
Peak acceleration (g)	0.588	1.491	0.766
Spectral intensity (cm)	0.0929	0.2122	0.1906
Predominant period (s)	0.1009	0.0714	0.0819
Mean period (s)	0.0967	0.1030	0.1277
Peak velocity (m/s)	0.0631	0.1553	0.1556
Peak displacement (mm)	3.584	6.862	5.482
Cumulative absolute velocity (m/s)	2.0725	5.4117	3.4846
Arias intensity (m/s)	0.4813	2.6155	0.9995
Arias duration (5-95) (s)	1.26	1.46	1.45

As already mentioned, the location of the earthquake was determined by the IGP as latitude 9°42'36"S and longitude 75°51'36"W (-9.71°N, -75.86°E) at a depth of 26 km; different calculations estimated the depth as being between 1.3 to 4 km.

While further investigation would be required to confirm this calculation, it is interesting to note the association between a shallow earthquake and the characteristics of the three components measured at the crest of the dam: very high peak accelerations and very high frequencies (predominantly very small periods).

The possible peak acceleration and velocity at the opening of the cavity detected in the hydraulic left sidewall of the headrace tunnel, distant 10.8km from the epicenter, were also estimated. It can be observed that, at the position where the opening in the left sidewall of the headrace was estimated to be, the mean PGA could have reached 0.06g and around 0.12g for the mean value plus one standard deviation.

4.6.3 Effects Observed on the Project Structures

Localized damage was observed after the earthquake on February 17th and was a result of the seismic event.

Dam area

A small shallow landslide was observed on the hillside on the right abutment near the dam, and a metric size rock rolled from the slope, as shown in Photos 4.5 (a) and (b).

Photo 4.5 - Right bank – landslide downstream of the dam

Region near the adit 2

After the earthquake a shallow landslide was observed near the entrance portal to the adit 2, distant approximately 8km from the epicenter (Photo 4.6).

Photo 4.6 - Adit 2 – landslide near the entrance portal

Chimao creek area

After the earthquake, the following events were observed in the Chimao creek area:

- Small shallow landslide on the left bank of the creek (Photos 4.7 (a) and (b));
- An area with a big volume flow of dirty water from the headrace tunnel outcropping on the left bank of the creek (Photos 4.8 (a) and (b)).

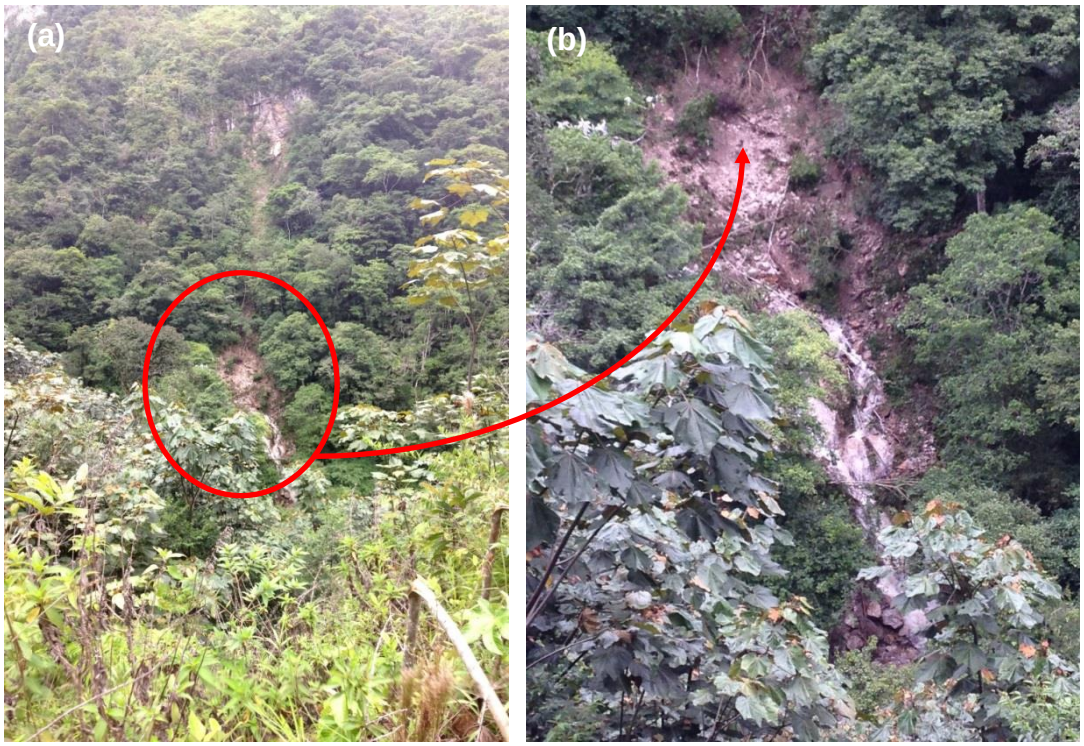

Photo 4.7 - Chimao creek – left bank – landslide around 100m upstream of the access bridge for adit 3

Photo 4.8 - Chimao creek – left bank – high-volume flow of dirty water was observed (later known as coming from the headrace tunnel) about 100m upstream of the access bridge for adit 3 the day after the earthquake. Water can be seen with important amount of solids in suspension.

4.6.4 General Considerations on the Earthquake

The earthquake recorded on February 17th, 2016 was felt as a short duration impulse by personnel in the offices on the site, which is approximately 2km from Chimao creek. This would indicate that the earthquake had a Modified Mercalli (MM) intensity of between III and IV in the area where the offices are located.

The seismic records from the accelerographs show that the earthquake was of very short duration, of the order of 1.5s at the dam site. The high peak accelerations of the three components recorded at the crest of the dam are substantially higher than expected even when an amplification factor of 2 to 2.5 due to the structural behavior is taken into account. The velocities recorded are within the normal ranges.

In particular, the recordings show very high frequency components. Calculations to determine the location of the earthquake using the three components of the accelerogram recorded at the dam appear to indicate that the earthquake was very close to the surface, at a depth of less than 4km.

In a number of localized areas near the dam and the adit 2, small landslides and some minor damage were observed after the earthquake. Using the NGA attenuation formulae (Power et al., 2006), the possible values of peak acceleration and peak velocity at the dam (at the rock base) and powerhouse were estimated. The possible peak acceleration and peak velocity at the opening of the cavity detected in the hydraulic left sidewall of the headrace tunnel were estimated; it is estimated that the horizontal acceleration could have reached something between 0.06g and 0.12g.

Because of the high volume flow of water outcropping in the region of Chimao creek and the considerable increase in the amount of water pumped out of adit 3, together with the almost 4.5-fold increase in the amount of water exfiltration from the headrace tunnel, it was decided to dewater the headrace tunnel.

4.7 Headrace Tunnel Dewatering Procedure

The dewatering procedure of the headrace tunnel was carefully thought and implemented, as not to further damage the tunnel.0

The gates at the Water Intake structure were closed on February 20th in the morning. The water level inside the tunnel was carefully monitored with three manometers installed in adit 3, in adit 4 and in the lower end of the headrace tunnel.

Due to the water leakage in the tunnel, and the lack of infiltration from the rock mass in the upstream section of the tunnel, the initial dewatering rate was very high - 65 meters in the first hour. To reduce the dewatering rate, one of the gates at the water intake was cracked and the dewatering rate dropped to 11m in the second hour, and 8m in the third.

A special device was installed to crack open the second gate in an attempt to further reduce the dewatering rate. Additionally, to gain better control of the dewatering rate, five pumps were installed close to the water intake. These pumps operated from the night of February 20th to the morning of February 23rd, and the average dewatering rate during these three days was around 1.2m/h, corresponding to a drop in the water level from

about elevation 1,090m.a.s.l. to 1,005m.a.s.l. if the first two hours of dewatering are ignored. This corresponded roughly to the prescribed dewatering rate of 1.0m/h.

On February 23rd in the afternoon, a few hours after the pumps had been shut down, one of the gates was completely closed. As a result, the water level in the tunnel dropped quite fast, and the gate had to be crack opened again. In five hours, the level inside the tunnel dropped 43m, reaching elevation 967m.a.s.l. During the following three days, the gates were successfully operated until they were finally closed and dewatering could be started from the drainage valve at the bifurcation downstream of the headrace tunnel in the spherical valve room. The average dewatering rate during these three days was approximately 0.3m/h, and the water level in the tunnel was at elevation 946m.a.s.l.

On February 25th in the afternoon, a site inspection showed that the surge of water at the left bank of the Chimao creek had ceased as the water level inside the tunnel reached elevation 950m.a.s.l., approximately. On the same day, the tunnel was accessed through adit 0 and a partial inspection was carried out down to adit 2. The water level inside the tunnel had stabilized at elevation 948m.a.s.l., which meant that the drainage valve capacity was approximately equal to the infiltration flow. On March 1st the drainage valves in the powerhouse used to drain the spiral casing could be operated, and dewatering was resumed slowly at around 0.15m/h until the dewatering valves at adit 3 were operated on March 6th.

Dewatering through adit 3 required that several drainage pumps were operated. These were operated for 3 days until the water level reached 920m.a.s.l., which corresponds to the tunnel floor under the surge chamber at chainage 14+000 approximately, being the highest point in the tunnel downstream of the siphon at Chimao creek. Dewatering through the bypass valves in the powerhouse is not possible from this elevation downwards.

Further lowering of the water level in the tunnel below elevation 920m.a.s.l. was not possible because of the high infiltration flows, particularly from the upstream stretch of the tunnel. Two boreholes were, therefore, drilled in adits 1 and 2 to install the ventilation system and construct small cofferdams so that the infiltration flows could be diverted to these holes and drained out of the adits.

On March 15th the water level inside the tunnel reached the elevation 898m.a.s.l. At this point, as foreseen in the dewatering procedure, a floating movable pumping system was installed inside the tunnel, allowing to dry the siphon at Chimao creek.

Figure 4.6 shows the dewatering curve and the main events registered during the dewatering procedure.

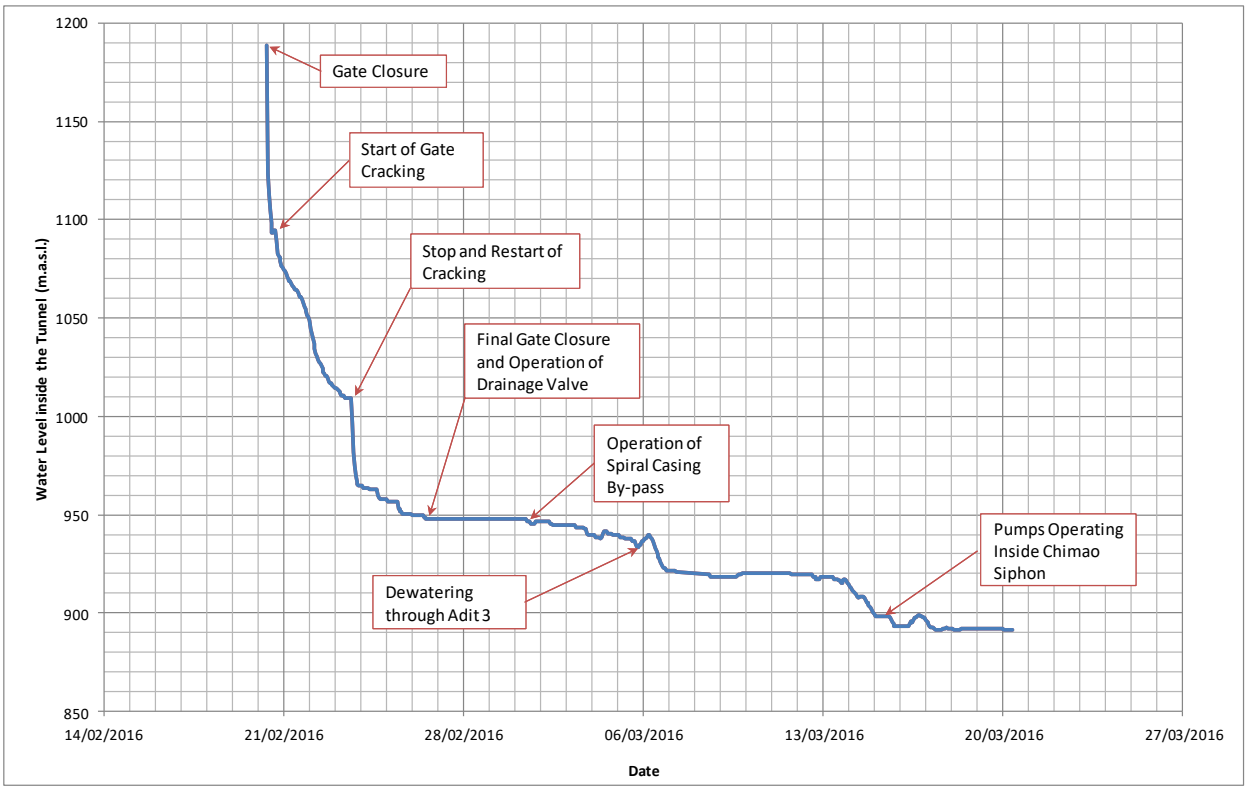

Figure 4.6 - Dewatering curve of the headrace tunnel and main events

4.8 Cavity Detected at Chainage 12+740

4.8.1 Initial Site Investigations by Speleologists

On March 17th, 2016, after most of the tunnel had been dewatered, a local failure of the shotcrete lining could be observed in the lower part of the hydraulic left sidewall of the tunnel at chainage 12+740, measuring roughly 1.5 x 1.5 m and triangular in shape.

This cavity was inspected by a team of geo-speleologists and called El Hoyo de la Beba; its internal topography mapped to collect all possible data that could help establishing its possible origin. Additionally, the geo-speleologists inspected and mapped the cavity at the left bank of Chimao creek where the outcrop of water was detected, this cavity being called El Suspiro de la Frescia.

El Hoyo de la Beba cavity is 1.50m wide and 1.50m high at the entrance (Photo 4.9), subparallel to the rock mass bedding layers, with an average dip/dip direction of 310/76 and extends more than 5m (the real depth could not be measured due to safety requirements) below the floor of the tunnel in the location it intersects the tunnel. The roof and walls consist of jointed, stable, gray to black rough limestone rock with layers up to 1.50m thick, with some indications of slickensides in the rock walls, and without any signs of dissolution.

Photo 4.9 - View of the entrance to the cavity on the hydraulic left sidewall of the headrace tunnel at chainage 12+740

El Hoyo de la Beba continues approximately 80m upstream of the point where it starts at chainage 12+740, reaching a maximum width in one of the sections of 8.6m and a height of 3m. It runs diagonally to the headrace tunnel and after 80m turns upward along an axis like a chimney rising more than 30m above the crown of the tunnel. The end of this chimney was not reachable due to the presence of many unstable blocks, which would put at risk the safety of the personnel involved in the activity.

No stalactites or stalagmites or other characteristic morphological features were found in the area inspected. Vertical rock bolts were observed on the floor of the cavity (Photo 4.10), suggesting that the area being inspected was immediately above the crown of the tunnel.

Photo 4.10 - View of a headrace tunnel rock bolt. The fact that the bolt is vertical suggests that the area being inspected is above the roof of the Tunnel

Based on the site inspection, the geo-speleologists concluded that the El Hoyo de la Beba cavity did not exist previously and that it established itself in a “stratigraphic fault” filled with friable intensively fractured material that became erodible when disarticulated and submitted to high flows and water pressures after the earthquake.

The cavity El Suspiro de la Frescia is located in the hydraulic right side of the headrace tunnel approximately subparallel to the axis and to the rock mass bedding layers. The inspection carried out by the geo-speleologists extended around 120m into the cavity, which is 1.5m to 10.7m wide and, in average, 3m high. Although in the inspection period the cavity was dry, a karstic process was associated to its origin, as well-developed stalactites and stalagmites were documented by the geo-speleologists (Photo 4.11).

Photo 4.11 - View of El Suspiro de Frescia cavity with stalactites and stalagmites

4.8.2 Internal Survey of the Cavity

A topographical survey of the El Hoyo de la Beba cavity was carried out with a portable laser scanner. Figures 4.7 and 4.8 show isometric side and front views produced as part of this survey, and Figure 4.9 shows cross-sections indicating the position of the cavity in relation to the headrace tunnel.

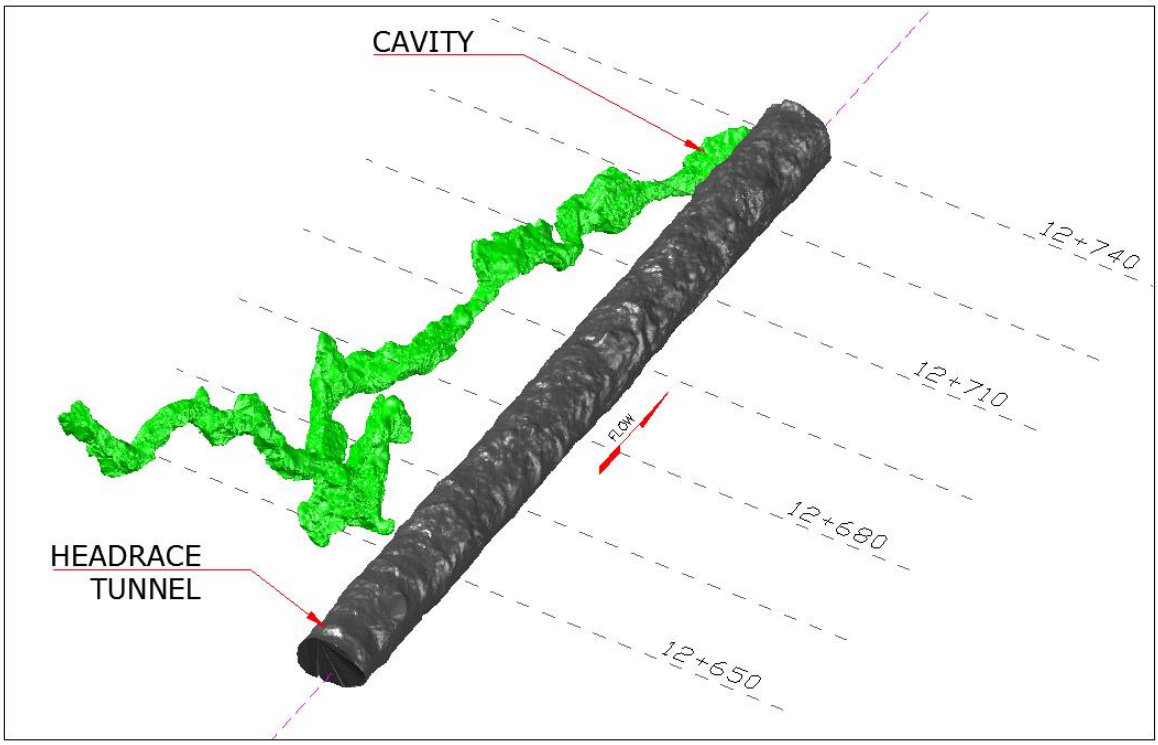

Figure 4.7 – Isometric side view of the El Hoyo de la Beba cavity

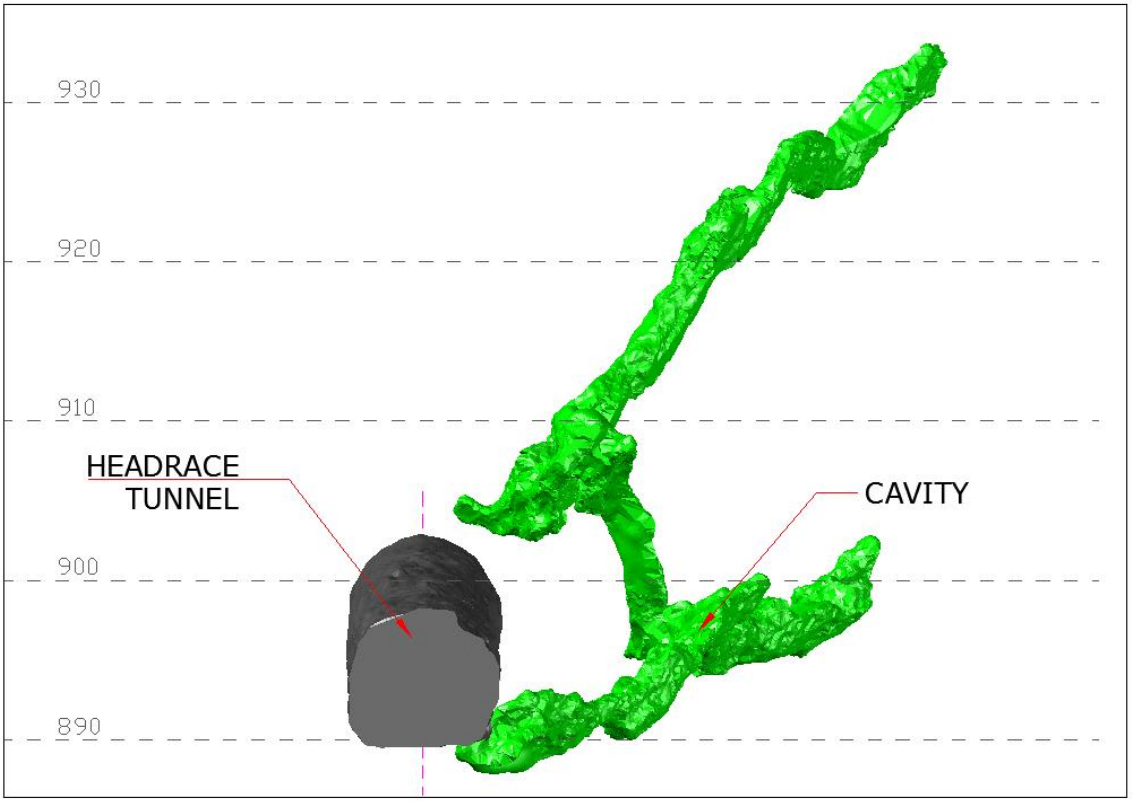

Figure 4.8 - Isometric view towards upstream of the El Hoyo de la Beba cavity

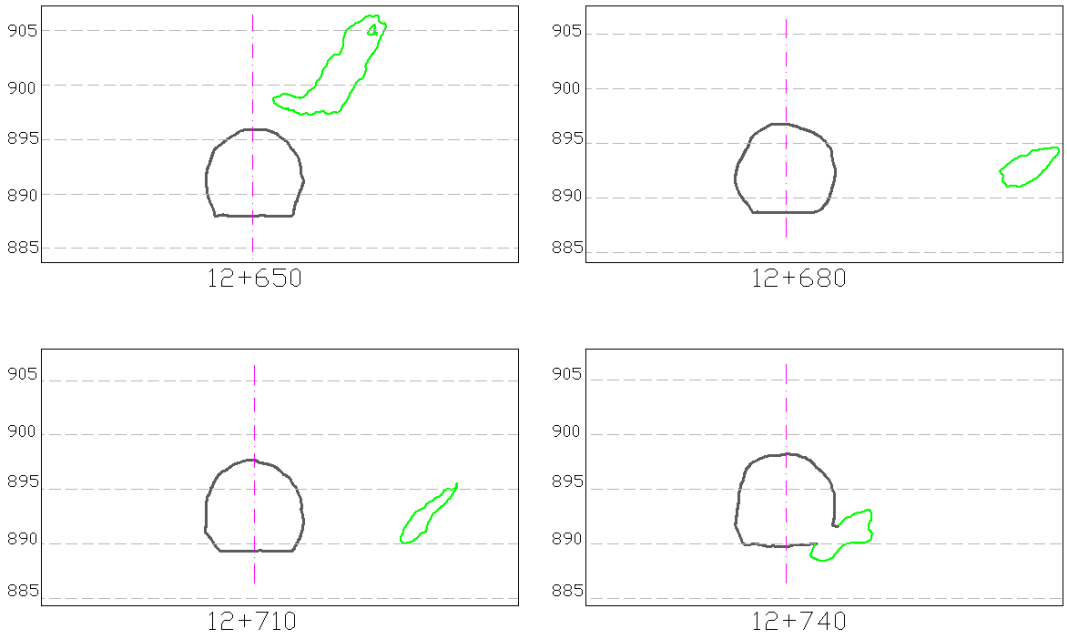

Figure 4.9 - Cross-sections of the headrace tunnel showing the position of the El Hoyo de la Beba cavity

Analysis of Figure 4.7 indicates that the cavity extends along a “stratigraphic fault”, that is, a fault developed along the orientation of the limestone bedding, slightly diagonal to the axis of the headrace tunnel between chainages 12+740, where it enters the tunnel, and approximately 12+680. From this point on, because of joints and / or sinistral faults, the cavity joined a karst conduit, approximately 110m upstream of chainage 12+740.

It is speculated that approximately around the elevation 950m.a.s.l. this cavity meets the karstic cavity El Suspiro de Frescia, which would have caused the surge of water in the left bank of Chimao creek. This probable connection between the two karstic conduits around the mentioned elevation is interpreted due to the fact that, during the dewatering process, at this water level in the headrace tunnel, the surge of water in the Chimao creek stopped completely.

4.9 Mechanisms Involved in the Formation of the Cavity

The inspections and investigations performed at the site of the incident revealed a large cavity in the rock mass adjacent to the headrace tunnel that could be accessed from the opening in the lining resulting from the failure. According to the geological survey described, the cavity extended about 80m upstream from the opening in the lining with an alignment almost parallel to the tunnel axis and then turned upwards into a chimney like shaft rising more than 30m above the tunnel crown (see Figures 4.7 and 4.8). At this point access to the cavity was blocked by accumulated debris (mostly rounded boulders) that could not be safely removed to allow further exploration. The initial 140 m of the cavern had rough walls, indicating that no karstic phenomena ever acted in this location; on the contrary the transition to smooth walls was generated by dissolution which was clearly seen and mapped.

The interpretation for the formation of this cavity is that it originated from the erosion of material that filled a stratigraphic fault. This fault was aligned with the bedding of the calcareous rock and was the result of differential movement along the bedding of the rock

that occurred during the tectonic history of the area. Its filling material was composed of sheared and crushed rock, originally in a very compact state, but which constituted a preferential seepage path. This fault zone had been intersected during excavation of the tunnel and had been defined as a Class V zone (according to Barton's Q index) for about 12m long. However, at the chainage where the failed lining was found, the rock mass had been classified as Class III during tunnel excavation and no weak or erodible materials were observed on the tunnel face, walls or crown. The support measures applied in this tunnel section were, therefore, those corresponding to Class III rock mass, and consisted of 10 cm thick fiber reinforced shotcrete on the crown and sidewalls and 3 m long, 25 mm diameter, passive bolts at 2 m intervals in the crown. The tunnel floor was lined with a 25 cm thick plain concrete slab poured over the compacted muck. No abnormalities were recorded when this section of the tunnel was excavated and the support measures were applied.

After filling and pressurization of the tunnel, which at this point had an internal pressure of 31bar, the water saturated the infilling material in the fault zone. It is interpreted that the earthquake acted as a trigger in the disarticulation of the infilling material, which when subjected to the high pressure of approximately 31bar, suffered a retrogressive erosion process starting from its interface with the karstic feature in the rock mass. This erosion retrogressed until it reached the location where it caused a loss of the passive support of the tunnel wall, leading to the localized failure of the lining. This karstic cavity was connected with an existing cavity that day lighted on the left bank of Chimao creek and constituted the duct through which the observed large flow of dirty water outcropped.

It is important to mention that the installation records of all rock anchors in the region, as well as their quality control load test, were analyzed, and showed no indication of the rock mass in the area being of weaker competence.

4.10 Design Solution to the Problem

Prior to the implementation of the necessary remedial works an intense investigation of the tunnel, along all its alignment, was performed using different geophysics processes and direct borings, in order to guarantee that no similar feature existed and could fail in the future pressurizing of the tunnel. Some regions where there were indications of possible presence of cavities were grouted.

The solution for the collapsed region was traditional, simple and quick to implement. The erosion cavity Hoyo de la Beba was filled with concrete until it became distant transversely to the tunnel – a transversal distance of 30 m was postulated as the criteria for concrete filling. The concrete lining previously installed at the Chimao creek was prolonged to a tunnel chainage where the design hydraulic gradient criteria was met in rock mass with reliable geomechanical characteristics.

4.11 Conclusions

The Chaglla HPP has been in successful operation since mid 2016; the concerns related to the behavior of the headrace tunnel during and after its pressurization for power generation have been surpassed.

5 CONCLUDING REMARKS

Some case histories are presented and discussed, trying to frame the physical behaviour(s) that lead to important gains in knowledge of geotechnical behaviour in important infrastructure projects, during detailed design and construction. Creativeness is an important aspect that guided decisions in these projects, and Prof. Victor de Mello's perspective on how to use creativeness is seen as present in all of them.

Many experienced engineers have studied and solved equivalent problems. To them these case histories may add little additional knowledge. To the younger colleagues, these examples may enlighten their decision taking process.

In all these case histories the importance of a sound geological model to support the design studies is present; the need to have this geological model alive throughout the site investigation for the project, and also throughout the actual construction of the works, updating or even fully revising the existing geological model due to information being gathered as the works progress, is crucial for the success aimed at. In some occasions, nature as materialised in the geo-environment, excited by meteorological factors, manifests itself through a different model than that accepted and studied previously.

Difficulties in budget and time constrains sometimes add an important factor in some contract models prevailing these days in many important infrastructure projects.

Broadly speaking, why so many projects undergo significant changes after start of construction or event failures continue to happen, and so much resources and time is lost due to these situations?

It is our understanding that geo-engineering, soil and rock mechanics and geology for engineering, has developed to a point in which sound physical concepts are recognized and understood. Mathematical tools have been developed to very sophisticated levels, in which the required in put parameters many times are not practically obtainable, other than in research related activities and projects.

Anticipation of a geological model is very important in order to plan and properly interpret data from a site investigation program; Fookes (1997, 2000) provides a very important contribution discussing and proposing basic geological models for different geological environments. Fookes (1998) also gives an important contribution when he clearly states *"if you do not know what you are looking for in a site investigation you are not likely to find much of value".* Keeping the model "open" to be re-discussed at the light of new information coming from the site, during construction work is of fundamental importance – early stages of excavation in a major construction site provides infinitely more information than localized boreholes.

The relevance of construction methodology and its inter-relation with design hypothesis also plays an important role, especially in soil-structure interaction behaviour, and should complement aspects of the geological model during design and construction.

The constant updating of the state of knowledge or of practice is crucial when pursuing the required optimizations in the major infra structure projects so needed by our societies. I hope that the discussion of these important geotechnical works add to the state of practice and knowledge.

As a last tribute to Victor de Mello in this occasion, I think it is valid to share one of his most used sayings, an Arab proverb:

He who knows not, and knows not that he knows not - He is a fool, shun him.

He who knows not, and knows that he knows not - He is simple, teach him.

He who knows, and knows not that he knows - He is asleep, wake him.

He who knows, and knows that he knows - He is wise, follow him.

which was discussed, in many interactions with Prof. John Burland before his death, as meriting revision and both proposing that the last line should be re-written and a further line should be added as follows:

He who knows, and knows that he knows – He is insufferable, use him

He who knows, and knows when he knows not – He is wise, follow him

6 ACKNOWLEDGEMENTS

I would like to share with you all my gratitude, *in memoriam,* to Prof. Victor de Mello, who taught and lead me in the field of applied geomechanics, opening my mind to the myriad of facets with which nature express itself, *"always considering that there is no reason for two things being equal".* His approach on how to tackle engineering problems, with sound concepts and wise thoughts, plays a very important part of my professional practice as well as of my private life, and is specially acknowledged.

Our gratitude has also to be extended to many colleagues, specially to Profs Georg Sadowski and Claudio Wolle, Mr. Carlos Manoel Nieble and Dr. Werner Bilfinger, who have a continuous and important participation, as well as Construtora Odebrecht, Construtora Andrade Gutierrez and Intertechne Consultores Associados, in facing and solving some of the geotechnical challenges faced during my professional practice. In the preparation of this technical paper, and the presentation that accompanies it, the collaboration and critical review of Mr. Bruno S. Dzialoszynski was greatly appreciated.

I also have to acknowledge the fact that numerous of Victor's friends incorporated me as their friends, sharing with me their enormous experience in life through geotechnical engineering; special gratitude is shared with Prof. Michele Jamiolkowski, Dr. David Carrier, Prof. John Burland, and Prof. Harry Poulos.

Finally, my gratitude to Dr. Purnanand Savoikar, Chairman of the IGS Goa Chapter of the Indian SSMGE, who transferred his enthusiasm in this task during the preparation of this Lecture. The gratitude is extended to all members of the Goa Chapter and to the Indian SSMGE.

7 BIBLIOGRAPHY

Babouchkine em Bogomolov, G.V. 1965. Hydrogeologie. *Ed. de la Paix.* 1965.

Barton, N.R., Lien, R. and Lunde, J. 1974. Engineering Classification of Rock Masses for Design of Tunnel Support. *Rock Mechanics.* 6, 1974, Vol. 4, pp. 189-239.

Benson, R.P. 1988. Design of Unlined and Lined Pressure Tunnels. *International Symposium of Tunneling for Water Resources and Power Projects.* 1988.

Bjerrum, L. and Andersen, K.H. 1972. In-situ Measurement of Lateral Pressures in Clay. *Proceedings to the Fifth European Regional Conference ISSMFE-Madrid.* 1972.

Bjerrum, L., et al. 1972. Hydraulic Fracturing in Field Permeability Testing. *Géotecnique.* 1972, Vol. 22.

Carlsson, A. and Olson, T. 1977. Hydraulic Conductivity of Swedish Crystalline Rocks. *The Bulletin of the Geological Institutions of the University of Uppsala.* 1977, Vol. 7, pp. 71-84.

Dale, T.N. 1923. *The Commercial Granites of New England. U.S. Geological Survey Bulletin 738.* Washington : Government Printing Office, 1923.

de Mello, L.G.F.S. 2005. Geotechnical Failures. *Jennings Lecture.* 2005.

de Mello, L.G.F.S., et al. 1987. The Foundation Treatment of Residual Soils Conditioned by Canaliculae: a Case Historie. *Anais da Conferencia Ibero-Americana sobre Aproveitamentos Hidraulicos.* 1987.

de Mello, L.G.F.S., Sadowski, G.R. and Nieble, C.M. 2004. Shear Resistance of Biotite Schists: Peak and Post-Peak Behaviour. *Advances in Geotechnical Engineering: the Skempron Conference, ICE, London.* 2004.

de Mello, V.F.B. 1977. Reflections on design decisions of practical significance to embankment dams. *XVII Rankine Lecture / Géotechnique.* 27, 1977, Vol. 3, pp. 281-355.

de Mello, V.F.B. 1972. Thoughts on soil mechanics applicable to residual soils. *III Southeast Asian Conference on Geotechnical Engineering.* 1972.

de Mello, V.F.B., et al. 2004. Reppraising historical coincidences that radically misled slope destabilization analyses of homogeneous earth dams. *Advances in Geotechnical Engineerin: the Skempton Conference, ICE, London.* 2004.

Fookes, P.G. 1997. Geology for Engineers: the Geological Model, Prediction and Performance - 1st Glossop Lecture. *Quarterly Journal of Engineering Geology.* 1997, Vol. 20 part 4.

Fookes, P.G. 1998. Judging the Lie of the Land - Meeting Report of the First Glossop Lecture. *Ground Engineering.* 1998.

Fookes, P.G. 1997. *Tropical residual soils, Geological Society Professional Handbooks.* London : Geological Society, 1997.

Fookes, P.G., Baynes, F.J. and Hutchinson, J.N. 2000. Total Geological History: A Model Approach to the Anticipation, Observation and Understanding os Site Consitions. *International conference on geotechnical and geological engineering; GeoEng 2000.* 2000.

Fossen, H. 2010. *Structural Geology.* 2010.

Haimson, B. and Fairhurst, C. 1967. Initiation and Extension of Hydraulic Fractures in Rocks. *Society of Petroleum Engineers Journal.* 1967.

Hencher, S.R., et al. 2011. Sheeting Joints: Characterisation, Shear Strength and Engineering. *Rock Mechanics and Rock Engineering.* 2011, Vol. 44, 1, pp. 1-22.

Holzhausen, G.R. 1989. Origin of sheet structure, 1. Morphology and boundary conditions. *Engineering Geology.* 27, 1989, pp. 225-278.

Kennard, R.M. 1970. The Measurement of Soil Permeability In-situ by the Constant Head Test. *PhD Thesis - University of London.* 1970.

Machado, A.d.B. 1983. The contribution of termites to the formation of laterites. *II International Seminar on Lateritisation Process, São Paulo.* 1983.

Morgenstern, N.R. and Vaughan, P.R. 1963. Some Observations on Allowable Grouting Pressures. 1963.

Norwegian Geotechnical Institute. 2013. Rock Mass Classification and Support Design. [Online] 2013. www.ngi.no.

Power, M., et al. 2006. The Next Generation of Ground Motion Attenuation Models (NGA) Project: an Overview. *Proceedings of the 8th Earthquake Engineering Research Center - Draft Report.* 2006.

Remy, J.P.P. et. al. 1985. Choice of the Foundation Treatment of Balbina Earth Dam. *15th International Conference on Large Dams.* 1985.

Santos, O.G. et. al. 1985. Experimental Grouting of Residual Soil of Balbina Earth Dam Foundation, Amazon, Brazil. *1st International Conference on Geomechanics in Tropical Lateritic and Saprolitic Soils.* 1985.

Sathler, G. e Camargo, F.P. 1985. Tubular Cavities in the Residual Soil of the Foundation of Balbina Earth Dam - Amazon - Brazil. *15th International Conference on Large Dams.* 1985.

Terzaghi, K. 1962. Dam Foundation on Sheeted Granite. *Géotechnique.* 1962, Vol. 12, 3, pp. 199-208.